DEVELOPMENT OF AN SMALL ELECTRIC RACE CAR

YIP ZHEN SHEN

UNIVERSITI TUNKU ABDUL RAHMAN

DEVELOPMENT OF AN SMALL ELECTRIC RACE CAR

YIP ZHEN SHEN

A project report submitted in partial fulfilment of the requirements for the award of Bachelor of Mechanical Engineering with Honours

Lee Kong Chian Faculty of Engineering and Science
Universiti Tunku Abdul Rahman

October 2025

DECLARATION

I hereby declare that this project report is based on my original work except for citations and quotations which have been duly acknowledged. I also declare that it has not been previously and concurrently submitted for any other degree or award at UTAR or other institutions.

Name : Yip Zhen Shen

ID No. : 2106623

Date : 22 September 2025

COPYRIGHT STATEMENT

This final year project report is submitted in partial fulfilment of the requirements for the degree of Bachelor of Mechanical Engineering with Honours at Universiti Tunku Abdul Rahman (UTAR). This final year project report represents the work of the author, except where due acknowledgement has been made in the text. No part of this final year project report may be reproduced, stored, or transmitted in any form or by any means, whether electronic, mechanical, photocopying, recording, or otherwise, without the prior written permission of the author or UTAR, in accordance with UTAR's Intellectual Property Policy.

ACKNOWLEDGEMENTS

I would like to express my deepest gratitude to my supervisor, Dr Wong Hong Mun for his invaluable guidance, support, and encouragement throughout the final year project. His suggestion and constructive feedback were crucial in solving the difficulties faced in the project so that the project can be completed on time with the best result.

I would also like to thank for Dr Kam Heng Keong from LKCFES and DMME as a final year project coordinator as he always provides necessary information and reminders for my final years project in UTAR.

In addition, I would like to express my eternal appreciation towards my family as they had given endless support whether physically or mentally as well as financially.

Lastly, to my dearest friends for their help, friendship, and support throughout the process of fabrication and experiment which has been instrumental to the success of this project.

ABSTRACT

This project aims to develop an electric racing car from a standard ride-on-car. Electric vehicles (EV) are recognized for the higher efficiency compared to traditional internal combustion engine vehicles. In addition, EV racing can be a good platform to understand everyday science. This can also be an effective method to spark children's interest in STEM (Science, Technology, Engineering, and Mathematics) education, where the students, children and young learners can gain hands-on experience in problem-solving, engineering skills and creativity when modifying the electric ride-on-car within an affordable budget. Pursuing this project, it first involves researching electric ride-on-car modification techniques, and performance components. Selected ride-on-car is then analysed to determine suitable design changes for an adult to drive. Required parts were fabricated using methods suitable for children to handle and subsequently installed on the car. The car was reinforced to support the weight and handling requirements for adult driving. Additionally, the stock 12V motor was replaced with a 24V motor, different gear ratio and wiring for improving the ride-on-car's performance. The modified car was then tested for weight distribution, shaft deflection, acceleration, and power consumption. The front wheel camber change due to heavy load is reduced about 75%. The rear shaft deflection was significantly improved 59% which would increase the durability of powertrain system. Performance improved notably, with the top speed increased 260% and the 0-13 m acceleration time dropped from 20.98 s to just 5.91 s. However, the upgraded motor consumed more electrical power which increase the power consumption from 0.0148 Wh/m to 0.1407 Wh/m. In short, this project successfully demonstrated that an electric ride-on car can be transformed into a cost-effective platform for STEM education.

Keywords: STEM awareness, racing, electric vehicle, modifications, energy efficiency

Subject Area: TJ1-1570 Mechanical engineering and machinery, TL1-4050 Motor vehicles

TABLE OF CONTENTS

LIST OF TABLES

LIST OF FIGURES

LIST OF SYMBOLS / ABBREVIATIONS

EV	Electric Vehicle
ICE	Internal Combustion Engine
PM	Permanent Magnet
BL	Brushless
AC	Alternating Current
DC	Direct Current
TV	Train Value
PRS	Power Racing Series
ABS	Acrylonitrile Butadiene Styrene
PP	Polypropylene
SLA	Sealed Lead Acid
Mph	Miles per hour
Km/h	Kilometre per hour
STEM	Science, Technology, Engineering and Mathematics
μ	Static coefficient
μ_{rr}	Static coefficient rolling resistance
F_{rr}	Friction force due to rolling resistance
F_N	Normal force
m	Mass
g	Gravity
a_x	Acceleration in x-direction
v	Velocity
P_w	Wheel Power
T_w	Wheel Torque
ω	Wheel angular velocity
η	Efficiency
τ_{in}	Motor input torque

LIST OF APPENDICES

CHAPTER 1

INTRODUCTION

1.1 General Introduction

Electric cars represent a revolutionary development in the automotive industry, playing an important role in reducing greenhouse gas emissions from vehicles. Nowadays, the innovations and new technologies in electric vehicles (EVs) still present challenges faced by many industries. An EV can be fully or partially (hybrid vehicle) equipped with electric motors and the energy storage system of the EV is rechargeable which is crucial for sustainable mobility. Implementation of the electric vehicle is important because it can provide a pollution-free transportation and less dependence of fossil fuel. The reduction of emissions is important for sustainability environmental, and EV does not release pollutants gasses like the traditional internal combustion engine (ICE) vehicle. EV electric motor is also performed better in terms of efficiency and unlike the internal combustion engine as it has the specify power range for maximum efficiency.

Furthermore, there are several significant components in designing an electric vehicle such as battery packs, electric traction motor, charging mechanism, thermal management system and the power electronics controller. The traction motor is the electric motor which may receive AC or DC current and transform electrical energy into mechanical energy in order to drive the wheel. Then, thermal management system is necessary to control the temperature of both the battery and electric motor to prevent overheating and enhancing the vehicle efficiency. Next, the power electronics controller is the key component as it serves as the brain of the EV and regulate the electric flow from the battery to motor and other electrical systems of an EV (“Understanding EV Technology”, 2024).

In addition, the performance and efficiency of an EV can be focus on the aspect as mentioned in the previous paragraph. In order to transfer the mechanical energy from the motor to the wheel optimally. Other than this, the electric motor can also generate electricity during braking and transfer the electricity back to the energy source which is battery pack. The powertrain

design for the vehicle must be optimised as it can affect the dynamic performance of the vehicle. Not only these, but the maximum output torque of the motor is also crucial as the selected transmission system must be able to handle the output from the motor. In the powertrain design of the EV, the number of motors can be 1 motor, 2 motor or 4 motor setups to propel the vehicle (Yu, 2017).

Electric vehicles have also proven to be an effective educational platform for STEM activities among children and students. In 2022, an international school in Kuala Lumpur launched the "Electric Vehicle in Education" (EViE) project, an extracurricular initiative in which the students collaboratively designed and built an electric race car. The program extended beyond engineering, requiring participants to apply skills in marketing analysis, project management, suspension tuning, and strategic planning to balance performance with battery efficiency. EViE program was not only limited to engineering students but it also provided opportunities for those interested in management, marketing and other supporting roles, making it a multidisciplinary learning experience. As with professional competitions, the project adhered to strict safety and technical regulations, including the requirement of a roll-over bar, a steel chassis and a Styrofoam crash box to absorb impact energy ("EViE – Electric Vehicles", n.d.).

Another EV program which related to STEM racing competition has also been organized at University of Kentucky in 2020, in collaboration with GreenpowerUSA and the Kentucky Energy & Environment Cabinet. The activity was launched with an ambitious hands-on STEM program aimed at fifth-grade students across the state. The initiative of the program, "STEM Education through Electric Vehicles" has empowered the students to design, construct and race one-person electric vehicles, engaging them deeply in science, technology, engineering, and mathematics. Funded by a $51,344 State Energy Program grant, the program integrated curriculum materials, vehicle kits and offers school training through CAER. Its goal was to transform theoretical learning into tangible experience for the students to apply scientific principles, engineering design and innovation to real-world vehicles as well as prepare young learners for their future careers in energy, manufacturing, and engineering fields (Melanson, 2020).

1.2 Importance of the Study

In recent years, there has been a noticeable decline in children's interest in STEM (Science, Technology, Engineering, and Mathematics) fields, which poses a significant concern for the future development and competitiveness of any nation. STEM education is crucial not only for technological advancement but also for fostering innovation and economic growth. To counter this trend, it is essential to introduce engaging activities that can spark curiosity and nurture young minds. Racing, with its dynamic and competitive nature, has historically served as a powerful motivator for technological development and offers an exciting platform for experiential learning in STEM. However, for such initiatives to be widely adopted and impactful, they must be financially accessible. This final year project addresses this challenge by proposing the development of a low-cost electric race car designed specifically for students and children. The aim is to create an affordable yet educational tool that can inspire interest in STEM through hands-on experience, teamwork, and creative problem-solving.

1.3 Problem Statement

An electric ride-on-car is built for children’s entertainment. It is also can be seen as a good platform to build upon as an introduction electric car racing, in hope to attract children’s interest to the field of science, technology, engineering and mathematics or STEM in short. To do so, there are many limitations needed to be overcome for this car. The said car material are Acrylonitrile Butadiene Styrene (ABS) plastic and Polypropylene (PP) which are soft and not suitable for rigorous demanding racing environment. Much rigidity in the chassis is needed. The car also has an DC motor that caters the load of a child’s weight and thus the power output from the electric traction motor is low and suitable powertrain re-design is deemed necessary for making this ride-on-car into a racing car. The wiring of this car will thus be unsuitable for the new motor performance. In addition, the selection of fabrication methods and tools used will be important considerations as children and high school students are going to perform all needed modifications.

1.4 Aim and Objectives

The aim in this project is to increase the performance of the electric ride-on-car and convert it into a race car application. The objectives of the project are:

1. To determine the required modifications needed for the conversion of an electric ride-on-car into an electric race car for children.
2. To perform all modifications to electric ride-on-car such as powertrain reinforcement, suspension reinforcement, electronic system and motor-gearbox modification.
3. To verify performance improvements made to the electric ride-on-car via the assessments like weight measurement, acceleration test, power consumption test and so on.

1.5 Scope and Limitation of the Study

This project focuses on modifying a small electric ride-on-car by upgrading the key components such as the powertrain, battery, motors, steering linkage, suspension and wiring systems. The drivetrain will be redesigned to support an adult's weight to ensure the car can be driven smoothly. The original motor and gearbox which were only sufficient for a child's load, will be replaced with higher-power rating motor with different gearing. Similarly, the suspension will be reinforced to handle greater loads and higher speeds. Finally, the wiring system will be upgraded to higher-rated specifications with optimized components' mounting location.

Testing will be conducted when both the mechanical and electrical parts are done. Then, the ride-on-car specification like speed and power rating will be obtained from GPS application and power consumption meter respectively. After that, the data collected will be further analysed to compare the specs of the ride-on-car for stock and modified versions.

The limitation of the project is the modification method for the electric toy car should not be too complicated and can be replicated easily as the modified ride-on-car is intended to be promoted to the high school students and children involve in this STEM racing activities. Equipment and machine used in this project should be common and available in a high school and their students had been trained on the proper ways to use it.

1.6 Contribution of the Study

This study aims to identify a suitable model of an electric ride-on-car and transform it into a small-scale electric race car via STEM cultural mission. Then, the project demonstrates the application of fundamental engineering principles combined with practical hands-on skills to achieve effective modifications. It further highlights the creativity and innovation involved in customizing an electric race car through cost-efficient methods, ensuring compatibility with competitive requirements while maintaining affordability. Ultimately, the project seeks to showcase not only the technical feasibility of such modifications but also their potential to inspire greater interest and engagement in STEM education.

1.7 Outline of the Report

This report is organized into 5 chapter to ensure clarity in presenting the project. Chapter 1, which is the introduction that provide about background of EV and briefing of STEM, importance of study, problem statement, aim and objectives, scope and limitation of the study as well as the contribution of this project and outline of the report. Literature Review will research about the related information on the electric ride-on cars. Chapter 3 will demonstrate the methodology adopted for the project, including design and simulation, material selection, fabrication, testing, and data collection. Chapter 4 will discuss the results based on the ride-on car assessment with reference to the project objectives. Lastly, chapter 5, Conclusion and Future Work are to summarizes the specification of the car compare with the objective and suggests potential design for further improvement.

CHAPTER 2

LITERATURE REVIEW

2.1 Introduction

The literature review for this section will focus on the related topics for modifying a small electric race car in different aspects. The first part was to review the low cost racing competition involving the electric ride-on-car and three wheeled electric race cars. Then, the potential modification plan and spare parts of the ride-on-car will also be studied with the outcome on the modification parts for this toy car.

Furthermore, the literature review will also include the deeper review on various powertrain configurations used in electric race cars, including electric system design principles and different types of electric motors. The working principles of DC motors, DC motors' dynamic braking effects and the role of bearings in powertrain efficiency will be examined. In the section, the car chassis designs and materials commonly used in toy cars are also investigated.

2.2 Low cost electric vehicle race series

The adaptation and transformation of children's ride-on-cars into competitive vehicles has become a unique platform for engineering creativity, innovation, and STEM engagement. Events such as the Power Racing Series (PRS) in the United States encourage participants to modify the electric ride-on-car and join the racing competition under strict budgetary and safety constraints. This culture of modification was further extended to ride-on-car drag races, where the draggy enhanced the motor output, gearing and battery spec to achieve short bursts of acceleration in straight path. In market survey, there were several modification methods could be done for the ride-on-car. These included modifying motor-gearbox and batteries with several configurations. Moreover, the Electrathon competition provided a more formalized racing environment for the high school students, emphasizing endurance, efficiency and better time laps by building electric racing vehicle from scrap.

2.2.1 Power Racing Series (PRS)

Power Racing Series which organized by a non-profit organization was a fun toy car racing competition for the public by using the electric ride-on-car initially made for kids and modified for racing application. This series encourages the people like the teenagers or adults to involve in this racing competition as it promoted and allowed them to learn more about the Science, Technologies, Engineering, Art and Mathematics (STEAM). In addition, the competition provided participants with opportunities to exchange knowledge and expertise regarding the modification of electric ride-on-cars (Power Racing Series, 2025).

The 2017 Power Racing Series (PRS) competition that held at Maker Faire Kansas City, set a modification budget cap at $500 for each electric ride-on car and excluding safety components such as braking systems. The car teams would either used existing ride-on-car bodies as the base frame or fabricated new custom frames to accommodate the motors, batteries and steering systems. Before competing, all vehicles were required to pass a brake test to ensure participant's safety. The event had also highlighted various mechanical and electrical issues encountered during endurance racing, including wheel detachment, motor failure, overheating and chain missing issue, requiring teams to perform rapid on-site repairs (Maker Faire Milwaukee, 2025).

Figure 2.1: Power Racing Series 2017 (Maker Faire Milwaukee, 2025).

2.2.1.1 Building electric ride-on-car for PRS from Mindtribe team in 2016

Mindtribe team was one of the car teams that involved in the Power Racing Series (PRS) in year 2016. This team initially bought a Lamborghini Aventador electric ride-on-car that would be modified and took part in the race. The total weight of the factory ride-on-car was about 33 lb and the maximum speed was 3 mph stated by the team. The first step that has been done was to teardown all the original parts from the electric ride-on-car and investigate all the features as shown in Figure 2.2. This allowed the team to segregate the different parts from the car to be analysed such as wheels, body panels, dashboard, steering wheel and so on.

Figure 2.2: Teardown electric ride-on-car's parts (Wu, 2016a).

This car also initially came with a 6V, 7AH battery with a DC motor to drive the rear wheel of the car. Another DC motor was to control the steering wheel at the front. The body panels of the car were made from the ABS plastic which offered high impact resistance and toughness. The whole body was made by a large injection mold with the natural ABS resin. Many of the body parts, rear components and plastic cover were connected by self-tapping screws. The wiring basically was using soldering joint with hot glue on top of it so that the wires would not be loosened (Wu, 2016a).

2.2.1.2 Decision on modification plan

Since the ride-on-car modification were limited by several rules set by the organizer of the PRS, this teams must fulfil the condition in the modification plan. For instance, the battery voltage maximum was 36 V, each team could only use $500 modification budget, braking distance must less than 18 inches from top speed and so on. Within the time constraint, the car teams agree that to purchase a go-kart frame directly instead of design a new one. Then, the team has also setup a Product Requirement Document (PRD) to decide the design require for the mod. Thus, there were 3 small teams divided to separate the task which were drivetrain, braking system, and steering team (Wu, 2016b).

The drivetrain group was responsible for designing the motor mount location, chain drive system, sprocket and axle. The aim of this group was to increase the torque of the motor and focus on the acceleration. Thus, the selected gear ratio for the sprocket was 1:5.5 with 8-15 Nm of theoretical wheel torque. A steel plate was welded on the frame with 4 drilled holes and the 800 W 36 V motor was mounted directly on the plate. The tension of the sprocket could be adjusted by increasing the height of the motor with the washers that tighten with the 4 bolts as shown in Figure 2.3.

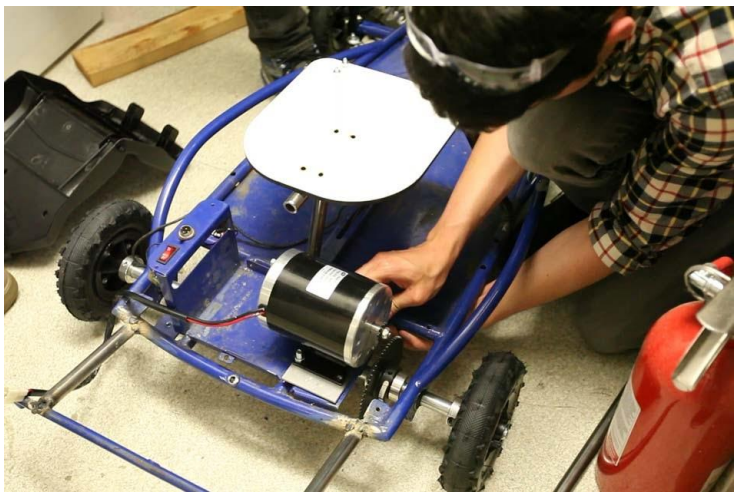

Figure 2.3: Drivetrain installation process (Wu, 2016c).

The braking system team not only responsible to brake, but also for throttle, wiring, battery, motor controller and so on. The group decided to use 3 units of 12 V batteries connected in series with 22 Ah rating to ensure the car could finish the race. In the battery selection, despite the lighter battery would be the best option for the car but the group decided to use lead acid batteries which weigh 20 pounds for each due to budget constraints. The braking system of the car was not upgraded and the belt brake from the go-kart was used back instead. This was because the car could only reach maximum of 12 mph and thus braking system of the car was not necessary to be upgraded.

Lastly, the steering group was to determine the best turning radius, driver posture and weight distribution of the car. Since the car did not have the differential, this group decided to choose the right tires which were 8-inch tires to let the inner wheel to drift during the corner in order to minimize the impact of same speed of the inner wheel and outer wheel during corner. As illustrated in Figure 2.4, the next problem was the tie rods with adjustable steering rods were not long enough to connect the new wheels. Therefore, the group use a trick which was to bend the steering rods slightly to fit to the new wheels (Wu, 2016c).

Figure 2.4: Steering linkage setup (Wu, 2016c).

Figure 2.5: Finished electric ride-on-car setup without car body (Wu, 2016c).

2.2.1.3 Strategy use on the race day

On the race day, the Lamborghini ride-on-car body was zipped tie directly on the go-kart frame as shown in Figure 2.6. Some body part was trimmed in order to fit the plastic body on the go kart frame to avoid the tire hitting the car body. With the driver, the total weight of the car was 260 lbs and reach the top speed of 12 mph under 8 seconds. The next strategy used was using a button to switch on and off of the car's electric system to preserve the battery power.

Figure 2.6: Modded Lamborghini ride-on-car (Wu, 2016d).

During the race, several technical issues faced by the teams such as tires wear, where the tires deteriorated rapidly during the halfway of the race, eventually becoming flattened. Thus, a temporary solution was to wrap the electrical tape around the tire and the race remained only very less time when the car back on track. The car motor start to smoke during the very last phase of the race due to motor overheat problem. However, the teams managed to bring the motor temperature down by blowing the cool air by leaf blower and a bag of ice. In the same race, there were some of the teams could not finished the race due the motor had burned out.

In summary, the race held by the PRS allow the car teams to exchange skills of modifying their karts after the race among different teams. For example, the people discussed about airflow design of the motor in the car to mitigate overheating issue. Participants also shared their respective insights on battery selection and methods of reducing overall vehicle weight in the event. In short, the race did not need require the best engineering knowledge and skill to build the car and win. This PRS race was for every skill level as some cars has proper design with full research, engineering skills and testing and some only for fun as well as enjoyment (Wu, 2016d).

2.2.1.4 Electric ride-on-cars' battery, motor and gearbox modification selection

Upgrading the battery in electric ride-on-car was the most common modification method to enhance the speed of the car. Every type of battery has its own properties with respect to the current discharge rate. In ride-on-car batteries upgrade, the most common batteries being used were sealed lead acid (SLA) and lithium batteries. For lithium batteries, the popular way was using the battery from the power tools. This type of battery generally gave faster discharge rate up to 5 times higher than seal lead acid batteries. However, if the dc motors and gears were not strong enough to cater the load, the motors could become overheated and the gears would be stripped easily. Due to safety reason, there were many users would choose SLA compared to lithium battery.

When upgrading the batteries, the voltage rating and amp rating were also important besides the type of batteries. ML Toys offered the batteries for 12 V, 18 V and 24 V with 12 Ah. The offered batteries were also having the 30% higher running times than the normal batteries. Then, higher voltage of the batteries would increase the motor speed directly. When choosing the batteries, it was also necessary to upgrade the fuse size as the factory fuse would be break easily when the batteries were upgraded with higher voltage and ampere (*"How to Start",* n.d).

Furthermore, there were also many types of motors for modifying a ride-on-car in the market. Different motors have respective voltage ratings, but there was also a common type of method to upgrade a ride-on-car which was to overvolt the factory DC motor. For example, a stock 550 dc motor was rated for 12 V, yet users often powered it with 18 V. The user has to take the risk of blowing the motors even though this method would enhance the motors' performance. Alternatively, an upgraded 550 DC motor was also available in the market which was rated for 18 V with 10% to 15% higher speed than the factory 550 motor. This upgraded 550 motor has also included the built-in cooling fan in the motor casing which the factory motor did not include. This would help to improve the heat dissipation of the motor as well as reliability.

Moreover, there was also a motor which larger than 550 motor was called 775 motors as shown in Figure 2.7. The larger motor tends to provide more torque than the smaller motor but it required higher voltage supply. When install a higher voltage rating and a large motor like 775 series motor, an aluminium motor mount was needed to secure the motor firmly, as the torque output could twist or damage the gearbox casing during operation. Despite the internal built-in cooling fan was already available for upgraded motor, the external heat sink has also been used to cool the motor and prolong the lifespan of the motor. Not only these, but an upgraded motor was also equipped with single or double ball bearings at each end of the motor casing to achieve higher speed and smooth operation.

When the motor has been upgraded, the gearbox of the electric ride-on-car would become one of the limiting factors in achieving higher speeds. As described earlier, the gear could be stripped due to the high instantaneous current of the lithium batteries. The same consequence would also happen in the gearbox where a high torque motor could break the gears easily if the gear material was not strong enough to sustain the motor output torque.

Conventionally, the electric ride-on-car was using steel pinion gear for motor but relied on plastic gears for the remaining gears. The first gear was generally the weakest gear in the gearbox of ride-on-car. To address this, the first gear could be replaced with a hardened steel version as illustrated in Figure 2.7, which not only increased strength but also reduced rotational friction as it was fitted with a ball bearing for smoother spinning operation. Beyond strengthening the material, the hardened steel pinion gear could also be installed with different numbers of teeth to alter the gearbox ratio (*"Staged Motor"*, n.d).

Figure 2.7: 775 motor with hardened steel first gear (*"Staged Motor"*, n.d).

In addition, there were also more extreme modification method of motor gearbox. For example, 2 units of 775 motor like Figure 2.8 could be installed on a same gearbox to run dual motor setup with aluminium mounting plate on the gearbox. This type of mod generally required first gear delete and provide higher top speed for the wheel. However, this type of modification method was not suitable for long run purpose as dual motor would draw more amps than single motor. For the aluminium mounting plate, the installation was not direct fit to the gearbox casing and it required trimming some material on the gearbox casing for mounting the plate on it by few screws. This plate also allowed wide range of number of pinion gear teeth adjustments from 10T to 21T (*"7R First Gear"*, n.d).

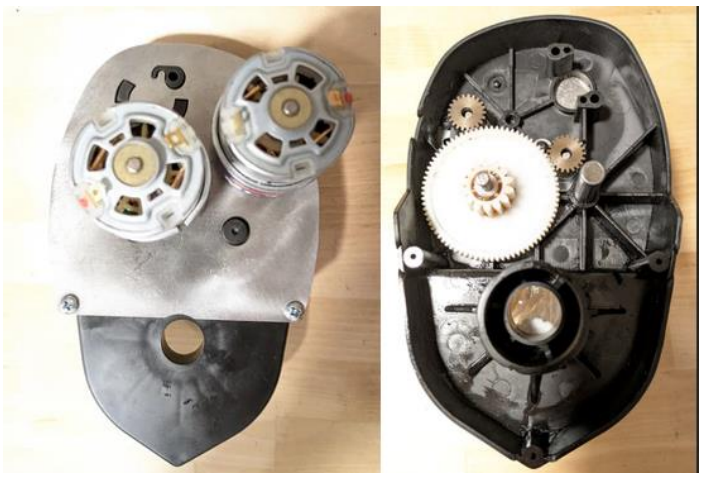

Figure 2.8: Dual 775 motor-gearbox setup with first gear delete (*"7R First Gear"*, n.d).

2.2.2 Electric ride-on-car in drags racing competition

Another type of racing competition for electric ride-on-car was the drag racing competition which the car competed on a straight track by using minimum amount of time. According to the race event held in Mount Vernon in year 2022, a drag racing competition was organized for the children from age of 3 to 9 years old with the race title of "The Central Ohio Power Wheels Drag Racing Series". The racetrack was setup with 60 foots long for 3 different classes of ride-on-car such as 24 V modified car, 12 V modified car and 12 V stock car categories ("Central Ohio Power", 2022).

In 24 V modified car class, the ride-on-car could be modified in terms of motor, gearbox, battery and other part of the car could also be modified. However, the rules stated that the wheelie bars, seat belt and helmet were required for the car for safety reason. However, the 12 V modified car class was only limited to modify the gears, motor and change their original tire to rubber tire or add rubber strip on it to improve traction. Lastly, only car paint and decals were permitted for 12 V stock class ("Power Wheels Racing", 2019).

In addition, the top speed of 12 V stock ride-on-cars was typically around 6 mph, but modified versions prepared for drag racing could reach the speeds up to 30 mph. As the car speed start to increase, the slick wheel usually required to add traction. For a modified 24 V powertrain drag series ride-on-car, the car could easily hit 18 mph on a 60 foots racetrack. For the battery modification, usually the car was installed with bigger power of battery and connect together with drill batteries. Not only these, but the car also equipped with golf cart solenoid that act like a relay to control large current and with first gear delete. In the drag race like Figure 2.9, there were few popular modified ride-on-car models participated for drag racing competition included Corvettes, Lamborghinis, and Ford Mustangs (Bellwood, 2024).

Figure 2.9: Ride-on-car drag race competition (Bellwood, 2024).

2.2.3 Electrathon competition

Electrathon racing is another type of competition that using 3 or 4 wheeled electric race vehicles with concept is similar to go-karting. One of the rules set by the organizer is the vehicle size only limited to 12 feet long and 4 feet wide. The battery weight is capped at 73 lbs, and only lead-acid batteries are allowed. Most importantly, the safety regulation also required the vehicle has braking system, roll bars and electric disconnect mechanism. Next, electrathon racing is a relatively low cost competition and has successfully attracted many participants from high school students, college students and technical school students. This competition provided opportunities for students to explore the subjects like AutoCAD, power electronics, aerodynamics, structural analysis and so on (Electrathon, n.d.).

In the East Central High school, there is an electrathon racing club that compete with the high schools and college in the race. 15 engineering students had built 4 electrathon vehicles from scrap metal and able to reach 40 mph. This club was following the mission of a local club which was called electrathon America. This local club was offering the STEM (Science, Technology, Engineering and Mathematic) educational hands-on learning. The car that builds from this group of students also participated in the Alamo City Electrathon Race, a competition designed to evaluate the energy efficiency of student-built vehicles. The winner was the car that able completes the most laps within the time and batteries capacities. Finally, this team won the race with 125 laps in 2 hours and this shown that the race emphasized more on endurance rather than speed.

The reflection from the students involved in this electrathon race shows that they had learn wide range of skills via this project in their high school. One student, for example, dedicated much of their free time to learn how to use a welding machine and an angle grinder to construct the car chassis. Another student also learnt about how to create the wiring system for the car, batteries testing and the electric component mounting location. The student who in-charge in batteries testing also learnt the technique to pre-heat the batteries to maximise the energy absorption of the batteries. These was how the students get fun during the process (Moore, 2024).

Figure 2.10: Fabrication process of the electrathon race car (Moore, 2024).

Figure 2.11: Preparation before electrathon endurance race (Moore, 2024).

2.3 Type of powertrain configuration

The powertrain is an essential subassembly for a vehicle to allow the power from the electric motor to be delivered to the wheel of the car. The configuration and design of the powertrain would determine the efficiency of the car in terms of transmission system, number of motors, type of motor, driveshaft configuration, number of wheels to be driven and so on. Table 2.1 describes the different types of powertrain configurations used in the race car.

Table 2.1: Different types of powertrain configuration in race car design (Badal, 2019).

Powertrain configuration		Explanation on the design
Single motor, rear wheel drive	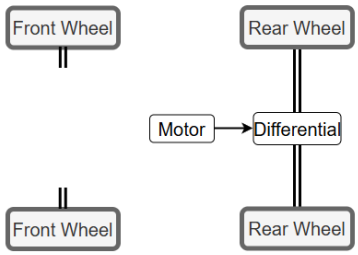	The motor is placed in middle of the car and drive a transmission with differential at the rear and send power to the wheel through two cv joint.
Single motor, front wheel drive	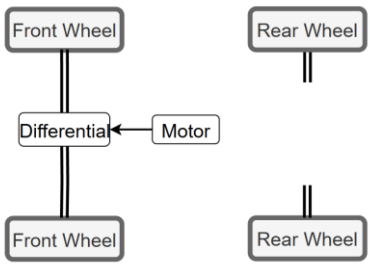	Similar to concept 1 but the transmission is placed in front of the car.
Single motor, all-wheel drive	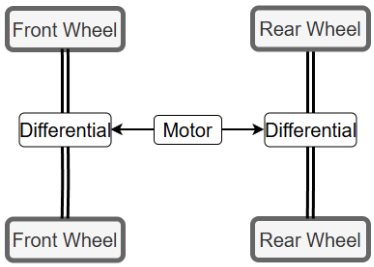	Two gearboxes are driven by single motor, this design allowed different traction to be allocated for front and rear side.
Dual motor, independent wheel drive (FRID EV)	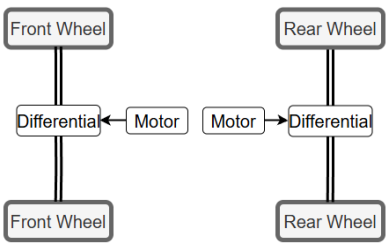	This design included to individual motor-gearbox system which can control the wheel from both sides

Dual motor, rear wheel drive	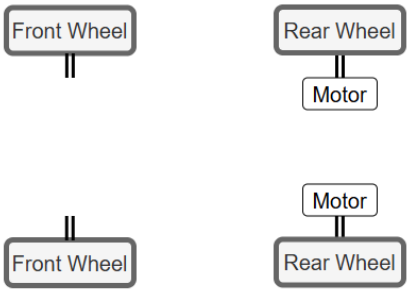	The motor is driving directly to the rear wheel and two independent motors allowed different rotational speed at both rear wheel
Dual motor, front wheel drive	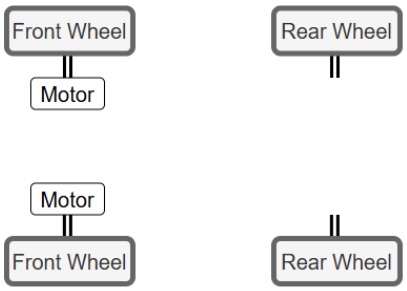	This is a similar concept with design above, but dual motor setup was attached to the front wheel hub of the car.
Three motor, front single motor, rear dual independent motor	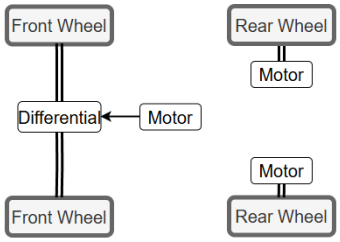	A motor in the front of the car used to drive both of the front wheel with gearbox and rear side included dual independent direct drive motor.
Three motor, rear single motor, front dual independent motor	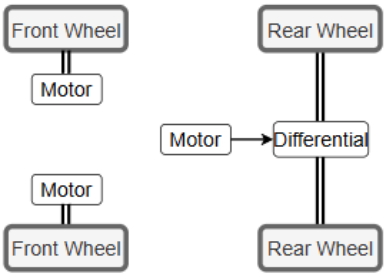	This configuration is the inverse setup from the idea above and dual motor at the front may help to save some spaces at the front of the car.
Four motor, all-wheel drive	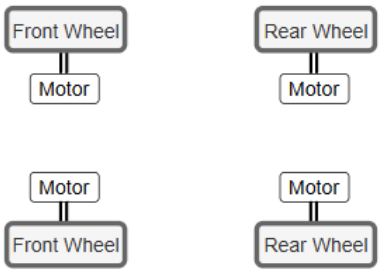	Four motors are attached to individual wheel hub and this setup can help the car to able to have different traction at individual wheel.

2.4 Electric system design for EV

The design of the electric system of the EV was essential as it directly influence the energy efficiency from the battery down to the wheel. For instance, the energy that could be recovered during the race was important as it determined the efficiency the electric motor. As shown in Figure 2.12, the electricity is first supplied from the battery and then flow to the inverter. The inverter's function is to convert direct current (DC) into alternating current (AC) which was required to drive the AC electric motor. This allowed the motor to drive the transmission system of the EV. Although energy losses within the electrical system are inevitable, a well-designed system could minimize these inefficiencies.

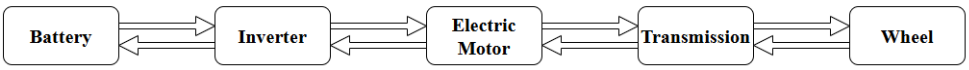

Figure 2.12: Electric conversion system in electric vehicle (Badal, 2019).

For a motor that used to be tested in this study was an AC synchronous motor with the product code of AMK DT7-75-20-XXW-3500 MOTOR and it produced the Torque speed graph in relation with the motor output speed in rpm was illustrated in Figure 2.13.

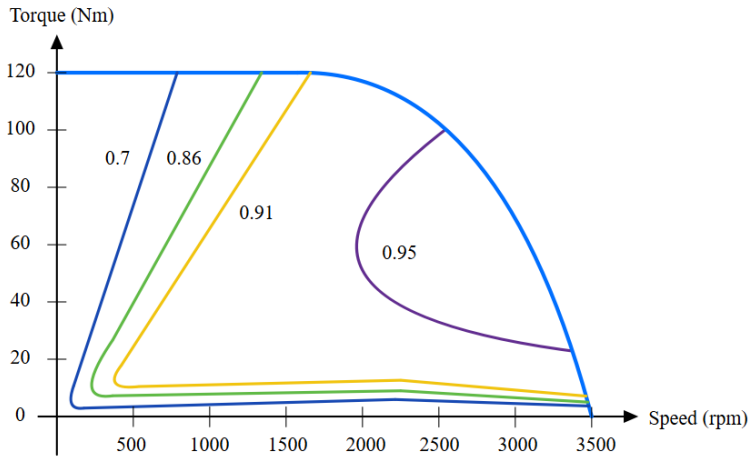

Figure 2.13: Torque speed behaviour of the AC synchronous motor (Badal, 2019).

When the motor speed increased, the output torque of the motor would be decreased due to the losses occur in the motor structure. When the motor speed increase, there were 2 typical main losses happened in a motor which were winding loss and iron loss. Winding loss happened when the current flow through the winding of the motor that made with enamel copper wire. This loss was also equal to the power loss in copper wire and this research was studying the 3 phases losses for this type of motor. Therefore, the amount of losses could be calculated by using the formula as shown below,

$$P_{cu} = I^2R \tag{2.1}$$

$$I = T \times k_t \tag{2.2}$$

where

- P_{cu} - power loss in winding
- R- winding resistance
- I- current flow to the coil
- T- torque output
- k_t- torque constant

On the other hand, the iron loss produced when the iron core of the rotor induced the magnetic field, and this loss was the sum of the hysteresis loss and eddy current loss. From the graph shown in above, the torque of the motor start to decrease as approaching the rated speed of 3000 rpm with small iron losses which are the 0.5% and 1% of the motor rated power for the hysteresis and eddy current loss respectively. These also showed that when the motor was working in the non-efficiency region like 0.7 efficiency, the losses would be higher compared to 0.95 efficiency region (Badal, 2019).

2.5 Different types of Electric Motor used for Electric Vehicle (EV)

Electric motor was a core component of the electric vehicle as it was used to propel the car. In many cases, electric motors were designed with the components that could handle harsh driving environments with different temperature, different humidity and high level of duty cycles. There were two main components used for the electric motor, the rotating component was called rotor or armature and the stationary component was known as stator. There were two types of energy used for the electrical motor which were called alternating current (AC) and direct Current (DC). These energy sources were used to generate the electromagnetic field that produced the same effect as the permanent magnet with different polarity.

Firstly, the DC electric motors which consist of two types of configurations which were brushed and brushless (BL). DC motors typically exhibited the characteristic of providing high output torque at low motor speeds. The DC motor could be just using permanent magnet (PM) to create the magnetic field at the stator side and did not require a separate excitation source. If the separate excitation was required, the rotor winding was connected in series with the coil on the stator side, this was known as series DC motor. The rotor or armature of the DC motor is made with multiple slots that were used for the copper windings.

On the other hand, another type of electric motor that consumed AC energy source which was called induction motor. This motor generally consists of 3 sets of winding on the stator side which generated magnetic field to react with the squirrel-cage rotor. This rotor was typically made from aluminium bar that arrange in close loop and short circuit design. Unlike DC motor, the induction motors' rotor did not require commutator and brush components and hence this reduced maintenance cost. Not only these, but the induction motors also have high efficiency at high speed and low torque range as the copper losses reduced when the speed increased.

Another electric motor that is widely used in EVs was the permanent magnet synchronous motor (PMSM) that was using three-phase AC windings on the stator side. The PM would then mount on the rotor side. Permanent magnets typically were rare-earth neodymium magnets (NdFeB) due to its high performance and it were mounted on the rotor side. This configuration

eliminated the need for brushes which further improve the durability and efficiency.

Lastly, a motor that was similar to the PMSM was called reluctance motors (RM) but it used the salient poles of magnetic flied on the stator and rotor side. The rotor was constructed with laminated silicon steel with multiple stacks. This type of motor was also using AC supply and the motor was controlled by switching the multiple of phase winding in the mode of 2 switches per phase on the stator. This was also meaning a pair of winding (phase) was excited based on position of the rotor when the 2 switches were triggered (Aarniovuori, Cao, Shah Bukhari, 2018).

2.6 Brushed DC Motor

DC motor, which was the motor that designed for running direct current (DC) input voltage and converting electrical energy to mechanical energy. It could also work in the opposite way by turning mechanical energy into electrical energy. This was working like a generator which produce electricity to recharge the source like battery. This two way operation of dc motor was widely used in the electrical vehicle to provide traction and magnetic braking while recharging the battery. DC motors also consist of two type of design which included brushed or without brushed. For a permanent magnet brush dc motor basically consist of 2 parts, the rotating part was called armature while the stationary part that provide constant magnetic field was called stator. For the brushed dc motor was used numerous turns of coil or windings in an armature with commutator ring so that the current could be passed into the coil and produce magnetic field to turn the coil. When carbon brushes contacted with the commutator that was spinning, the spark would be generated as short circuit between two split ring surfaces. Figure 2.14 shown in below illustrates the general construction of the DC motor that work with permanent magnet.

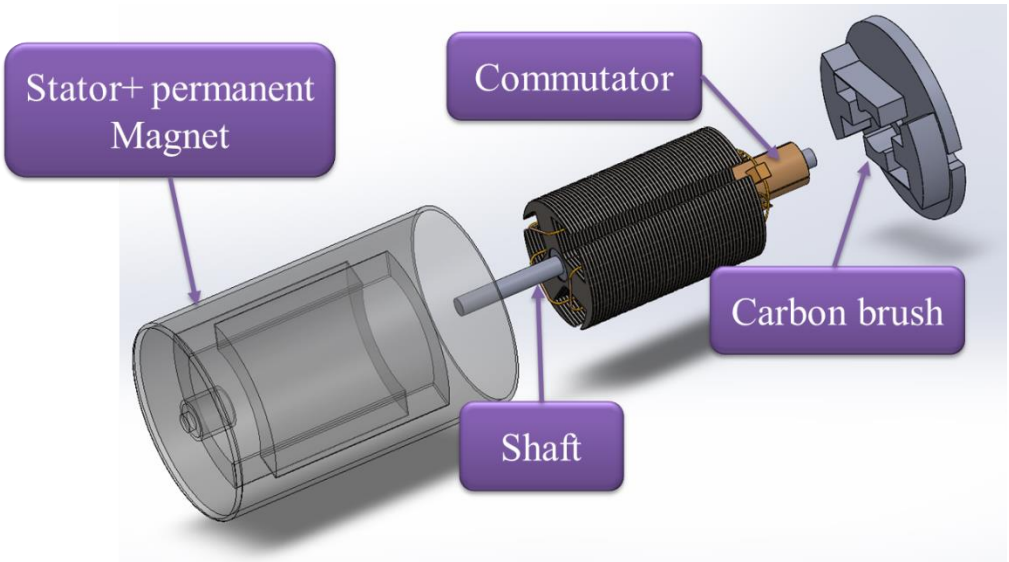

Figure 2.14: DC motor internal design (Mohammed Salah, 2009).

2.6.1 DC motor working principle

Figure 2.15 below shown the typical working principle of DC motor with single-turn coil. When the current carrying conductor passing through the constant magnetic field B, both sides of the coil generate the rotating torque of the motor T_m and it could be obtained by multiply the force F with distance from the shaft to the coil, r.

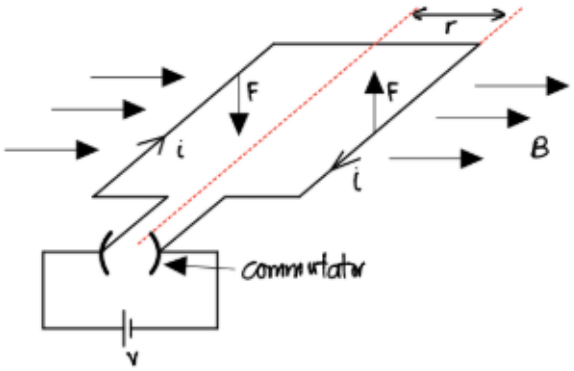

Figure 2.15: Force exerted on single coil when current passing through the coil (Mohammed Salah, 2009).

By using the reality dc motor, the number of turns could be varied depends on the requirement, this was also meaning that the motor torque T could be calculated by using the following equation,

The motor torque for single turn coil initially was given by,

$$T_m = 2Fr \tag{2.3}$$

Then, for the force generated by the current carrying conductor,

$$F = BIL \tag{2.4}$$

where

B – magnetic field exerted to the coil

I – current applied to the conductor

L – length of the conductor that crossing the magnetic field

Thus, the motor torque becomes

$$T_m = 2N(BIL)r \tag{2.5}$$

Let,

$$k_t = 2NBLr \tag{2.6}$$

Then,

$$T_m = k_t I \tag{2.7}$$

where

$k_t -$ torque constant

$N -$ number of turns of the conductor.

Next, when the current was applied to the coil, there was one parameter would produce at the coil cross section surface and perpendicular to it as shown in Figure 2.16 was called the magnetic flux Φ and the formula was given by,

$$\emptyset = BL2rcos\theta_m \tag{2.8}$$

Where θ_m was the angle of the rotating coil between the normal line to the magnetic field B. Then, for the magnetic flux linkage λ,

$$\lambda = N\emptyset = NBL2rcos\theta_m \tag{2.9}$$

According to Faraday's law, if the coil that rotate in the magnetic field, it would generate opposite EMF and it would depend on the magnetic flux linkage and varies with time which yield the equation as shown below,

$$EMF, e = -\frac{d\lambda}{dt} \tag{2.10}$$

Since the angle θ_m was also the angle travelled by the coil, the angular speed of the coil, ω_m could be obtained as shown in below,

$$\omega_m = \frac{\theta_m}{t} \tag{2.11}$$

$$\lambda = NBL2rcos(\omega_m t) \tag{2.12}$$

$$\frac{d\lambda}{dt} = -\omega_m NBL2r[sin(\omega_m t)] \tag{2.13}$$

Then, the back emf become,

$$e = \omega_m NBL2r[sin(\omega_m t)] \tag{2.14}$$

When angle $\theta_m = 90°$, the coil provided maximum back emf as $\sin(90°) = 1$.

$$e = \omega_m NBL2r \tag{2.15}$$

$$e = k_b \omega_m \tag{2.16}$$

where

k_b – back emf constant

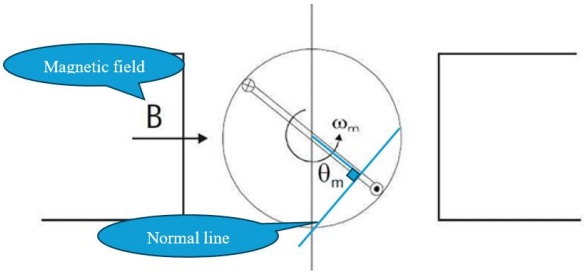

Figure 2.16: Illustration of angle between magnetic field and normal line (Mohammed Salah, 2009).

2.6.2 Dynamic braking or reverse current braking of DC motor

Dynamic braking was one of the techniques that utilised electrical energy to stop the rotation of the motor which similar to the mechanical brake, but the electrical energy was used instead. So, the general unit used for energy was the product of force and distance, measuring in Joules, J. Another term that usually used to describe the mechanical power was called the horsepower which equal to 550 ft.lbs/sec. For electrical power, watts were typically used as the standard unit. Through this statement, the following paragraph will discuss the electrical circuit for dynamic braking effect of the DC motor (DeLuca, C., 2020).

According to a previous study, rotating torque that was generated at the wheels of the car and formed the traction motion. In contrast, the opposite torque or counter torque created by the motor will be the braking torque to decelerate the vehicle from certain speed. When the dynamic braking was triggered, the DC motor that connected with the parallel resistor allowed the motor generate braking force when the applied voltage was removed. The energy of the DC motor would be dissipated via the resistor and the DC motor would work as a generator. This was meaning also some energy was wasted and some energy would be recharged back to the source. Consequently, the value of additional resistor, R_{add} need to be considered wisely.

The relationship of braking torque was proportional to the current flow through the motor coil and smaller value of R_{add} allowed more current to flow and hence generated more braking torque to stop the load. The braking design therefore needed to account for the load to be stopped within the shortest possible time. When the dynamic braking was applied, the back emf, E_a of armature of DC motor would be generated and hence the armature current would also be produced as described in the equation (2.17) and (2.18) shown below. The negative sign come from the back emf of rotating coil.

$$I_a = \frac{-E_a}{R_a + R_{add}} \tag{2.17}$$

The braking torque will be,

$$T = k_t \emptyset I_a \tag{2.18}$$

In addition, another braking method that provided the same result as the dynamic braking to stop the DC motor with the additional resistor R_{add} was reverse current braking method. However, reversing current braking was the method that applied input voltage to DC motor with opposite direction when this braking was needed, and the motor was still rotating in the default direction. This result in addition of input voltage to armature V_a with the back emf of armature E_a like the explanation in previous paragraph. Thus, the overall current in the armature would be greater than dynamic breaking method as this method provides higher braking torque than dynamic breaking method from the DC motor. Thus, the relationship between armature current to the braking torque of the DC motor as shown in the following step.

$$I_a = \frac{-(E_a + V_a)}{R_a + R_{add}} \tag{2.19}$$

$$T \propto I_a \tag{2.20}$$

Lastly, the study also done the simulation that compared the braking method in DC motor. The rotational speed of motor ω_m between 450 to 500 rad/s was simulated for a period of 10 s in simulations in order to able the motor run in constant speed. Then, the respective braking method were implemented to the same DC motor. The results shown that the dynamic braking method wasted lesser power during braking (14000 W) compared to reverse current braking (25000 W). This could also be explained by the equation above where this reverse current method yields higher armature current than dynamic braking method (Serteller, and Ustundag, 2017).

2.7 Vehicle dynamics in tractive force and braking force

When a car parked on horizontal flat road, there are two normal forces acting at both left and right tires at the front and rear respectively. A car with 2 symmetric axles where 1 axle is connected to a pair of tires, it is equivalent to a rigid beam with two supports. The horizontal distance from each of the axle to the centre of gravity of the car will be represented by a_1 and a_2 as shown in Figure 2.17.

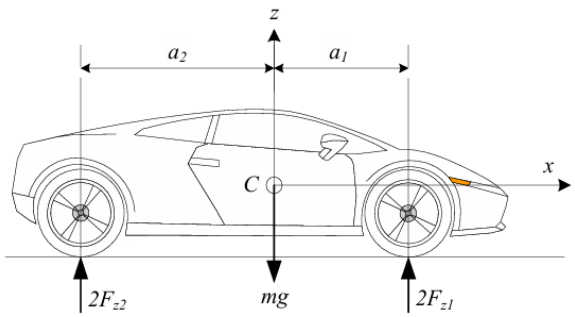

Figure 2.17: Parked car with horizontal road (Jazar, 2008).

Thus, if the y-axis is pointing out of the page and the normal forces acting on the tires under static equilibrium condition can be represented by,

$$\sum F_z = 0 \tag{2.21}$$

$$\sum M_y = 0 \tag{2.22}$$

Then,

$$F_{z1} = \frac{1}{2} mg \left(\frac{a_2}{l}\right) \tag{2.23}$$

$$F_{z2} = \frac{1}{2} mg \left(\frac{a_1}{l}\right) \tag{2.24}$$

$$l = a_1 + a_2 \tag{2.25}$$

On the other hand, the braking force applied from the 4-wheels needed when the vehicle is on an incline road as shown in Figure 2.18 is given by,

$$2F_{x1} + 2F_{x2} = mgsin\emptyset \quad (2.26)$$

$$2F_{z1} + 2F_{z2} = mgcos\emptyset \quad (2.27)$$

In static condition, the maximum angle $\emptyset_M$ of inclination occur and the car start to slide down, and the braking force for 4-wheels can be written as,

$$F_{x1} = \mu_{x1}F_{z1} \quad (2.28)$$

$$F_{x2} = \mu_{x2}F_{z2} \quad (2.29)$$

Where, the μ_{x1} and μ_{x2} represented the coefficient of friction of the tire. Then the equation of equilibrium will become,

$$\mu_{x1}F_{z1} + 2\mu_{x2}F_{z2} = mgsin\emptyset_M \quad (2.30)$$

$$2F_{z1} + 2F_{z2} = mgcos\emptyset_M \quad (2.31)$$

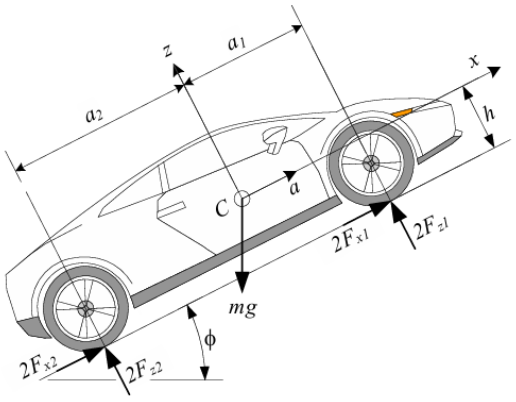

Figure 2.18: 4-wheel braking force under incline angle (Jazar, 2008).

When the car is accelerating on the horizontal road, the horizontal will no longer be equilibrium and newton second law is applied as shown in the Figure 2.19. The three equations, only for the forces acting in vertical direction and moment of y-axis are equal to zero.

$$\sum F_x = ma \quad (2.32)$$

$$\sum F_z = 0 \quad (2.33)$$

$$\sum M_y = 0 \tag{2.34}$$

Hence, the traction force F_x for both wheels will be,

$$2F_{x1} + 2F_{x2} = ma \tag{2.35}$$

$$2F_{z1} + 2F_{z2} = mg \tag{2.36}$$

The newton second law equation can be replaced by substituting the friction coefficient equation into this equation. Thus,

$$2\mu_{x1}F_{z1} + 2\mu_{x2}F_{z2} = ma \tag{2.37}$$

Assume all tire has the same friction coefficient of μ_{x1} and μ_{x2}

$$2\mu_x(F_{z1} + F_{z2}) = ma \tag{2.38}$$

The acceleration, a of a vehicle can be positive or negative sign depending on the car is accelerating or decelerating. By inserting the equation $2F_{z1} + 2F_{z2} = mg$ into newton second law equation. It yields the result,

$$\pm\mu_x g = a \tag{2.39}$$

These showed that the required braking force will depend on the acceleration of the car tire friction coefficient.

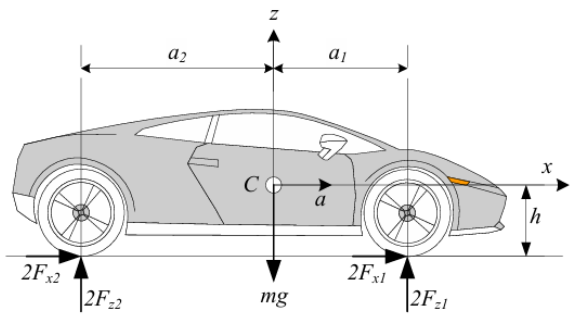

Figure 2.19: Acceleration of the car on horizontal road (Jazar, 2008).

2.8 Importance of bearing in friction reduction and its effect in different real-life applications

Ball bearings played a crucial role in reducing friction between parts that move relative to each other by converting the sliding friction to rolling friction. When two surfaces slide across each other, the friction was substantially higher because of large contact areas of resisting motion. In contrast, ball bearings used steel balls between two races which consist of inner and outer rings. This dramatically lowered the resistance, reducing heat and wear. Ball bearing has also been used in different high-precision components such as watches, rotating shafts in machinery and skateboard wheels with different coefficient of friction. Precision machining of the bearing races and balls was very crucial with smooth and polished surfaces. This would further reduced frictional torque and improved performance. Lubrication like oil or grease was also vital as it maintains the oil film between contact points, preventing metal-to-metal contact so that the bearing could be operated smoothly.

Furthermore, bearing efficiency was not just reducing friction, it also translated directly into better mechanical efficiency, less energy losses, lower operational temperatures, quieter operation and prolong equipment lifespan. In automotive applications, bearings were considered critical components in wheels, steering columns, drivetrain assemblies and engine systems. Ball bearings not only assist in improve fuel efficiency and reduced emissions. This bearing also provided smoother motion over rough terrain and help absorb or transmit loads while maintaining rotational stability. In industry such and food and beverage and power plant industry, ball bearings are ubiquitous as they were used wherever there was rotational or linear motion needed such as electric motor, generator, conveyor system and so on (SLS, 2020).

2.8.1 Types of bearing used in vehicle and its internal friction

The type of bearing usually used in vehicle were ball bearing and taper roller bearing as shown in Figure 2.20. The former type of bearing is designed for working in high rotating speed condition and the latter is usually used for high load application. However, there was still some torque friction occur in the bearing when the ball is sliding against its bearing housing. The torque friction was the resistance created by bearing rolling resistance and seal sliding resistance of the rotating bearing (Yokota, 2020).

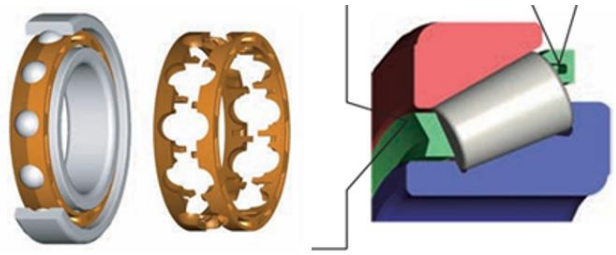

Figure 2.20: Ball bearing and tapered bearing assembly (Yokota, 2020).

Moreover, an efficient bearing design not only decrease the torque loss and increase the axial load capacity, but the oil agitation problem would also be minimised, and the lifespan of the bearing would be prolonged indirectly. The latest model of the ball bearing developed by the JTEKT company with new expansion raceway design was to increase the amount of oil available in the ball bearing' ball. Consequently, this design significantly reduced the torque loss of the rotating part with high axial load by 48% compared to the conventional deep groove ball bearing. These showed that the bearing type was important part for the rotating part of the vehicle (Yokota, 2020).

2.8.2 The effect of rotational speed of the bearing

According to the researcher of deep grove ball bearing test with various rotational speed, the lifespan of bearing tends to be determined by the oil thickness between the raceway and the ball surface. The experiment has been done by this researcher by using the rotational speed of 1910, 3820, 5250, 7640, 11500, 14870, 18750 and 20190 with the unit of per min, min^{-1}. The relationship between the speed and the oil thickness in inversely proportional to each other for certain range of speed. When the speed start increasing to 2000 min^{-1}, the amount of air bubbles starts to form inside the bearing. Then, the amount of oil thickness present on the rolling ball of the bearing decreased when the rotating speed increased. When the speed start exceeding about 7700 min^{-1}, the oil film thickness has become constant and this has resulted in the oil starvation problem which can increase the wear at the interface of the rolling ball and the raceway (Hideaki, et al., 2024).

2.9 Type of car's chassis and material properties of ABS and PP

Automotive chassis refers to the structural framework of a car and it holds everything including the engine and transmission, the suspension, steering mechanism and often the body panels. Different chassis types vary in strength, weight, rigidity, manufacturing complexity and suitability for different types of cars. The were total of four main types of chassis which included ladder frame, backbone, monocoque and tubular chassis.

The ladder frame chassis was the earliest type of chassis and most fundamental structural designs in the automotive industry. Constructed from two longitudinal beams connected by multiple smaller lateral beams, it resembles the form of a ladder. Its inherent strength makes it highly suitable for vehicles designed to transport heavy loads such as trucks, buses, commercial vehicles and off-road vehicles. However, the design was limited in its ability to resist torsional stresses, which results in reduced handling performance and agility. Consequently, due to its relatively high weight, this design was not suitable for hatchback and performance cars.

The backbone chassis employs a central structural of rectangular cross-section and cylindrical tube, running the length of the vehicle to connect the front and rear suspension assemblies. This cylindrical tube at the central of the bone also enclose the driveshaft, protecting it from damage when the vehicle used for off-road driving. The backbone design offered superior torsional toughness compared to ladder frames and able to absorb more impact energy. However, it introduced challenges such as complex servicing requirements as all the components had to be disassembled if repair works was needed on drivetrain assembly.

The monocoque, unibody chassis and it was called "single shell" in French. This chassis had been integrated the structural frame and body into a single cohesive shell. In this configuration, the crumple zone has been integrated into the chassis to absorb and distribute mechanical stresses, eliminating the need for a separate supporting frame. This integrated cage design had enhanced the torsional rigidity, improved agility and reduced overall weight. Monocoque construction dominates modern passenger cars, including sedans, hatchbacks and most electric vehicles due to its balance in efficiency, safety and performance. However, it requires significant capital

investment for small-batch production and structural damage can be costly to repair.

The tubular or space frame chassis was an advanced three-dimensional framework composed of interconnected steel or alloy tubes, often arranged in triangulated formations to maximize rigidity. This geometry provides excellent torsional stiffness and strength while minimizing weight, making it highly advantageous for racing, performance vehicles and off-road applications where agility and safety are paramount. Despite this design has many benefits, the tubular chassis still presented challenges in terms of design complexity, high production costs and not suitable for mass production. It is most often employed in niche or racing contexts such as lightweight high performance cars and specialized off-road vehicles (Sharma, 2025).

2.9.1 Ride-on-car chassis

The Bentley JE1008-CEN Apocaday ride-on car's plastic body structure acts as a single integral shell and could be considered a simplified monocoques chassis design without the car roof (tub design) Figure 2.21 and Figure 2.22. According to its parts list, the "vehicle body" was identified as a core component in part number 1 and attached by others significant components such as the axles, wheels, steering assembly, powertrain and suspension directly onto this molded body shell. There was no separate internal subframe or structural components within the body, indicating that the plastic body itself was engineered to carry load and transmit structural forces. This design approach simplifies assembly by integrating the chassis and frame.

Because the vehicle body serves as the structural tub chassis, several implications follow for strength, safety, and performance. The body must provide sufficiently rigid mounting points for the steering assembly, motor-gearbox, suspension and other areas that concentrate load and torque. It must also accommodate the battery housing and wiring under the seat, with access for charging and fuse protection integrated into the design. Furthermore, given a maximum user load of 30 kg and speed of 3-5 km/h, indicating that the plastic vehicle body were used to cater the load statically and dynamically

("BENTLEY JE1008-CEN", n.d.). The ride-on-car body could be made from 2 types of materials which included ABS (Wu, 2016a) and PP ("12V Kids Electric", n.d.).

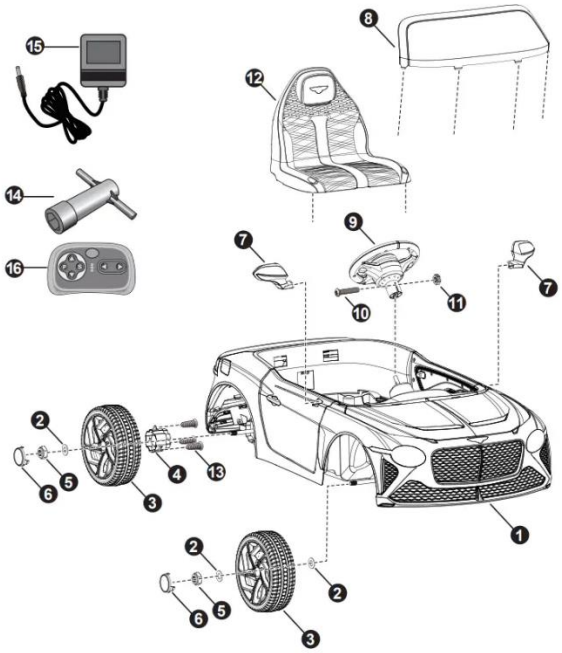

Figure 2.21: Exploded view of Bently ride-on-car ("BENTLEY JE1008-CEN", n.d.).

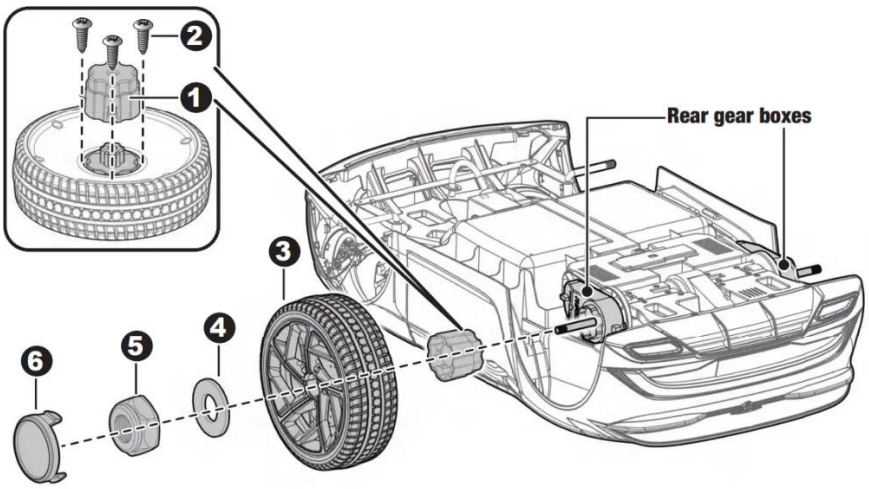

Figure 2.22: Exploded view of Bently ride-on-car with powertrain assembly ("BENTLEY JE1008-CEN", n.d.).

2.9.2 Material properties of the Acrylonitrile butadiene styrene (ABS) with automotive applications

The Acrylonitrile butadiene styrene (ABS) was one of the thermoplastic polymers that consists of excellent mechanical properties and widely used in the automotive industry. One of the advantages of using this plastic was because it could be reheated and reshaped into different forms without significant changes to its material characteristics. ABS was also equipped with high impact resistance, heat resistance, corrosion resistance, toughness, shiny surface and so on. Because of these qualities, it was commonly used in the automotive components such as body kits, interior panels and wheel covers. Figure 2.23 shown an ABS specimen that was used to carry out an experiment for determining its several mechanical properties test such as flexural strength, impact resistance, ultimate tensile strength, yield strength and so on (Mohd. Ali, et al., 2022).

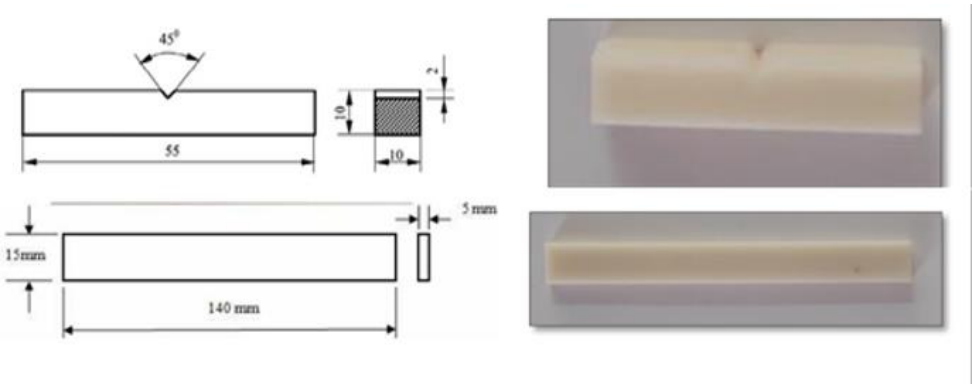

Figure 2.23: Acrylonitrile butadiene styrene (ABS) specimen dimension for impact test (Mohd. Ali, et al., 2022).

The study showed that the ABS specimen with 10 mm thickness could absorb the impact energy of 32 J and impact strength of 3200 J/m^2. A pendulum striker was used to undergo this impact test with 45 degrees striker' angle, the notch was formed by releasing the pendulum at a higher position and hit the specimen until fracture occurred. After the specimen has been tested with several experiments, the experimental data of the material properties were recorded in the Figure 2.24.

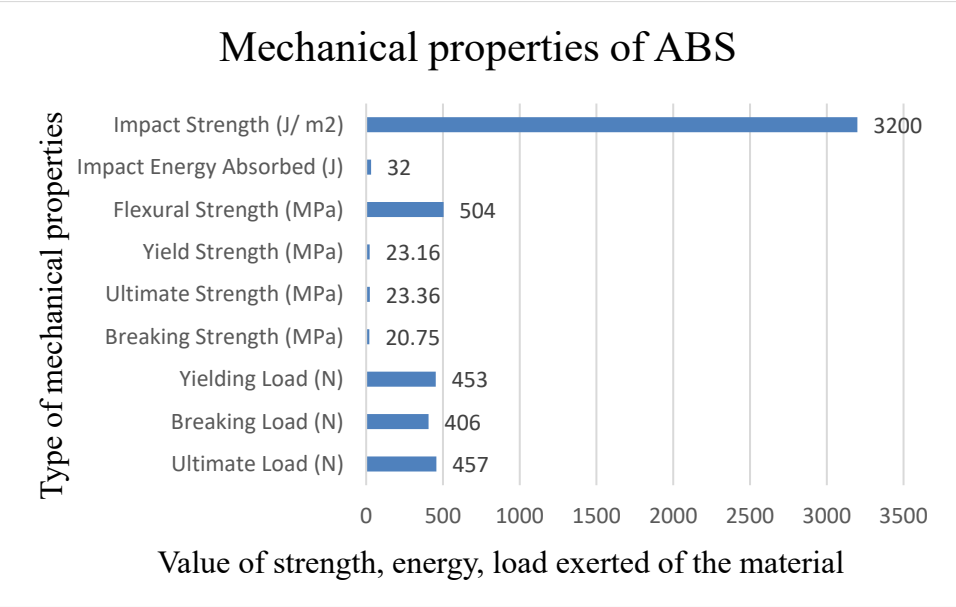

Figure 2.24: ABS material properties of the study (Mohd. Ali, et al.).

2.9.3 Material properties of the Polypropylene Plastic (PP) with automotive applications

Polypropylene (PP) is one of the widely used plastics material for automotive parts, valued for its low cost, excellent moldability, and mechanical properties. According to Sumitomo company, over half of the plastic components in automobiles are made from PP compounds, including bumpers, instrument panels, door trims and other interior and exterior parts. The company reported that in 2007, roughly 3.75 million tons of PP globally (approximate 8% of all PP consumption) and about 690,000 tons domestically (Japan) (with 23% of national PP consumption) were used in automotive manufacturing (Kanzaki, Moritomi and Watanabe, 2010).

The reasons of using PP in automotive parts was not only due to the cost, but also its material properties. Polypropylene (PP) is a linear hydrocarbon polymer valued for its versatility. Some of its key mechanical properties are that it is semi-rigid, tough, has good fatigue resistance, and so on. PP has also higher softening point which is about 160 °C, greater hardness and rigidity, yet a lower density. PP can also be further divided into 2 categories which were homopolymer and copolymer. The data shows that PP's density is about 0.905 g/cm³, tensile strength for homopolymer and copolymer grades is 33 MPa and 25 MPa respectively. PP also maintains good breaking strain of 150 % and 300 % for homopolymer and copolymer respectively. The heat distortion temperatures were around 100-105 MPa/°C for low deformation under load.

The material’s processing and stability attributes are also notable, PP can be easily undergoing injection moulding process as it has low melt viscosity which helps in molding complex and large parts. However, its performance was based on the resin grade, melt flow index, and fillers content. PP also has good chemical resistance and relatively good weatherability when properly stabilized. PP also exhibit poor UV resistance, significant creep under sustained load and can suffer oxidation when contact with copper (Hindle, n.d).

2.10 Summary

In short, the mission of STEM (Science, Technology, Engineering, and Mathematics) has been promoted among children and high school students through several racing competitions such as the Power Racing Series, Power Wheel Drag Race and Electrathon racing. This mission aimed to encourage students to be innovative and creative in modifying electric cars within a set budget. At the same time, it provided them with valuable hands-on experience in vehicle modification. STEM education also trained students in decision-making, such as selecting appropriate batteries, motor power ratings, chassis setups and gear ratios. Moreover, when something broke during a competition, teams were required to work together to address the problem, thereby improving their problem-solving and collaboration skills.

Apart from that, the electric vehicle was composed of several key parts that worked together to enhance its overall efficiency and performance. These included braking power, friction reduction, body materials, weight, motor design, and battery voltage. When modifying a stock ride-on car, these aspects needed to be carefully considered and balanced with design decisions. For instance, battery voltage and the type of motor controller directly affected the motor's power output. Likewise, the drivetrain setup influenced how effectively that power was transmitted to the wheels. Even smaller components, such as deep groove or journal bearings, played a crucial role in reducing friction and supporting the load of the car. Finally, the body of the car had to be strong enough to withstand the extra stress of carrying an adult driver under extreme driving conditions.

CHAPTER 3

METHODOLOGY AND WORK PLAN

3.1 Introduction

The methodology for this project involved total of 8 sections which would be described in the workflow of the project shown in Figure 3.1. The process begins by understanding the project title, followed by extensive research on the different ride-on-car models available in the market and their potential for modification as well as the parts available to modify the car. This initial stage of the project is about the identification of suitable components and modification strategies based on research information in order to achieve the objective.

Once sufficient background research is conducted, the design and simulation of the required parts will be in the next stage. For instance, steering linkages, rear shaft assemblies, suspension system, gear trains, and other reinforcement structures will be created and simulated via SolidWorks to validate their functionality before fabrication. After that, the selected materials and parts are procured, fabricated and installed to the ride-on-car according to the proposed design, ensuring that the modifications are done correctly based on the specification and dimension.

After fabrication, the modified ride-on car undergoes a series of assessments to evaluate its performance. These tests included weight measurement, shaft deflection measurement, drivability assessments, acceleration and power consumption test by using GPS-based applications. The collected data are then analyzed and check whether the vehicle meet the required standards. If not, the methodology allows for iterative improvements through redesign and re-testing. The collected data is to be then systematic documented, data analysis for the weakness of the car. Last step is the report writing, providing insights on the current design for future enhancements.

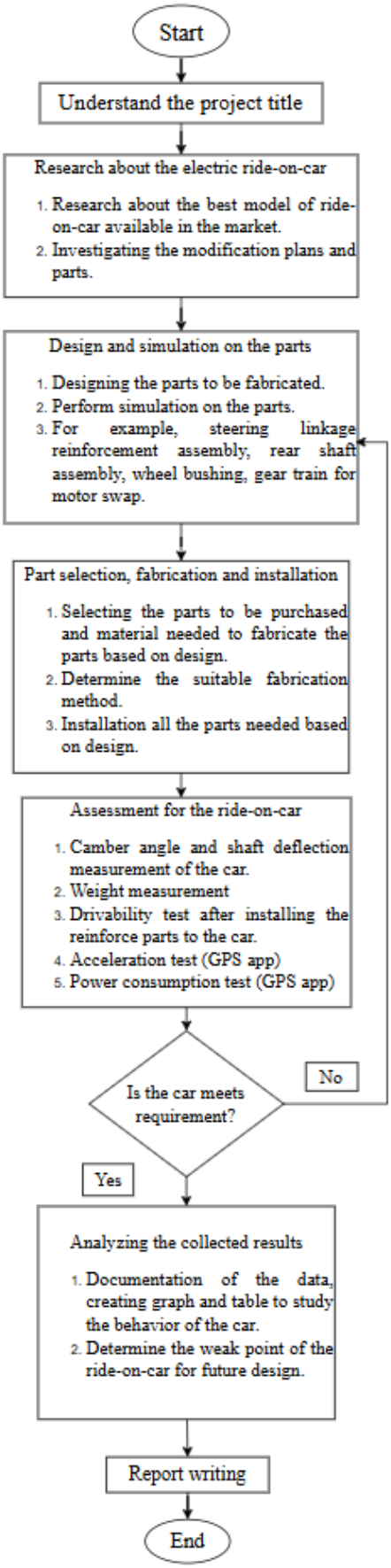

Figure 3.1: Workflow of the project.

The small electric car that has been purchased was the Ferrari ride-on-car and equipped with dual RS380 DC motors. The traction motors were also powered by 2 units of 6V batteries that connected in series with a small motor controller. The car originally was made for a kid to ride on it and the detail specification of the car will be shown in Table 3.1 below.

Figure 3.2: Small electric car to be modified.

Table 3.1: Selected small electric car original specification.

Part	Description
Motor spec	Brushed DC motor, (6V-14000rpm) *3 sets 2 sets for rear wheel, 1 set for steering remote
Battery type	Lead-acid battery
Battery spec	(6V4AH) *2 units
Motor controller	12V rated input voltage and include remote receiver
Driving mode	Self-driving (Not autonomous driving) or using remote controller
Speed control	3-speed selection
Powertrain configuration	Rear wheel drive (wheel hub direct drive with single speed gearbox)
Car weight	16.9 kg
Wheel size	9 in or 230 mm in diameter
Wheelbase	600 mm
Track width	600 mm
Lightning system	Front and rear led light
Suspension system	Dual spring system for front (independent suspension) and rear size (dependent suspension) respectively

Figure 3.3 below depicts the bottom view of the overall powertrain setup for the car. 3 sets of 12 V motor with gearbox were included and both the rear wheel were not dependent on each other, allowing them to spin at different speeds. At the front side of the car, a 4 bar linkage mechanism was included for steering purpose. The front wheels were connected to two identical turning rods, with one spring mounted on each side. Each spring was positioned on the left and right sides' short pivot bar. The turning rods were mounted at the front strut mount location of the car and secured with two pins. This four-bar linkage system was controlled by a hook that was attached to the steering wheel, as shown in Figure 3.22. For more information detail review of the car, the review would be allocated at Appendix A.

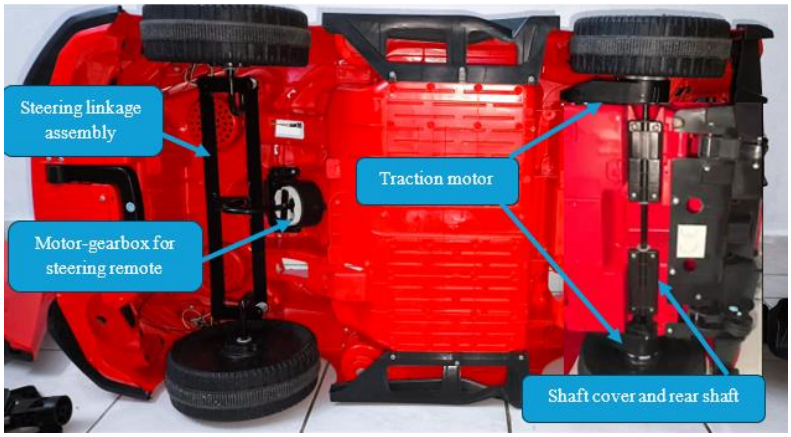

Figure 3.3: Overall setup for powertrain of the car.

To modify this commercially available electric ride-on-car for racing purpose, several modification sections needed to be considered to ensure that the vehicle fulfilled the requirements necessary to achieve the objectives outlined in the introduction. Four main aspects of the car were identified for improvement which included drivetrain modification, suspension conversion, motor-gearbox modification and wiring redesign. Every modification plan will be included with the information like problem encountered, design concept, the required equipment and materials with dimension and fabrication process.

3.2 Rear drivetrain reinforcement

The car body initially was manufactured by using plastic which was combination of ABS and PP and the rear shaft was enclosed only by 2 plastic covers and compressed by two small springs. From the first testing with an 80 kg load, excessive deformation of the rear axle was observed and obvious changes in static wheel camber as shown in Figure 3.4. This may cause by the low quality and tinny steel used in the ride-on-car like steering linkage, rear shaft and springs as it was categorised in low price ride-on-car model. In addition, all 4 tyres were also rotating wobblily and rubbing with the car fender frequently when the car was driven in the first testing section. To tackle this shaft deformation issue, which was causing the car could not be drive normally, stronger and thicker size of materials were needed to replace the stock rear shaft assembly to support the load required based on the design requirement.

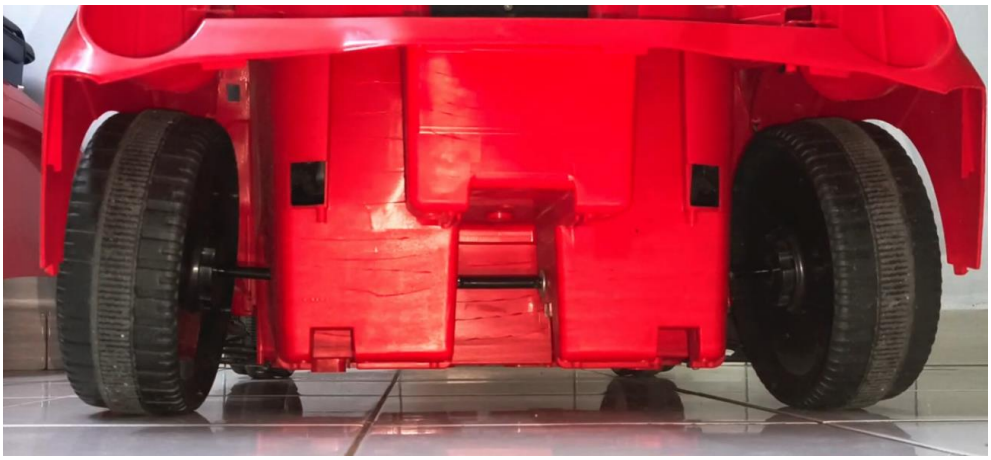

Figure 3.4: Deflection of shaft when loaded with driver.

3.2.1 Rear drivetrain reinforcement design

According to Figure 3.4, the original rear shaft with 9.5 mm diameter showed significant deflection once the driver sits on the car. This issue was attributed from the quality of the factory mild steel shaft, the smaller shaft diameter and the mounting method of the original assembly. Due to the load demand, the selected shaft's material would be mild steel. Based on the simulation result obtained from the SolidWorks, the 16 mm diameter of mild steel shaft results showed much lower vertical displacement (0.2635 mm) in than a proper 9.5 mm mild steel shaft (2.115 mm) as shown in Figure 3.5 and Figure 3.6. The design of rear shaft is particularly suitable for high school students as it introduces them to use fundamental engineering skills and knowledge of CAD software in terms of stress analysis, deflection analysis, boundary condition and so on. The 16 mm rear shaft also was a common size available in the and hence no heavy machinery involved which could be easily obtained by them.

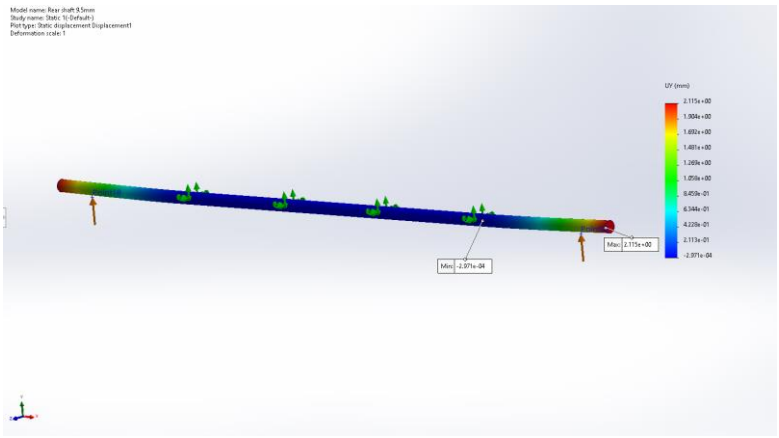

Figure 3.5: Simulation result for deflection of 9.5 mm shaft.

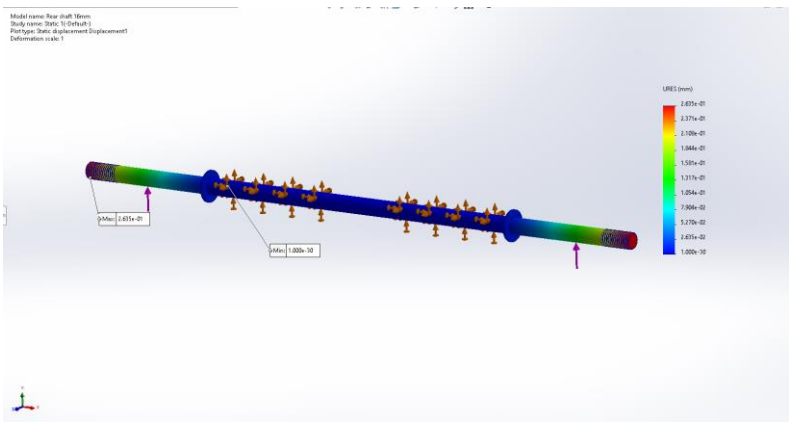

Figure 3.6: Simulation result for deflection of 16 mm shaft.

On the other hand, the nylon wheel bush and its housing would be required as shown in Figure 3.7. These parts were necessary because the drivetrain was designed to incorporate with a 16 mm rear shaft. The original plastic wheels were designed only with 10 mm shaft support structure as shown in Figure 3.8. Hence, this structure had to be removed as 16 mm shaft would larger than the outer diameter (OD) of this structure and hence a custom bushing was needed. The fabrication of nylon bush would involve the use of lathe machine and not suitable for children to do so. However, an alternative approach could be using the special size bearing to replace the outer bush while reusing the 9.5 mm rear shaft assembly, as the load demand of the ride-on-car for a child was significantly lower than that for a teenager.

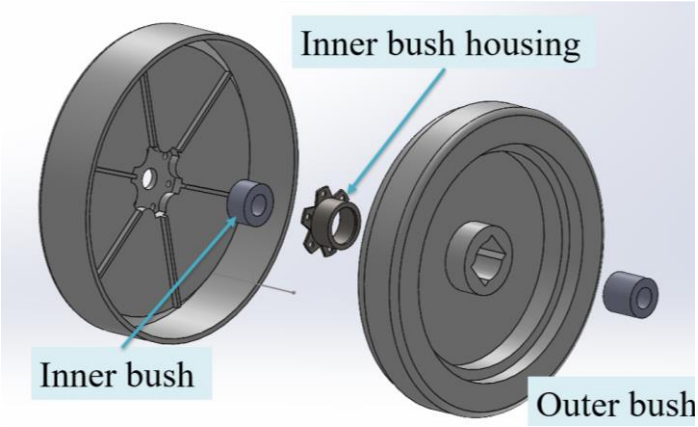

Figure 3.7: Modified plastic wheel.

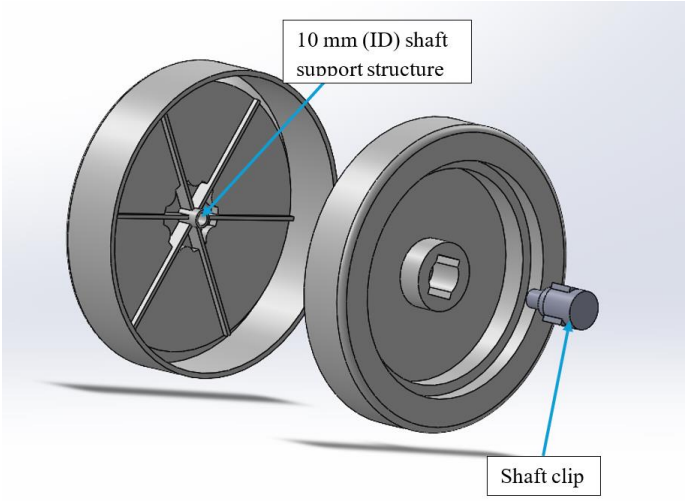

Figure 3.8: Stock plastic wheel.

Table 3.2: Equipment to be used in fabrication rear drivetrain assembly.

Equipment	Usage
Metric die with the size of $M16 \times 2.0$	To create male thread to lock the rear wheels by nuts.
Horizontal bandsaw machine	To cut the shaft to required length
Lathe machine	Reduce the diameter of the nylon bushing for rear wheels
Vertical bandsaw machine	Create the wheel hub reinforce pattern
Vernier calliper	Measuring the shaft and thread dimension
Epoxy glue	Reinforcing the plastic wheel
Sandpaper	Remove surface rust from mild steel rod
Stone grinding machine	Create chamfer for both end of the rod
Table vice	Holding the workpiece
WD-40 lubricant	Lubricate the die when making M16 thread

Table 3.3: Material used for the reinforcement rear drivetrain.

Material name	Outer diameter, OD (mm)	Inner diameter, ID (mm)	Total length (mm)
Mild steel rod	16	0	600
Outer nylon bush	30	16	27
Inner nylon bush	32	16	19
Steel bicycle wheel hub	70	32	20
Nylon lock nut, M16	24	16	16

3.2.1.1 Procedure to produce the rear shaft

1. A 600 mm long with 16 mm diameter of mild steel rod was prepared by using the horizontal bandsaw machine to cut off the excess rod as shown in Figure 3.9.

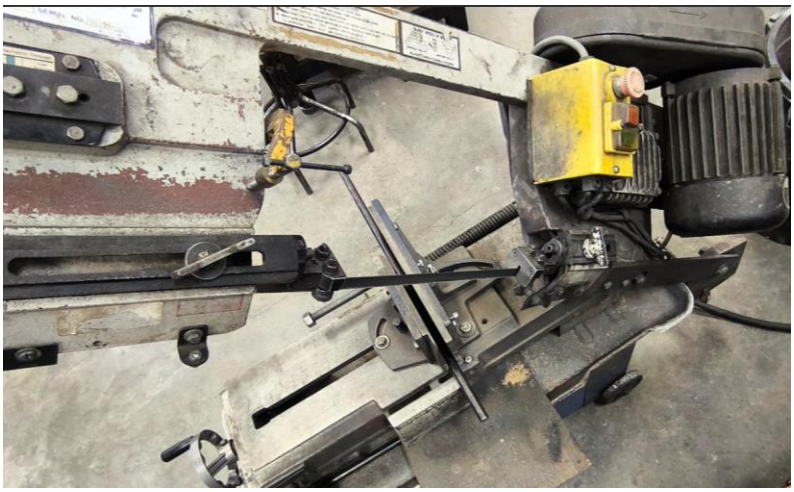

Figure 3.9: Cutting the 16 mm diameter shaft into length of 600 mm.

2. Rust removal on the mild steel rod surface was done by using sandpaper and wash with water together.
3. The edges on both end of the rod was then grinded with the stone grinding machine to create chamfer.
4. The rod was clamped on the table vice firmly so that it would not move while doing thread.
5. A metric die $M16 \times 2.0$ was used and insert to the handle. Tighten the 3 screws on the handle before starting to make thread.
6. Insert the die on top of the rod and pressed firmly on the die while turning the handle in clockwise direction as a default direction as shown in Figure 3.10.

Figure 3.10: Process to make $M16 \times 2.0$ with 30 mm length.

7. WD-40 lubricant was applied to the interface of the die and the shaft surface to ease the external threading process.
8. While turning the die in clockwise direction, rotate the handle in opposite direction to make sure the chips has fall off and continue rotate in default direction until the thread length of 30 mm was achieved.

Figure 3.11: $M16 \times 2.0$ with 30 mm length thread.

9. Step 6 to 8 were repeated for another end of the rod.
10. Test fit the thread created with a M16 nut to ensure the nut could be entered smoothly.

3.2.1.2 Procedure for making wheel bushing for front side and gearbox side of the plastic wheel

1. A plastic wheel is divided into front side as wheel as gearbox side as illustrated in Figure 3.12.

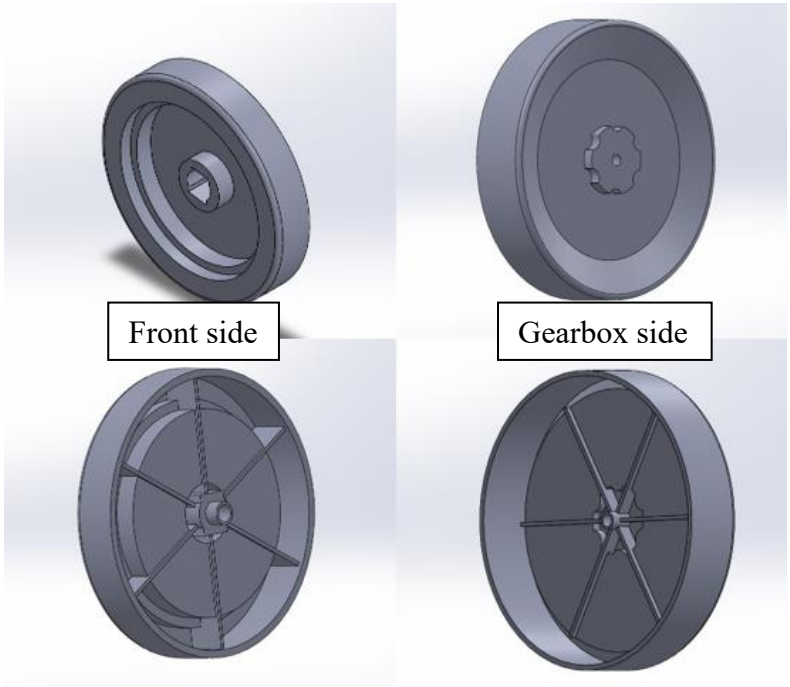

Figure 3.12: Detail view of original plastic wheel.

2. 2 pcs of standard size (32 mm of diameter and length) and 2 pcs of standard size (35 mm of diameter and length) of nylon bush were prepared and mount one of it on the chuck of the lathe machine.
3. The nylon bush was remount and turned on the lathe machine by few times to ensure the cylindricity of the raw material.
4. Before the nylon bush was cut, the cutter post of the lathe machine was tightened firmly with a slight angle position.
5. The lathe machine was turned on, the outer diameter of the bush was cut from 32 mm to 30 mm by a decrement of 0.5 mm adjustment from the cutter traversing wheel as shown in Figure 3.13.

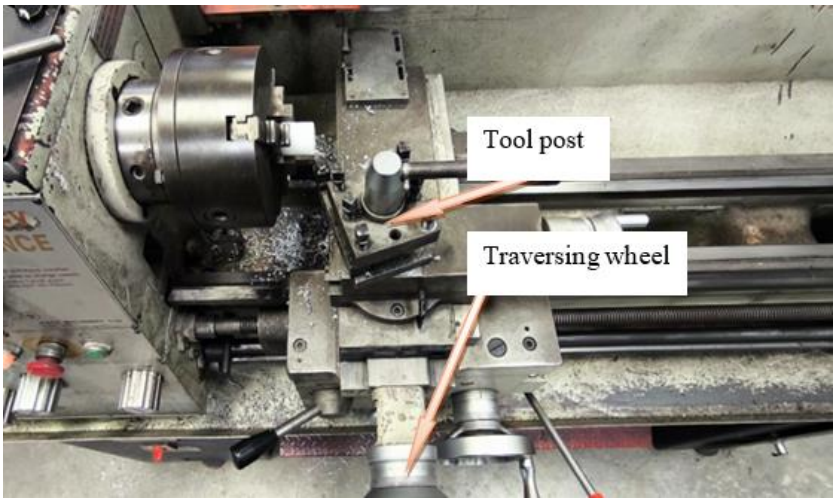

Figure 3.13: Nylon bush cutting process.

6. The nylon chips were clean during the cutting process for better accuracy of final product and avoid hitting the user as shown in Figure 3.14.

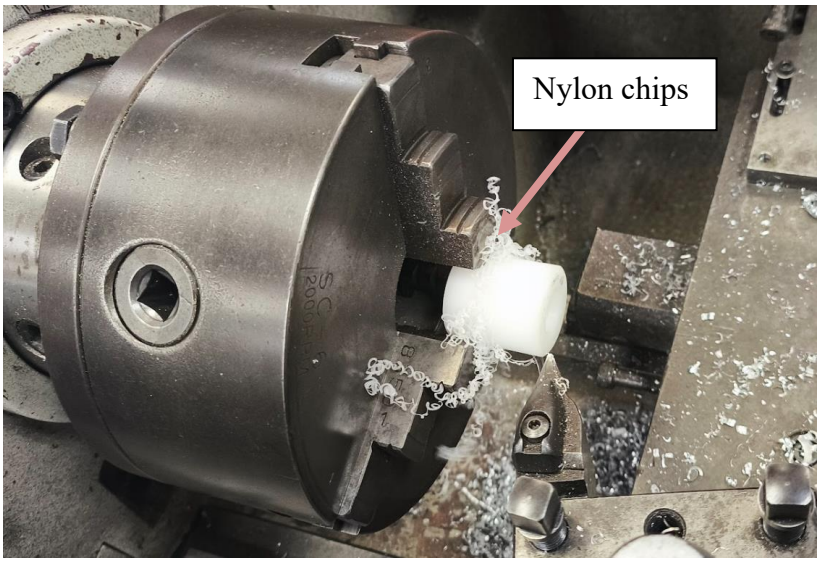

Figure 3.14: Chips removing process.

7. After step 4 and 5 were done, the 30 mm of outer diameter would be the final product as shown in Figure 3.15.

Figure 3.15: Final product of nylon bush.

8. Using a 16.5 mm diameter of drill bit and mount it on the tail stock of the lathe machine.
9. The machine was turned on and the drill bit was feed to create a center hole of 16.5 mm on the nylon bush like Figure 3.16.

Figure 3.16: Drilling process for the bushing with 16.5 mm of hole.

10. The drill bit was removed from the chuck and setup the tool post cutter for facing machining process to ensure the flatness of the end bushing surface.
11. The material would be cut by 1 mm for each end face so that the final result would be 30 mm of length.
12. Steps 2 to 10 were repeated for the bushing of another front side of the wheel as well as the remaining 2 pcs of 35 mm diameter nylon bushing for two gearbox side of the wheel.

13. After another 30 mm diameter nylon bushing was done, the bushing could be fitted into the front side wheel bush housing as shown in Figure 3.17.

Figure 3.17: Nylon bushing for frontside of wheel.

14. The extra material of nylon bushing was cut by using jig saw.

3.2.1.3 Procedure to create custom inner bush housing for gearbox side wheel

1. A bicycle wheel hub was prepared and marking with the cutting line as well as performed rough cut by using jig saw.
2. Comparing the pattern with the gearbox side wheel with the custom bush housing. The remaining cutting lines were marked.
3. Cutter blade was used to remove the plastic rib (support material) inside the wheel as shown in the highlighted portion in Figure 3.18.

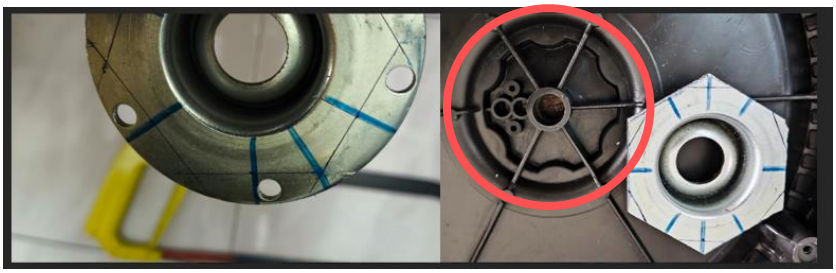

Figure 3.18: Rough cut for the inner bush housing.

4. The remaining material on the wheel hub was cut by using vertical band saw machine and trim off the excess the material by using grinding stone in order to fit into the wheel like the Figure 3.19.

Figure 3.19: Test fit of the inner wheel housing.

5. Total of six 5 mm holes on the wheel were drilled and the 32 mm nylon bush created early was fitted with the inner wheel housing and prepare to rivet process.

Figure 3.20: Test fit the inner wheel housing with nylon bushing.

6. The inner wheel housing was then rivet on the gearbox side wheel. Then, the cavities were filled with epoxy glue to
7. enhance the wheel casing strength as depicted in Figure 3.21.

Figure 3.21: Rivet process and epoxy glue filling process of the inner wheel housing.

3.3 Suspension modification

3.3.1 Front suspension spring delete

Figure 3.22 shown the factory configuration of the front suspension and steering linkage system of the ride-on-car. It also shown that the original design for front suspension system was integrated with steering linkage assembly. It was observed that the springs became fully compressed under the driver's weight, resulting in significant steering difficulties when turning the steering wheel. Not only this, but the front wheels of the ride-on-car also exhibited the increase of negative camber when loaded due to the entire turning rod (steering axis) deflection as shown in Figure 3.23. To increase the rigidity of the front suspension and steering linkage assembly, the springs have to be removed and install with reinforce structures.

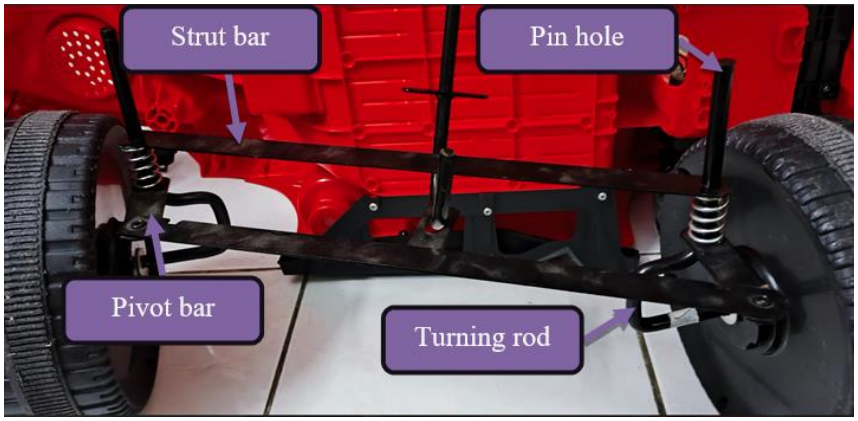

Figure 3.22: Front steering linkage and spring assembly.

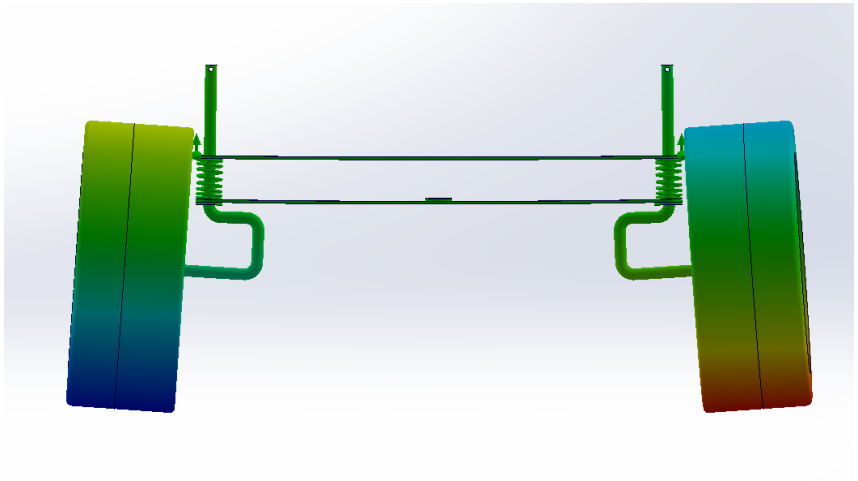

Figure 3.23: Illustration of wheel camber change.

The reinforcement of the front steering linkage assembly shown in Figure 3.24 could be achieved by adding an upper and lower strut bar that made by aluminium hollow square bar. Upper strut bar's primary function was to resist the camber change. The lower strut bar was not only used for reducing the camber change but also to secure the entire front steering linkage onto the car body so that the forward and backward movement of this steering linkage could be limited. Aluminium was selected for the strut bars due to its lightweight properties and moderate strength. Although it would wear out faster than using mild steel and would be replaced frequently. This was because the selected material (Aluminium) could be easily fabricated via normal tools like hacksaw and hence suitable to be replicated by the children and high school students. Aluminium was also considered as a high cost-effectiveness and relatively low cost material. For the turning rod reinforcement, steel block was selected due to its weldability with high carbon steel turning rods was higher than aluminium material. The steel block was to ensure the turning rod would not be deformed under heavy load and welding machine should be commonly available in most of the high school.

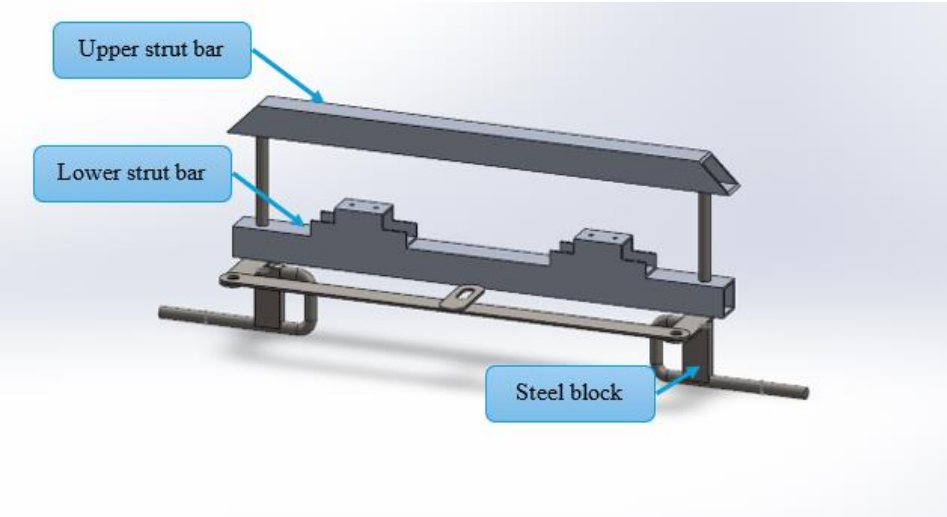

Figure 3.24: Steering linkage reinforcement.

The simulation results shown Figure 3.25 and Figure 3.26 below indicated a significant reduction in steering turning rod deflection after the reinforcement was implemented. Initially, the steering turning rod exhibited a maximum Y-deflection of 7.135 mm under 400 N load on each side, which

contributed to excessive negative wheel camber. Following the installation of the aluminium strut bars and steel block, the deflection was reduced to 0.6528 mm. This improvement demonstrated that the strut bars and steel block effectively increased the rigidity of the steering linkage system by redistributing the applied load and minimizing bending of the shaft.

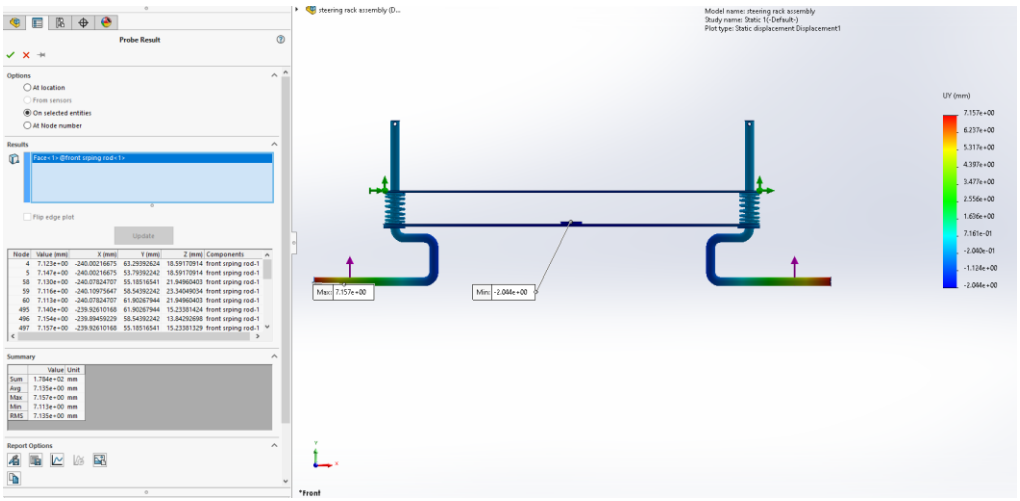

Figure 3.25: Average Y-displacement (7.135 mm) of stock steering linkage (400 N each side).

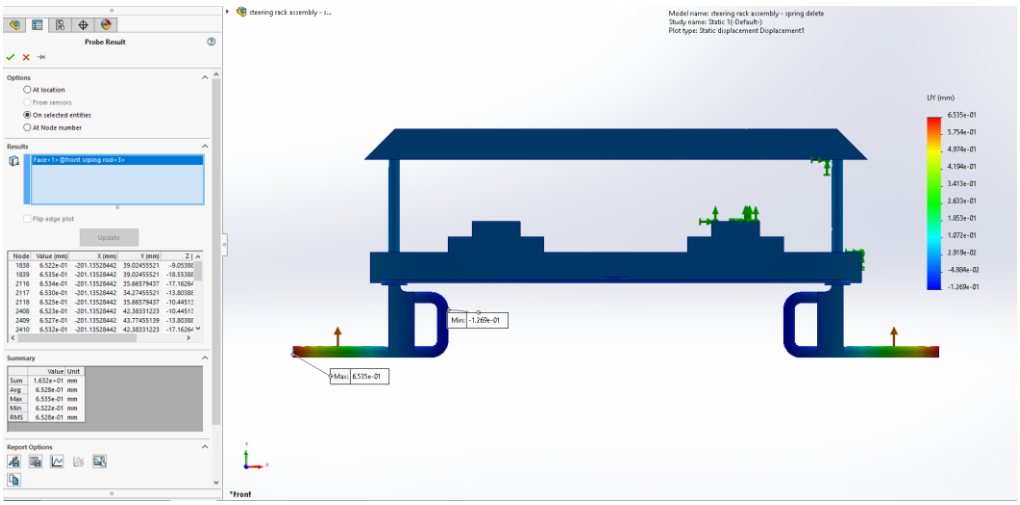

Figure 3.26: Average Y-displacement (0.6528 mm) of reinforced steering linkage (400 N each side).

Table 3.4: Equipment list for steering linkage reinforcement.

Equipment	Usage
Screwdriver	Pry out and insert the locking pin of turning rod
Hack saw	To cut the reinforcement bar into certain length
Electric drill	Drilling the holes for reinforcement bar
Table vice	Holding the workpiece for cutting
Rivet gun	Attach the steering linkage to body of the car
Cutting blade	Trimming the strut mounting area of the car body

Table 3.5: Material needed to upgrade the suspension setup and steering linkage system.

	Parts	Spec (mm)	Material	Quantity (pcs)
1	Bushing	10.2*16*20	Aluminium	2
2	Hollow square bar	25.4*25.4*2	Aluminium	4
3	Steel blocks	10.5mm thick	Mild steel	2
4	U-clip	M10	Stainless steel	2
5	Rivet pin	Ø4.8	Aluminium	10
6	Self-tapping screw	M4	Zinc coated steel	8

3.3.1.1 Procedure of turning rod reinforcement

1. Two steel blocks were prepared and fabricated by using horizontal band saw machine as shown in Figure 3.27.

Figure 3.27: Welding block fabrication process.

2. The steel blocks were sanded and fitted into the turning rod welding area by using grinding stone.
3. The turning rod was clamped on the table vice and the paint was removed by using filler.

Figure 3.28: Paint removing process.

4. The turning rod was welding with the steel block with the thickness of 10.5 mm by using MIG welding.

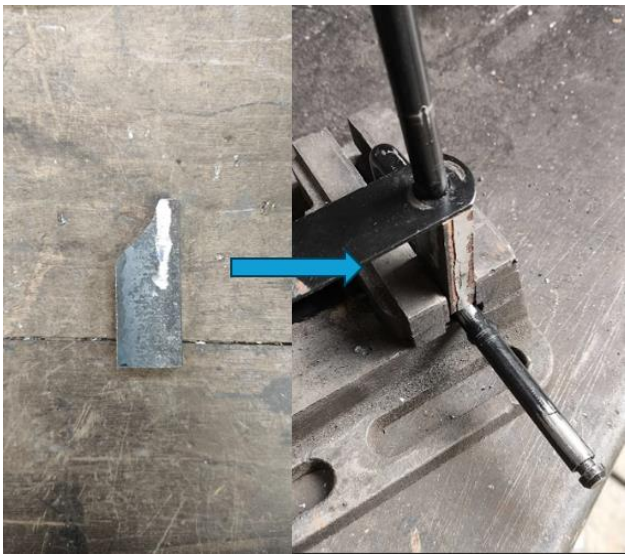

Figure 3.29: Clamping of steel block for welding process.

5. The finished product for strengthening the turning rod would be as shown in the Figure 3.30.

Figure 3.30: Reinforced turning rod.

3.3.1.2 Procedure to modify the front suspension setup

1. Two pcs of aluminium hollow square bar were prepared with the length of 410 mm and 400 mm by hack saw.
2. By using cutting blade, the area that obstruct the bar to mount on the pin hole was trimmed by using cutting blade.
3. The bar was placed on top of the pin hole for hole location marking purposes.
4. The prepared hollow square bars in step 1 for the length of 410 mm was clamped on the table vice.
5. Both ends of the bar were cut with 45 degrees of angle as shown in Figure 3.31.

Figure 3.31: Strut bar fabrication.

6. Two holes were created by using electric drill with 9.5 mm diameter based on the marking.
7. Step 3 to 6 were repeated for the second bar which was 410 mm of length and without cutting both end of the bar in 45 degrees.
8. Two additional aluminium square bracket to support the 410 mm long bar were prepared by cutting it using vertical band saw machine and drill two 5 mm holes for each bar.

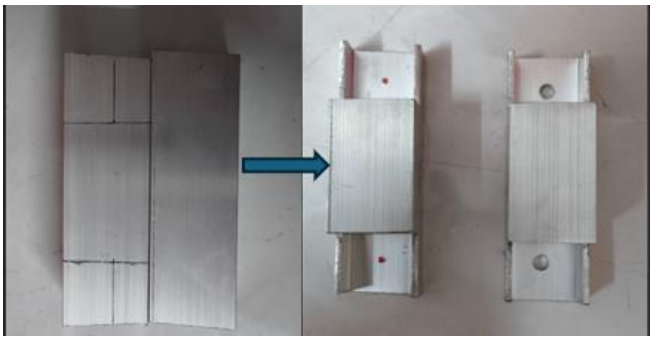

Figure 3.32: Additional bracket for 410 mm long bar.

9. The additional brackets were mount on the lower half strut bar with 410 mm of length by using rivet pin.

Figure 3.33: Lower half steering linkage reinforce bar.

3.3.1.3 Installation of the reinforce bar for steering system

1. The steering linkage turning rod is removed by prying out the locking pin from the top mount.

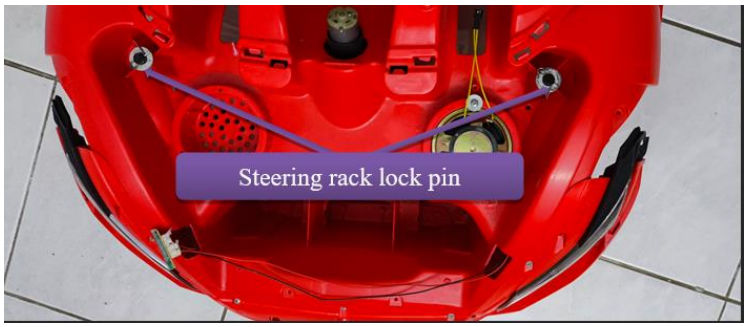

Figure 3.34: Steering linkage lock pin.

2. The aluminium bars fabricated from the steps above were installed based on the sequence as in the Figure 3.35.

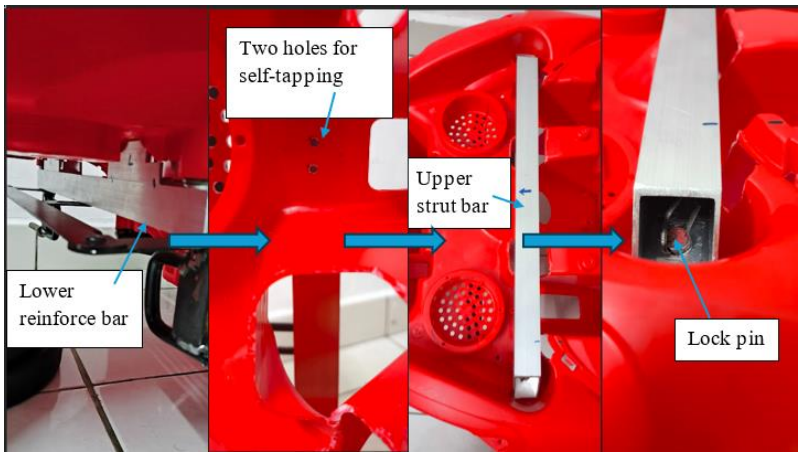

Figure 3.35: Steering linkage reinforcement installation sequence.

3. By using the M10 shaft clamp, the steering column was clamped on the reinforce upper and lower bar with M4 self-tapping screw by using 8 mm socket as shown in Figure 3.36.

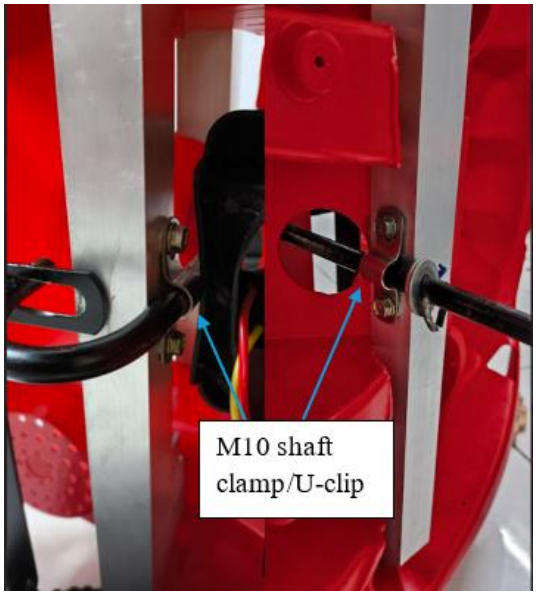

Figure 3.36: Steering column holding method.

3.3.2 Rear suspension delete design

After the rear shaft has been fabricated, the next step was to use the shaft and combined with two steel plate to replace the factory plastic shaft cover. Not only these, but the rear springs were also removed as the factory suspension was changed to rigid type suspension system as shown in Figure 3.37. The selection of fabrication was to weld the two steel plate on the shaft as this method was more direct and particularly suitable for the high school students. On the other hand, for the children perspective, mild steel plate joining method was not limited to this as M16 shaft-clamp could be used to secure the shaft on the plate after drilling the mounting holes on the plate. By using this method, the steel plate should be replaced with thicker aluminium plate as the load demand would be lesser if compare with high school students.

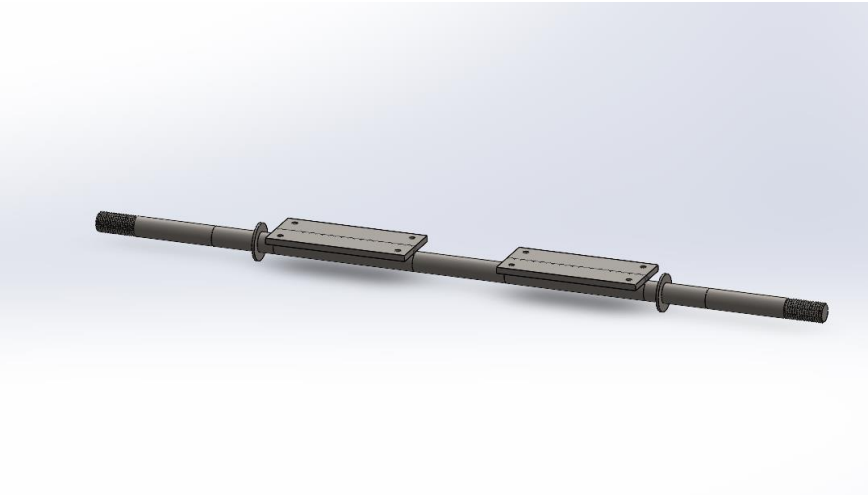

Figure 3.37: Rear shaft assembly.

Table 3.6: Equipment list for rear suspension deletes.

Equipment	Usage
MIG welding machine	To weld the 2-steel plate together with the rear shaft
Horizontal bandsaw machine	To cut the mild steel plate into required dimension
Vertical drilling machine	To drill the screw holes for each steel plate
G-clamp	For holding the workpiece

Table 3.7: Material needed to upgrade the suspension setup and steering linkage system.

	Parts	Spec, L*W*H (mm)	Material	Quantity (pcs)
1	Shaft cover	115*49.5*5 mm	Mild steel metal sheet	2

3.3.2.1 Procedure to fabricate the shaft cover

1. Prepare a mild steel metal sheet with A3 size, the marking line was made on the sheet metal based on the required shaft cover dimension.
2. Clamp the mild steel metal sheet on the horizontal bandsaw machine and align with the saw blade.
3. The machine was switched on and press down the handle to cut the metal sheet base on the marking line.
4. Repeat step 2 to 3 for another shaft cover.
5. The shaft cover was then sent to the vertical drilling machine after finishing cutting process.
6. Centre punch was used to create the small dent holes so that the drill bit would not misalign with the required holes' position as shown in Figure 3.38.

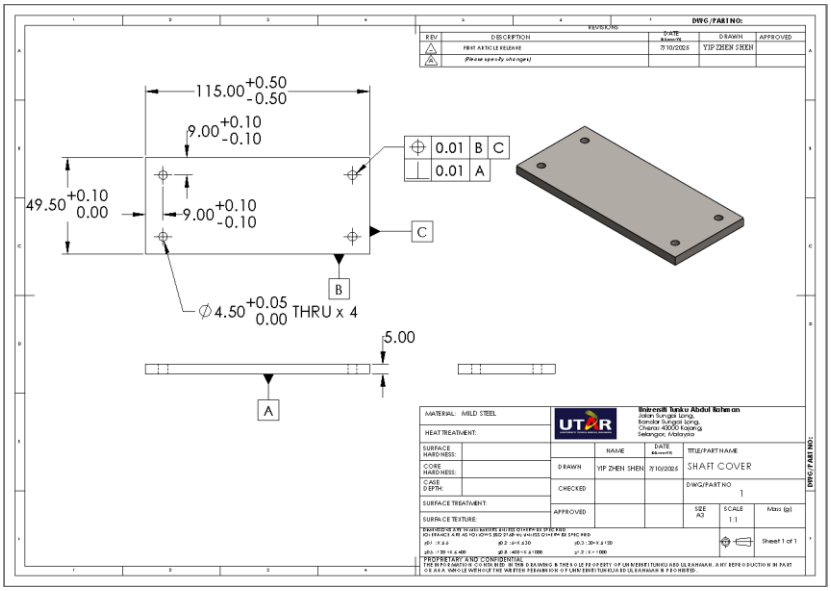

Figure 3.38: Engineering drawing for shaft cover.

7. 3 mm drill bit was used and lock into the chuck of the drilling machine.
8. Turn on the machine and press down the drill bit by using the machine handle.
9. The machine was turned off after drilling 8 holes for 2 plates
10. Repeat step 7 to 9 by using 4.5 mm drill bits.

3.3.2.2 Preparation for welding the shaft cover with the rear shaft

1. The rear shaft and the cover made were transfer to the car body rear suspension location for doing marking.
2. The shaft covers were screw into the car body first and followed by placing the shaft on top of it.
3. A M12 hex bolt (17 mm spanner) was used to determine the shaft location which adjusted the wheelbase of the car for shaft cover like Figure 3.39.

Figure 3.39: Adjustment of the shaft for marking.

4. Measuring tape was used to measure the distance from the end of the shaft to the side of the shaft cover which was 146 mm for left and right side shown in Figure 3.40.

Figure 3.40: Measuring distance from the end of the shaft to cover plate.

5. The marker pen was used to draw the line on the shaft cover which represents the shaft position.

3.3.2.3 Process to weld shaft cover with rear shaft

1. The 16 mm shaft and cover were clamped on the table by using g-clamp but not clamp firmly.
2. The 16 mm shaft was aligned with the cover based on the marking made previously.

Figure 3.41: Workpiece holding method.

3. The MIG welding machine was turned on together with the CO2 gas vessel.
4. Fully tighten the g-clamp and recheck the shaft alignment.
5. Spot weld the shaft with the cover for opposite side to secure the welding location.
6. The shaft was full welded for both sides for each plate.

7. The fully weld rear shaft and cover assembly was showed in the Figure 3.42.

Figure 3.42: Fully welded rear shaft assembly.

8. Two washers were spot weld also from a distance of 131 mm from both end of the shaft as a stopper for the gearbox and the final product would show in Figure 3.43.

Figure 3.43: Final product of rear shaft assembly.

9. The reinforced 16 mm rear shaft assembly was trying to be installed back to the car by using 4 self-tapping screws for each side shown in Figure 3.39 to ensure the parts could be installed without major interference.

3.4 Installation and testing of the rear shaft assembly

After the reinforced rear shaft assembly has been fabricated, the next step was to conduct the rear shaft measurement for the rear shaft assembly for both stock and reinforced condition. The measurement that to be taken was to determine the difference stock and reinforced rear shaft assembly in order to encounter the obvious deflection of rear shaft shown in Figure 3.4, the measurement of rear shaft deflection was done by using the following steps.

3.4.1 Procedure to measure the rear shaft (9.5 mm diameter) deflection under heavy loaded condition

1. The dead weight of 80 kg was prepared by using the dumbbell plates.
2. The floor of the testing room would be the datum Z to measure the shaft deflection.
3. The shaft was assumed to be straight and hence the initial distance was measured from the floor to the wheel centre by using measuring tape. The result was recorded.
4. The dumbbell plates were distributed to the rear seat and middle section of the car with weight distribution of 60 kg and 20 kg respectively.
5. The next measuring distance would be the distance from the floor to the upper surface of the shaft. The distance was also measured by using the same tool and the result was recorded.
6. The dead weight was removed from the car gently to avoid any destructive accident to the car body.

3.4.2 Procedure to install to the 16mm rear shaft assembly onto the car body

1. The wheels of the car were removed from the original shaft by releasing the shaft clip.
2. Total of 8 screws were unscrewed from the car body by using crisscross pattern as the plastic shaft cover (original rear shaft assembly) was under tension from the springs.
3. After that, the original rear assembly could be removed from the car and the reinforced 16 mm diameter shaft assembly

shown in Figure 3.43 was installed back to the car by using same number of screws.

4. By using the rear wheel sets that prepared with the wheel bushing, installing the wheels to the shaft. Using two M16 lock nuts for each end of the shaft and tightening the nut together to prevent the wheels from coming out from the shaft.
5. For the front wheels, the wheel housing was fitted with 2 bearing (6200 ball bearing) for each wheel. The factory plastic shaft clips were replaced by the circlips (for 6 mm diameter groove) and the circlips were installed by using plier.
6. By using the same approach in the procedure to measure the rear shaft (9.5 mm diameter) deflection in section 3.4.1, the rear shaft deflection was recorded.

3.5 Installation and testing front steering assembly with and without reinforcement

The following section showed the procedure needed to measure the strut mounting point distance and the wheel camber angle difference by using measuring tape and a camber angle application for both with and without the reinforcement of steering linkage assembly.

3.5.1 Procedure of measuring the strut mounting point distance and camber angle difference under heavy loaded condition

1. The measurement was started without the aluminium strut bar.
2. The dead weight of 80 kg was prepared by using the dumbbell plates.
3. The floor of the testing room would be the datum Z to for the measurement setup.
4. The dumbbell plates were distributed to the rear seat and middle section of the car with weight distribution of 60 kg and 20 kg respectively.
5. By using measuring tape, the distance x_1 from strut mounting point 1 to point 2 was measured by referring to Figure 3.44.

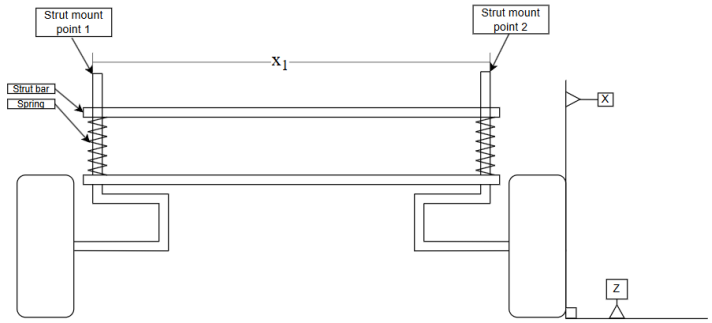

Figure 3.44: Strut mounting point distance illustration.

6. Camber angle application in phone was used and placing a battery at either side of the phone so that the phone's screen (datum X) would be 90 degrees to the floor (datum Z). The illustration of the experiment setup would be shown in Figure 3.45.

Figure 3.45: Measurement setup for wheel camber angle.

7. Once the datum setup has been done wisely, the reading of camber angle was set to zero in the application.
8. Placing the phone against the front wheels of the car, the camber angle was recorded.
9. Steps 5 to 8 were repeated after installing the upper and lower aluminium strut bar.

3.6 Weight test before and after reinforcement of front and rear suspension assembly

Once the reinforced front and rear suspension assemblies has been fabricated, the weight test needs to be done for the calculation on the performance testing result for both conditions (without and with reinforcement). In this section, the equipment need was the ride-on-car and one weighing machine.

3.6.1 Process to weight the car with and without driver (without reinforcement)

1. The original ride-on-car was prepared with body kit installed as well as the plastic wheels.
2. However, for motor-gearbox assembly and battery were not installed to the car as these components would be changed after modifications shown in section 3.7.
3. The front right wheel was placed on the weight machine after calibration and the result was captured.
4. The process was repeated for the remaining wheels.
5. Step 3 and 4 was repeated again with driver (load) and the result was obtained.

3.6.2 Process to weight the car with and without driver (with reinforcement)

1. The reinforced assembly was installed to the ride-on-car such as 16 mm rear shaft assembly, reinforced steering linkage assembly and plastic wheels with bushing.
2. For the front wheels, the wheel housing was fitted with 2 bearing (6200 ball bearing) for each wheel. The factory plastic shaft clips were replaced by the circlips (for 6 mm diameter groove) and the circlips were installed by using plier.
3. The front right wheel was placed on the weight machine after calibration and the result was captured.
4. The process was repeated for the remaining wheels.
5. Steps 3 to 4 were repeated again with driver (load) and the result was obtained.

3.7 Motor-gearbox modification

3.7.1 DC motor upgrade of the electric vehicle (EV)

The car factory setting initially consisted of two brushed DC motor wheel hub drive setup. A DC motor is rated for 12 V and 17000 rpm as well as 25 W to 30 W of input power. However, the car is purposely modified for carrying the load is a teenager instead of a kid according to the objective. Thus, the dc motor needs to be replaced and add-on another 12 V battery in series so that the total voltage supplies targeted become 24 VDC.

Figure 3.46: DC traction motor (upper one is steering remote motor).

In the SolidWorks model shown in Figure 3.47 was the modified RS380 gearbox configuration with first gear delete to accommodate the RS895 motor. The upgraded RS895 motor with its higher power rating, was integrated into the redesigned gearbox to improve acceleration and top speed. The simulation results shown in appendix D, Figure D.3 further verified that the nylon gears could withstand the input torque of 1 Nm provided from the RS895 motors and did not exceed the yield stress of the nylon material ($\sigma_{yield,nylon} = 139$ MPa). The method of doing modifications on motor swap in RS380 gearbox would be suitable for both children and high school students as this only required basic hand tools with proper gear installation. Difficulties of fabrication would be considered as easy to moderate level and aim for achieving the goal which was to increase the performance of the car.

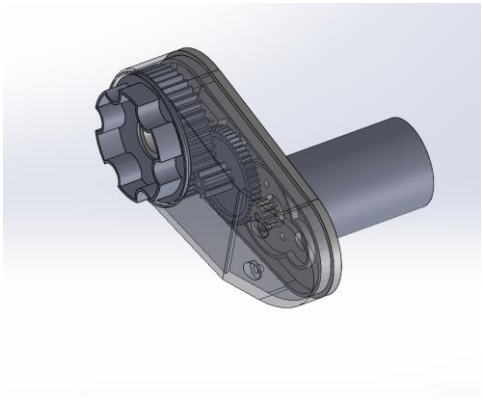

Figure 3.47: RS380 gearbox with first gear delete.

Table 3.8: Equipment needed to modify RS380 motor-gearbox.

Equipment	Usage
Soldering iron	Joining between wire to terminal pin of dc motor
Suction pump	Remove excess unwanted soldering iron tin
Cutter blade	Trim off the excess material on the gearbox casing
Sandpaper	Resurface the output gear holder and sharp edges
Screwdriver (cross head)	Remove the screw from the gearbox and motor
Electric drill	Create holes to mount the new motor
Allen key	Tighten the pinion gear on the RS895 motor

Table 3.9: Material needed to upgrade the motor-gearbox assembly and wiring system of the EV.

	Part	Material	Spec	Quantity (units)
1	DC Motor RS895	-	360 W	2
2	RC pinion gear	Hardened steel	Module 1.0 and 5 mm ID	2
3	Lead acid Battery	-	12 V	2
4	AB epoxy glue	Resin and hardener	-	1
5	Screws	Steel	M4	4

3.7.1.1 Process to upgrade motor-gearbox assembly (first gear delete)-part 1

1. Disassemble the motor-gearbox set from the ride-on-car using screwdriver.
2. Using cross head screwdriver, total of 6 screws were removed from the gearbox casing. 4 at the rear casing and the other 2 at the front side of the casing as shown in Figure 3.48.

Figure 3.48: Disassemble of gearbox.

3. The motor was removed by unscrewing the 2 screws that holding the motor.
4. All the gears and shaft were removed as shown in Figure 3.49 followed by scraping out the grease from the gearbox using cutter blade.

Figure 3.49: Separation of gearbox internal part.

5. The AB epoxy glue was mix evenly by using 1:1 ratio of resin and hardener.
6. The prepared epoxy glue was filled in the gearbox output gear cavities to strengthen the gearbox casing which represented by the Figure 3.50 below.

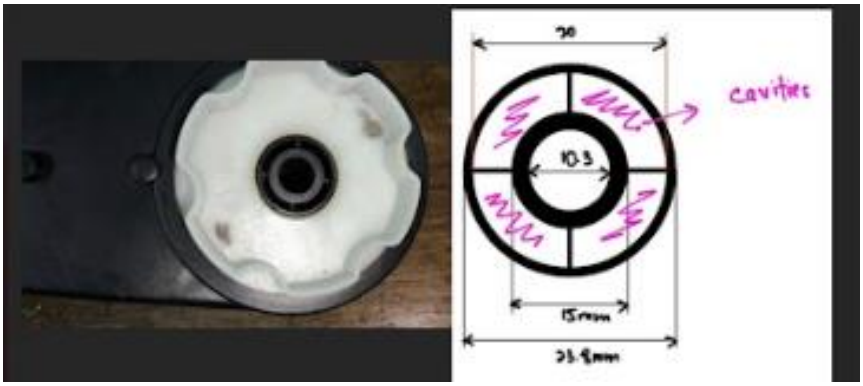

Figure 3.50: Cavities of the output gear support filling process.

7. By placing the gearbox in a room temperature space and let it dry for 1 to 2 days.

3.7.1.2 Process to upgrade motor-gearbox assembly (first gear delete)-part 2

1. After the epoxy glue has cured, a 13 mm drill bit was used to enlarge the output gear hole by using vertical drilling machine.
2. Step 1 was repeated by using 15 mm drill bits and increased up to 16.5 mm drill bits for better outcome.
3. The excess plastic chips were sprayed out by using air compressor and the result of enlarging the holes would be shown in Figure 3.51.

Figure 3.51: Outcome of drilled output gear holes.

3.7.1.3 Process to upgrade motor-gearbox assembly (first gear delete)-part 3

1. The excess plastic material that used for mounting the original motor was removed as highlighted in Figure 3.52 with red colour circle by using cutter blade.
2. Pre-drill a 4 mm diameter hole at the first gear center shaft location for mounting the RS895 motor later.

Figure 3.52: Fabrication of the new motor mounting location.

3. The predrilled hole was then enlarged to 17.5 mm diameter and this hole's position could be referred from engineering drawing in Figure 3.53. Datum A represented the original middle gear location and extend it by 32 mm to the right side for 17.5 mm hole.

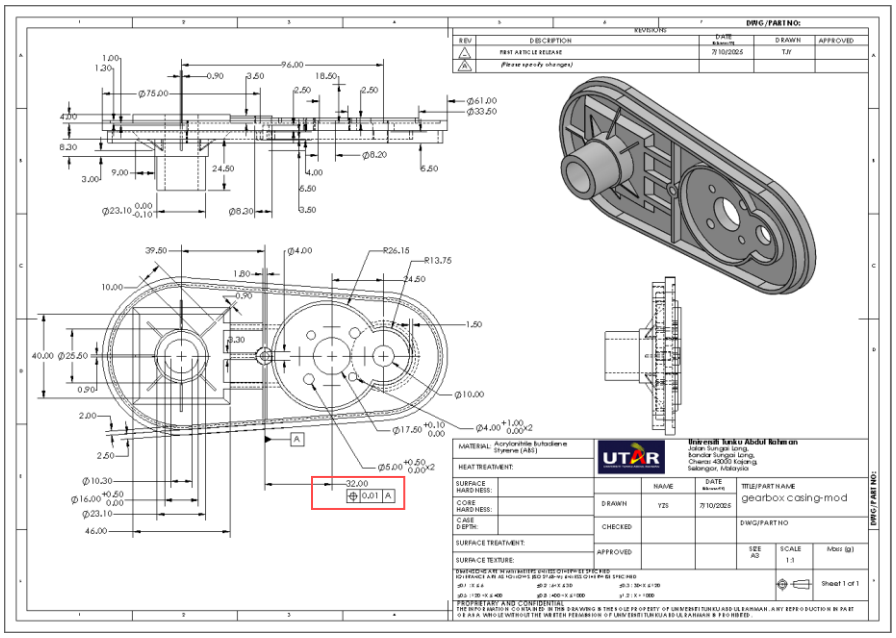

Figure 3.53: Engineering drawing for 895RS motor location.

4. Two 4 mm holes and two 5 mm holes could also be drilled approximately by using the paint marker to draw the hole location. The tolerance given was for the gear mesh purpose when installing the RS895 motor.
5. 2 pcs of M16 washer (spacer) were used to mount in between the back casing to the motor housing.
6. The marking was draw on the screw's head on the motor itself. The motor was press on the back of the spacer firmly and release to ensure the holes position.
7. The spacer was fabricated by boring the 17 mm hole (actual diameter of M16 washer) to 17.5 by using grinding stone as shown in Figure 3.54.

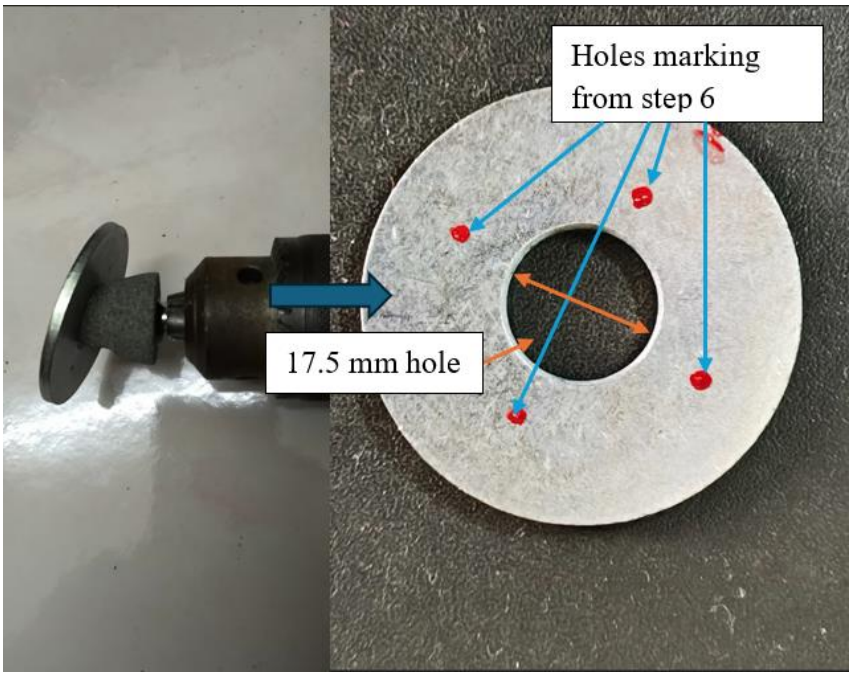

Figure 3.54: Motor spacer boring process.

8. Then, the washer was drilled by using 4 mm and 5 mm drill bit to create the mounting location.
9. The 17.5 hole that was drilled in step 2 was used to align with the washer and transfer the 4 holes location to the back of the gearbox casing by using paint marker.
10. The pinion gear on the motor shaft was tightened with allen key.

Figure 3.55: Pinion gear installation.

11. The middle gear and output gear were installed on the gearbox and test fit with the pinion for gear mesh adjustment.

12. The gear mesh between middle gear and pinion should have the sweet spot between tight and loose meshing.
13. The screws were tightened once the gear mesh was done.
14. Each of the gear was pasted with the grease to minimize the friction.
15. The casing of the gearbox was covered back together with the modified casing as shown in Figure 3.56.

Figure 3.56: RS895 motor-gearbox set with first gear delete.

16. The steps from 1 to 14 were repeated for another set of motor gearbox only after the first testing of the ride on car performance has been executed with dual RS380 motor-gearbox.
17. Two RS895 motor-gearbox was connected to 24 V battery source to ensure the gear could run smoothly before installing to the car.

3.8 Electronic design and testing plan of the small electric car at stock condition

Figure 3.57 illustrated the electrical components of the stock electric ride-on-car which included headlights and taillights, a speaker, three 12V motor (2 for traction and 1 for remote steering), 2 units of 6V batteries with a 10-amp fuse, a charging port, a motor controller, a dashboard control panel and steering horn buttons. The detail illustration of the original dashboard wiring is provided in Appendix A, Figure A.6, Figure A.7 and Figure A.8.

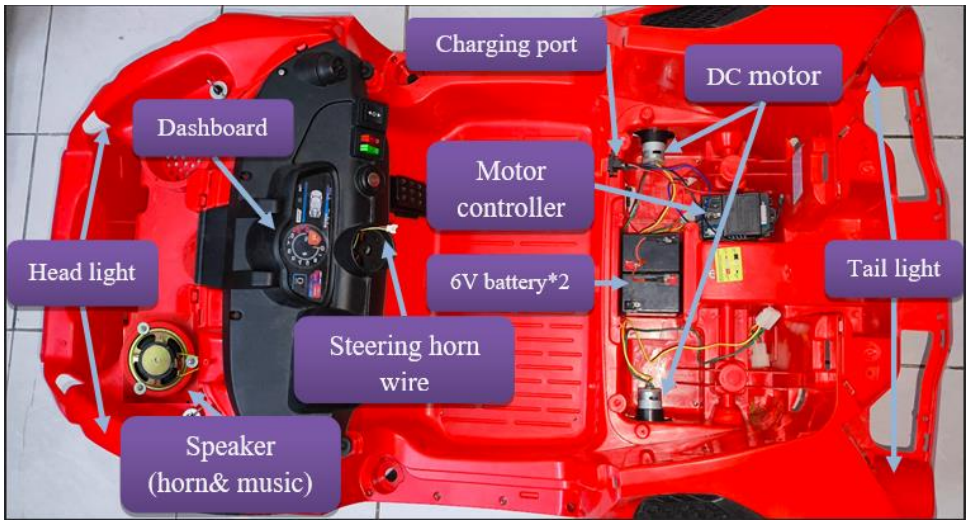

Figure 3.57: Overall electrical components location of the car.

Since 2 sets of RS895 DC motor are intended to replace the stock 12 V motors with input voltage of 24 VDC and majority of the vehicle's weight distribution is concentrated at the rear when a driver is seated, it is necessary to relocate the rear electrical components to alternative positions. The redesigned wiring system will focus on optimizing the use of available space for electronic components in order to improve the efficiency of current flow compared to the original layout. Furthermore, since one of the original 6 V batteries contained a defective cell, a new 12 V battery will be used for initial testing. The required equipment and parts for the wiring redesign are listed in Table 3.10 and Table 3.11.

Table 3.10: Equipment for fabrication of wiring hardness.

Equipment	Usage
Soldering iron	Joining between wire and wire, or wire to terminal pin
Crimper	Connect copper wire together with terminal pin
Lighter	Sealing the exposing wire with heat shrink
Cutter	Cut wire in certain length
Wire stripper	Remove insulator from the wire
Electric drill	Create hole for cable tie to pass through

Table 3.11: Electronic parts of the wiring design of the stock car.

	Part	Material	Spec	Unit
1	Heat shrinks sets	PVC	Diameter, 2-13mm	1
2	Terminal pin (50 pcs)	Copper	Female	1
3	Fuse	Tinted copper plate	10 A	1
4	Lead acid battery	-	12 V	1
5	Cable tie (20 pcs)	ABS	10 inches long	1

3.8.1 Preparation to test the ride-on-car based on selected electronic components before upgrading

1. To conduct the test, the important components that were selected to be used for the ride-on-car consist of dual RS380 motor gearbox sets, 1 unit of 12 V battery, a motor controller with on/off switch, power consumption meter, control panel for forward drive, reverse drive and ignition (kill switch).
2. The electronic components setup for the car remained the same as factory setting. These included the motor controller, batteries, motors which would be placed underneath the driver seat. While the control panel for music and also the dashboard was removed from the car.
3. The only additional wiring has to be changed was the power consumption meter and the connection was completed based on the wiring diagram shown in Figure 3.58 and soldering process in Figure 3.59.

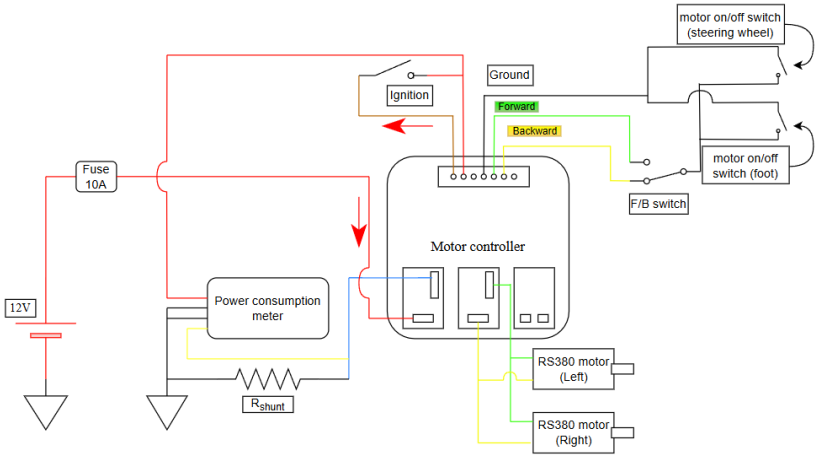

Figure 3.58: 12 V wiring diagram with power consumption meter.

Figure 3.59: Wiring hardness fabrication process.

4. All the connection created by soldering must be covered by heat shrink which would be heated by the lighter.
5. Then, the final looks of the wiring connection with newly added power consumption meter would be illustrated in Figure 3.60.

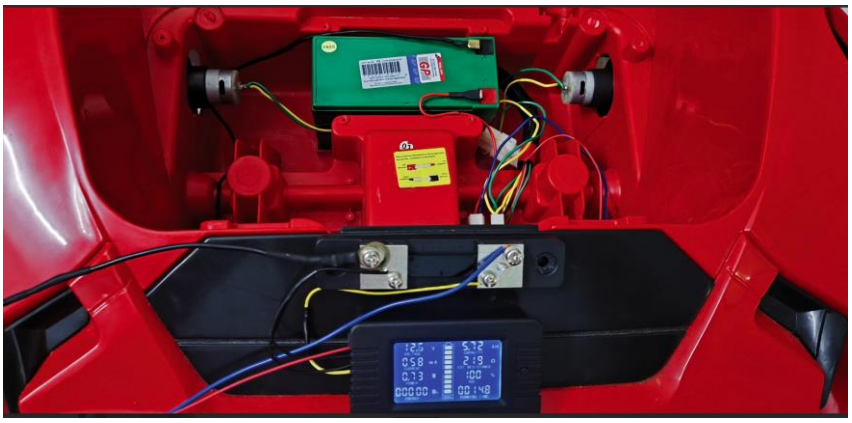

Figure 3.60: Addition power consumption meter connection.

3.8.2 First testing on the car performance with stock setup

Since the car was installed with the reinforced drivetrain and suspension assembly, the car now could be tested with the following tests which were power consumption test, acceleration test and motor temperature measurement. The location for the testing the ride-on-car would be at the parking basement. Table 3.12 shows the equipment needed to conduct the first test.

Table 3.12: Equipment needed to conduct the first test.

Equipment	Purpose
Phone- GPS apps	• To measure the top speed of the car • To measure the G-force over for a time interval
Measuring tape	To measure the length of the track to be tested
Power consumption meter	To measure the power consumption of the battery during efficiency test
Thermometer probe	To measure the motor temperature
Stopwatch	Measure the time for power consumption test and acceleration test

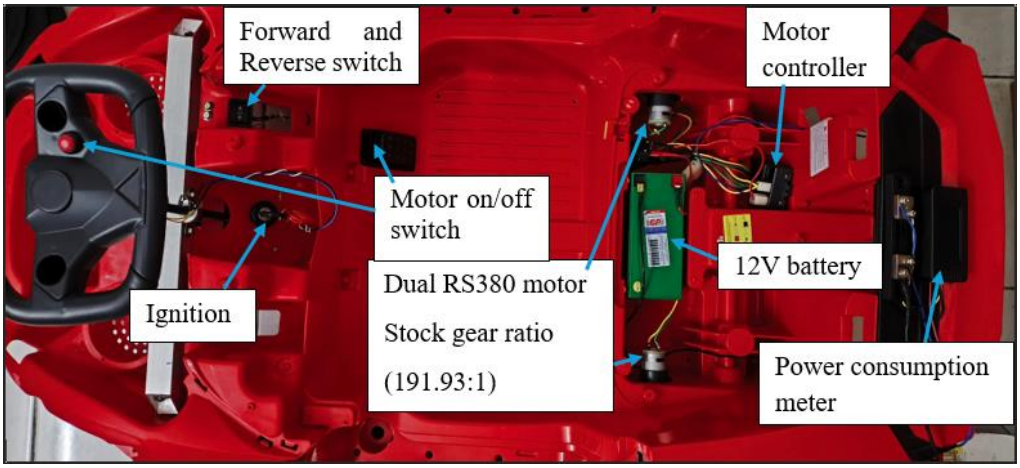

Figure 3.61: Ride-on-car electronic component and powertrain layout.

3.8.2.1 Acceleration test of 12 V stock car

The location of testing the ride-on-car would be located at the parking basement. Acceleration test would be testing on the time required for the car to travel from starting point to ending point. The total distance for the test was 13 m along a straight path as shown in the Figure 3.62 and the distance was measured using a measuring tape. Prior to the test, the phone GPS application has to be calibrated for the accelerometer function and start logging button was pressed. When the test began, the stopwatch was started simultaneously and stopped when the car reached the ending point of the test route and the time was recorded. The stop logging button was pressed in the GPS app and the data for the G-force with time interval and top speed of the car was obtained. This procedure was repeated for 3 times to obtain the average results. For the peak power measurement, the reading was captured on power consumption meter when the car started to move from standstill condition. The value recorded was the total peak power produced by the dual DC motor (RS380 motor).

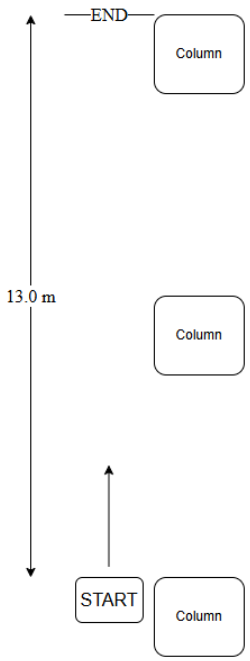

Figure 3.62: Acceleration test track length.

3.8.2.2 Power consumption with stock condition

Power consumption test, which required to measure power needed drive the ride-on-car over a specified number of laps in the basement. Based on the measurements taken with the measuring tape, the total distance along the circular route was approximately 27 m/lap. 5 laps were required to test the power consumption of the car. Before the test began, the power consumption meter was calibrated and reset to zero. When the test has started, the stopwatch was start counting the time and time required per lap was recorded. Figure 3.63 represented the sketch of the testing route.

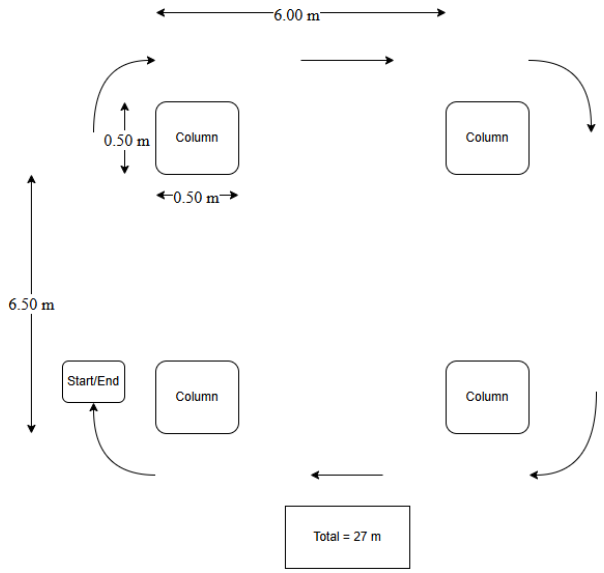

Figure 3.63: Power consumption track length.

In addition, the total power consumption recorded was subsequently used to estimate the range of the electric ride-on-car for the stock configuration. Not only these, but the recorded lap times were used to calculate the average power consumption per lap (Wh/lap). When the power consumption test has been completed, the motor temperature was measured by using a thermometer probe. The probe was placed on the motor housing immediately after the test finished. The reading was taken once the temperature reading stabilized or reached steady-state conditions. The purpose of doing the temperature measurement was to ensure the motor could withstand the endurance driving conditions without overheating.

3.9 Electronic design and testing plan of the modified powertrain small electric car

A new wiring design on the modified ride-on-car was needed as the new set of RS895 motors would draw more amps than RS380 motors and the car would be upgraded and operated with 24 V battery. There were few new electric components added in the system, which included a 4-pin relay, another 12 V battery and standard size 35 A fuse as shown in Table 3.13. Using the procedure in section 3.9.1 and section 3.9.2 below, the new wiring design was fabricated with the same tools as shown in Table 3.10.

Table 3.13: Electronic parts for modifying ride-on-car.

	Part	Material	Spec	Unit
1	Heat shrinks sets	PVC	Diameter, 2-13 mm	1
2	Wire braided sleeve	PTFE	Diameter, 5 mm Length, 5 m	1
3	Terminal pin (50 pcs)	Copper	Female	1
4	Fuse with holder	Tinted copper plate	10 A	1
5	Fuse with holder	Tinted copper plate	35 A	1
6	4 pin relay	-	24 V, 40 A	1
7	Copper wire (1m long)	Copper	12 awg	4
8	Lead acid battery	-	12 V	2
9	Cable tie (20 pcs)	ABS	10 inches long	1

3.9.1 Procedure to locate the electrical components of the ride-on-car

1. All electrical components were installed on the ride-on-car without wiring hardness at the first step.
2. In the design, two 12 V batteries were installed. The first battery was installed in the original battery location while the second battery was positioned below the front hood of the ride-on-car after removing the plastic material that interfered the battery installation.
3. Two fuses with fuse holders were mounted near the rear battery. Once the locations for the fuse holders were determined, two 5 mm holes were drilled for each fuse holder and secured with cable tie.
4. The ignition key, motor on/off switches, power consumption meter with shunt resistor were located at the same position as in test 1.
5. The 4-pin relay and motor controller were mounted on the rear side of the car body instead of installing under the driver seat.
6. Then, the required wire lengths were determined by measuring the distance between two connection points. By using the same technique for wiring hardness fabrication in test 1, The connections were completed by referring the wiring diagram in Figure 3.64.

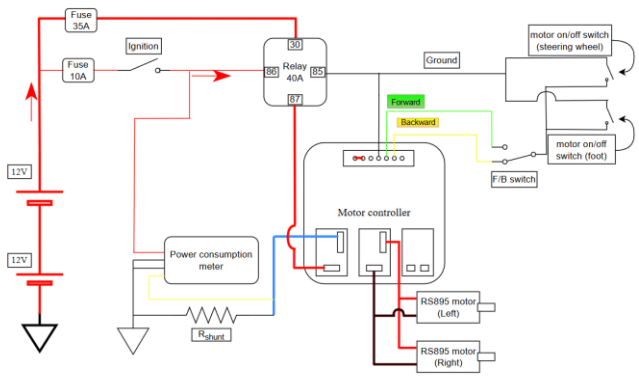

Figure 3.64: 24 V Wiring diagram for modified ride-on-car.

3.9.2 Upgrading internal component and wiring of the motor controller

By referring to Figure 3.66, three capacitors that come from the original motor controller was rated for 25 V with 220 µF and 330 µF. In the latest operating battery voltage, which was total of 24 V nominal voltage and it would become higher than this voltage in reality up to 26 V. According to Figure 3.65, a single bulk capacitor in the motor drive circuit was connected parallel with an output motor and they will receive the same voltage during motor startup (Kinnaird, 2024). Hence, the capacitor voltage rating must be rated above the supply voltage to safely handle the voltage spike (Redaktionsteam, 2025).

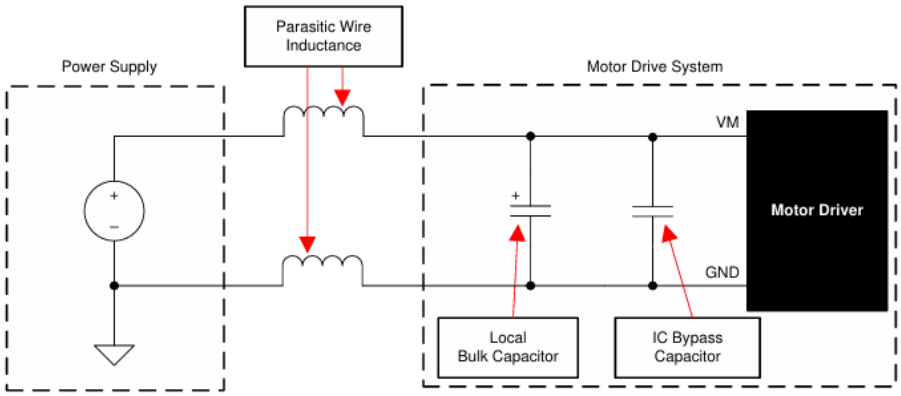

Figure 3.65: Single motor drive circuit (Kinnaird, 2024).

For safety reasons, the capacitor which use to control the soft start function of the dual motor must be changed to higher voltage rating by using the steps below.

1. The motor controller was disassembled and the capacitors were shown in Figure 3.66.

Figure 3.66: Internal component of the motor controller.

2. The original capacitor was removed from the pcb of motor controller by using soldering iron as shown in Figure 3.67.

Figure 3.67: Removing original 25 V capacitor.

3. The capacitor with 50 V with 330 µF was resoldered to the pcb of the motor controller. Based on Figure 3.68, additional soldering tin was added to the shunt resistor in order to allow more current flow to the DC motor.

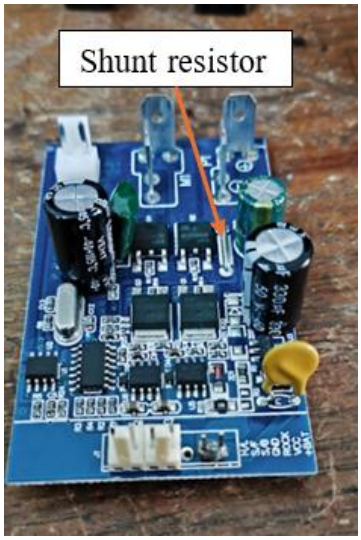

Figure 3.68: Soldering 50V capacitor and shunt resistor.

4. Step 2 to 3 was repeated for the remaining two capacitors with same 50 V with 330 µF specification of capacitors.

5. In the input and output of the motor controller, a 10 awg wire was soldered directly to each pin for dual motor connection and battery input connection. Then, two 12 awg wire (red and black) were soldered to 10 awg wire on the motor output side and two Y-connection was formed.
6. The bullet terminal was crimped on the 4 pcs of 12 awg wire and the negative terminal of motor controller was crimped with a SC6-8 cable lug by using crimper.
7. On the control side of the motor controller, the 7-pin female connector was removed from the pcb board. The VCC and +BAT pin was joint together by using soldering iron.
8. There were only 4 pins being used which were ground, forward, backward and light. However, the light pin was not connected to the lightning system of the car.
9. The pcb female pin was inserted on the 4 pcs 24 awg wire and crimped by using crimper. Then, the female pins could be inserted to the 2-pin connector.
10. Hence, the upgraded motor controller would become as shown in the Figure 3.69 and the entire wiring system would be illustrated in Figure 3.70.

Figure 3.69: Upgraded motor controller.

Figure 3.70: Overall wiring setup for modified ride-on-car.

3.9.3 Second testing on the modified ride-on-car performance

In the test of the modified ride-on-car, same type of test would be carried out like the previous test which consisted of acceleration test and power consumption with same tools and procedures. In this section, parking basement would also be used for the test with same track length and procedure to conduct the test.

3.9.3.1 Acceleration test of 24 V mod ride-on-car

In the acceleration test, the procedures below showed the steps required to perform the test.

1. A straight route with a distance of 13 m was measured.
2. The starting point and ending point were marked by referring the parking space line.
3. When the car was positioned at the starting point, the accelerometer in the GPS application was calibrated and pressed start logging button. The top speed reading in another application was calibrated to zero before the test.
4. The phone's stopwatch was started when the test began.
5. When the car passed through the ending point, the data logging was stopped and the time was recorded.
6. The test was repeated for 3 times to get the average result.

3.9.3.2 Power consumption with modified powertrain

In this section, the track length was also using 27 m in the circular route as shown in the Figure 3.63. The number of laps to undergo the test was equal to 5 and the following section was the process to perform the test.

1. Before the test start, the required track length in the parking basement was measured using measuring tape.
2. 1 to 2 laps were used to familiar the track and the latest setup of the car in order to obtain the consistent lap time.
3. Power consumption meter was set 0 before the test start.
4. Stopwatch was pressed when the driver has ready for the real 5 laps and the time per lap was recorded.
5. After 5 laps, the power consumption reading was recorded and the temperature of the motor was measured.

CHAPTER 4

RESULT AND DISCUSSION

4.1 Comparison between original and reinforce (with strut bar) steering linkage assembly.

Due to the camber change was too high, the steering linkage mounting location has also been deformed and causing the entire wheels and turning rods assembly could be steered left and right easily.

Figure 4.1: Movement (free play) of turning rod and wheel assembly due to excessive camber increment.

By using 2 steel block, aluminium lower and upper strut bar as the reinforcement of the steering linkage assembly, the camber change has been minimized by visual inspection when the car was loaded with driver as shown in the Figure 4.2.

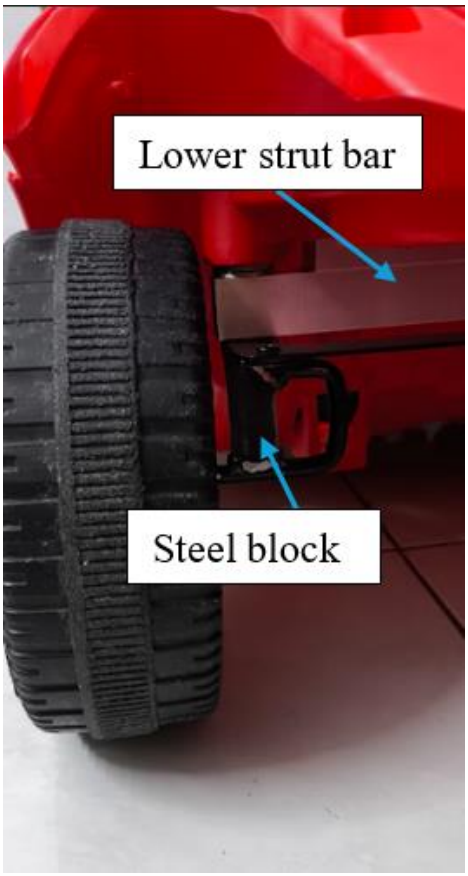

Figure 4.2: Camber change under load after reinforced steering assembly.

Figure 4.3 demonstrates the static wheel camber angle changing direction for configuration 1, 2 and 3. Configuration 1 represents the original assembly without applying the load while 2 and 3 represents the wheel angle changes with respect to datum X. Point 1 and point 2 represent the distance between two strut mounting point (edge to edge distance) when viewed from 2D. When the load was applied onto the ride-on-car, the edge to edge distance was measured by using the measuring tape with the distance of 373 mm and 377 mm for X_2 and X_3 respectively as shown in Figure 4.4. Hence, the relative change of the reinforcement steering linkage to the configuration that without aluminium strut bar could be calculated as shown in the step below.

If edge to edge distance is X, the relative change of distance is,

$$relative\ change\ distance, X = \frac{X_{after} - X_{before}}{X_{before}} \times 100\% \qquad (4.1)$$

Consider the configuration 2 and 3 where the steering linkage assembly without and with the reinforcement respectively. The relative change of distance X_2 and X_3 is given by,

$$X = \frac{X_3 - X_2}{X_2} \times 100\% \tag{4.2}$$

Thus,

$$X = \frac{377 - 373}{373} \times 100\% \tag{4.3}$$

$$X = 1.07\% \tag{4.4}$$

In short, the result indicated that around 98.93% of free play has been eliminated via the new aluminium strut bar design.

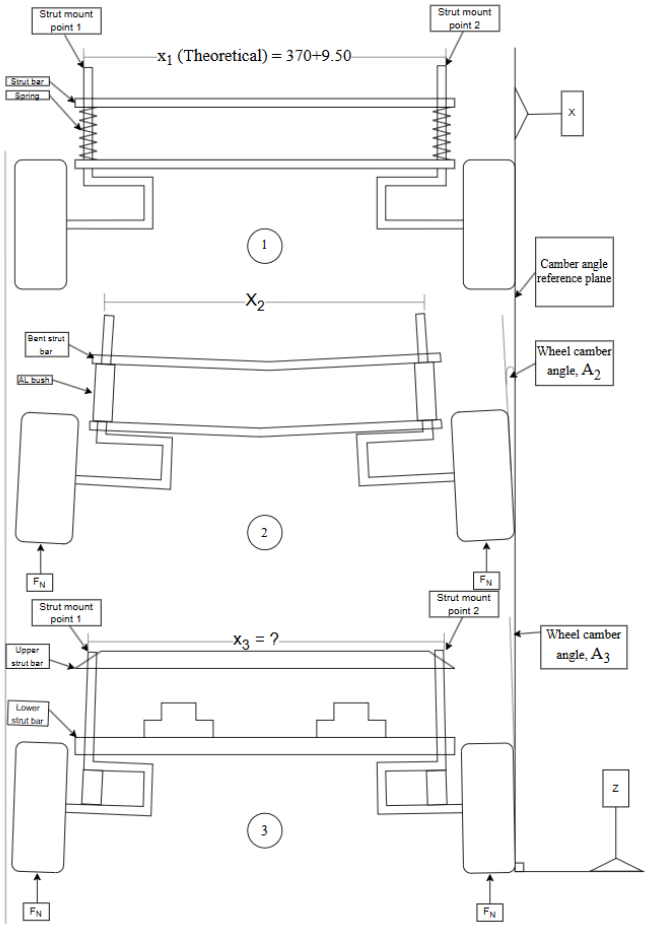

Figure 4.3: Wheel camber angle diagram (Front view of the car)

Figure 4.4: Edge to edge distance measurement without strut bar (upper portion) and with strut bar (lower portion).

On the other hand, the camber angle was also measured by using the camber angle application shown in Figure 4.5 and Figure 4.6 for left wheel and right wheel.

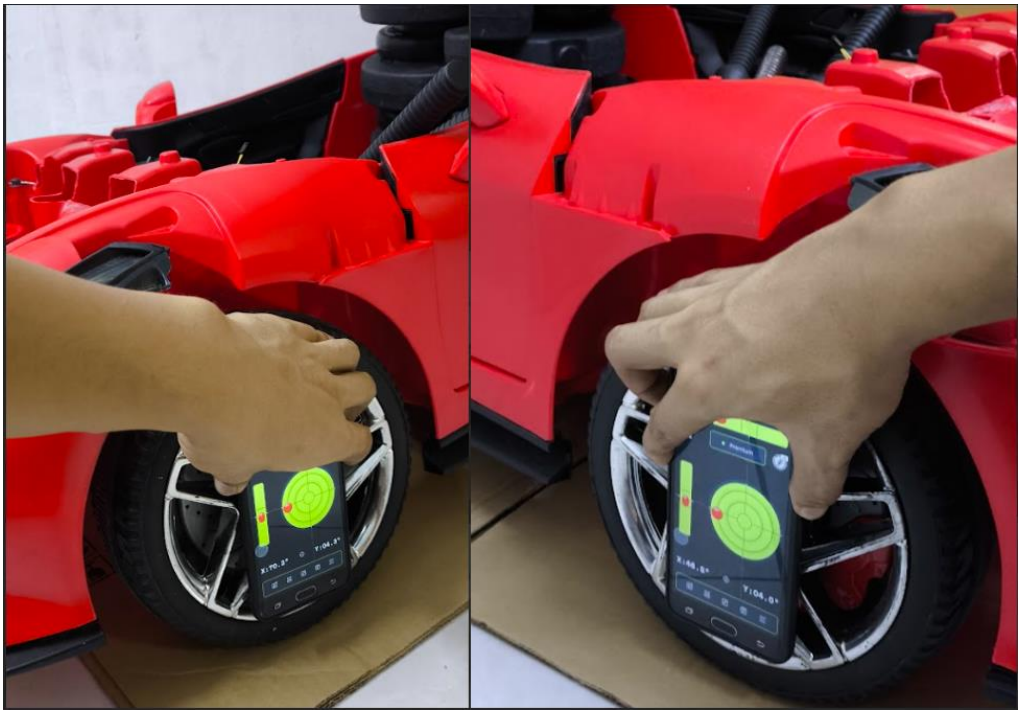

Figure 4.5: Wheel camber measurements without aluminium strut bar (1eft and right wheel).

Figure 4.6: Wheel camber measurements with aluminium strut bar (1eft and right wheel).

Table 4.1: Camber angle measurements data.

Front wheel camber angle	Wheel camber without aluminium strut bar, A_2	Wheel camber with aluminium strut bar, A_3
Left	4.3°	0.9°
Right	4°	1.0°

For left wheel, the relative change of camber angle, A_L can be calculated as,

$$A_L = \frac{A_3 - A_2}{A_2} \times 100\% \tag{4.5}$$

$$A_L = \frac{0.9 - 4.3}{4.3} \times 100\% \tag{4.6}$$

Hence,

$$A_L = -79.07\% \tag{4.7}$$

Same process was done for right wheel's relative change of camber angle, A_R and hence,

$$A_R = -75.00\%$$

In short, both front left and right wheels' camber change has been reduced about 79.07% and 75% for left and right wheels respectively.

4.2 Comparison between original rear shaft assembly and reinforced version rear shaft assembly

Figure 4.7 below showed the experiment setup of the deflection of the original rear shaft assembly by using measuring tape. The car was loaded with 80 kg of dead weight.

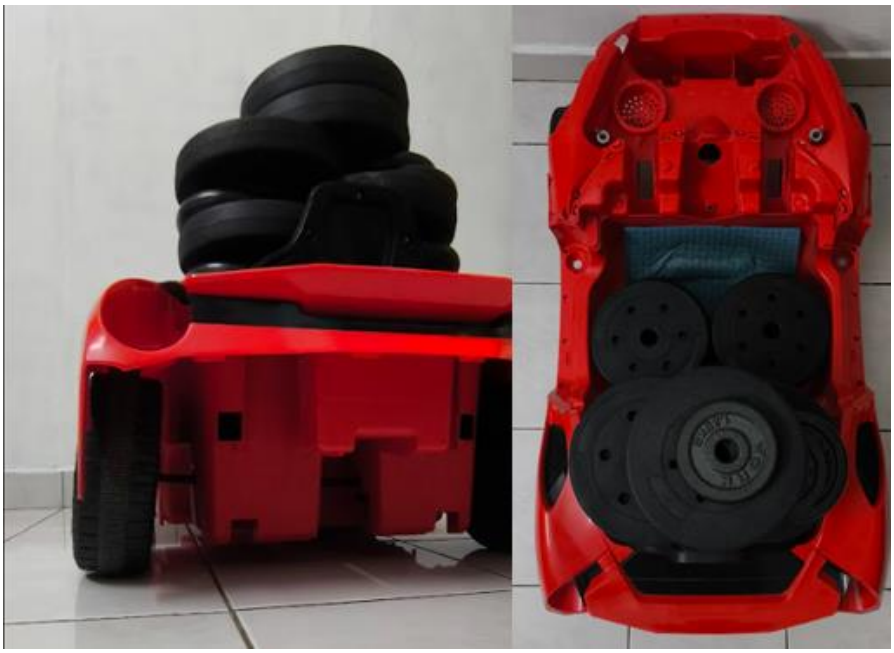

Figure 4.7: Experiment setup for rear shaft deflection measurement.

The distance measured from the floor (datum) to the wheel centre was equal to 115 mm as shown in Figure 4.8. After the car was loaded with 80 kg of dead weight, the measured distance was 100 mm from the floor to the upper surface of the 9.5 mm rear shaft. By using a simple free body diagram shown in Figure 4.8 to illustrate the deflection of the shaft, the deflection could be obtained by using the steps below,

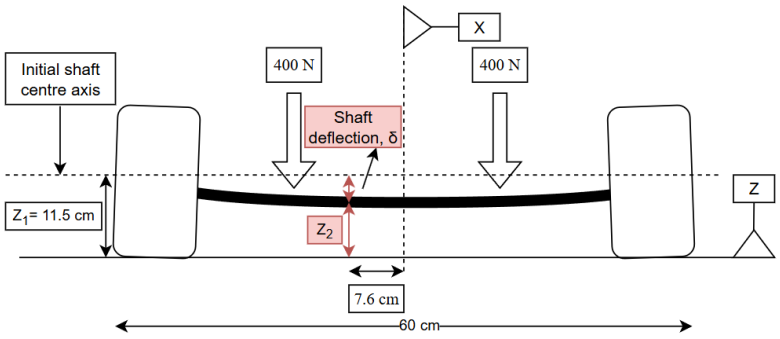

Figure 4.8: Free body diagram of shaft deflection.

$$shaft\ deflection, \delta = z_1 - z_2$$

Where,

z_1 - the distance from the floor (datum) to the wheel centre.

z_2 – the distance from the floor to the upper surface of the rear shaft

Thus,

$$\delta = (115) - [100 - \left(\frac{9.5}{2}\right)]$$

$$\delta = 19.75\ mm\ (shaft\ deflection)$$

Figure 4.9: Result for shaft deflection from unload to loaded with 80 kg weight.

Figure 4.10: Result for shaft deflection after changing to 16 mm shaft (115 mm from datum).

$$\delta = (115) - [115 - \left(\frac{16}{2}\right)]$$

$$\delta = 8\ mm\ (shaft\ deflection)$$

As a result, the shaft deflection measured from datum Z was reduced from 19.75 mm to 8 mm as shown in Table 4.2 and the rear wheels no longer rubbing with the car body under heavy load.

Table 4.2: Summary of the shaft deflection for original and upgraded version assembly.

	Original assembly (9.5 mm diameter shaft)	Upgraded assembly (16 mm diameter shaft)
Shaft deflection (mm)	19.75	8

4.3 Weight distribution test result before and after installation of reinforcement components.

Figure 4.11 showed the weight distribution at the front left (FL), front right (FR), rear left (RL) and rear right (RR) of the ride-on-car before installing the reinforcement components, with and without driver (load). According to the measurement, the total weight of the car was 16.9 kg without driver and 103.95 kg with the driver. The results indicated that the majority of the weight (68.6 kg) was distributed to the rear of the car when the driver was seated. Consequently, the overall weight distribution of the car that included the driver was 34:66, meaning that 34% of the total weight was carried by the front and 66% by the rear.

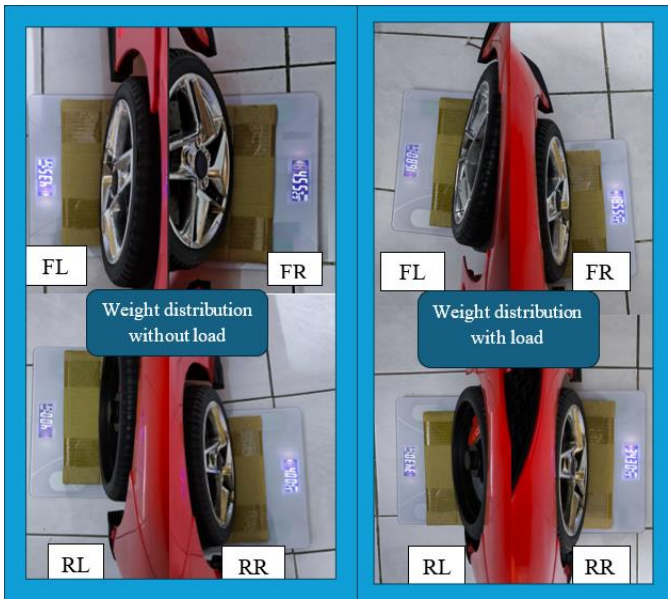

Figure 4.11: Weight distribution diagram before the installation of reinforcement components.

After the car has been upgraded to stronger front and rear assemblies compared to the original setup, the total weight of the car alone had increased to 23.8 kg without the driver and 119.45 kg with the driver weight as shown in Figure 4.12. The new weight distribution of the car with the driver has become 39:61. Where about 61% of the total weight concentrated at the rear of the car with driver. These results indicated that the weight distribution approached a 40:60 ratio after installing the critical reinforcement components. A summary of the results was presented in the Table 4.3 and Table 4.4.

Figure 4.12: Weight distribution diagram after suspension reinforcement.

Table 4.3: Weight distribution of the car before upgrading the suspension.

Without load	Mass (kg)		Mass (kg)	With load	Mass (kg)		Mass (kg)
FL	4.35	FR	4.55	FL	16.80	FR	18.55
RL	4.00	RL	4.00	RL	34.30	RL	34.30
Total weight (kg)	16.90			103.95			
Ratio	53:47			34:66			

Table 4.4: Weight distribution of the car after upgrading the suspension.

Without load	Mass (kg)		Mass (kg)	With load	Mass (kg)		Mass (kg)
FL	6.30	FR	6.30	FL	22.95	FR	23.10
RL	5.85	RL	5.35	RL	38.85	RL	34.55
Total weight (kg)	23.80			119.45			
Ratio	53:47			39:61			

4.4 Motor-gearbox specifications

In the stock RS380 motor-gearbox setup, this motor datasheet stated the rated motor no load speed was 17000 rpm with 12 V input voltage. The original gear ratio was also calculated based on the steps and Figure 4.13 below.

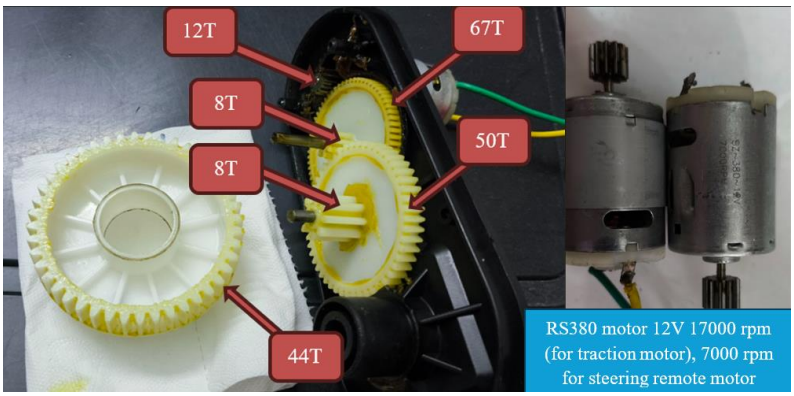

Figure 4.13: Original RS380 motor-gearbox setup.

$$Train\ value, TV = \frac{Product\ of\ driven\ gears\ teeth}{Product\ of\ driver\ gears\ teeth} \tag{4.8}$$

By using equation above, the train value is given by,

$$TV = \frac{67 \times 50 \times 44}{12 \times 8 \times 8}$$
$$TV = 191.93$$

The theoretical angular velocity ω_{out} of the wheel could be obtained as,

$$TV = \omega_{in}/\omega_{out} \tag{4.9}$$
$$\omega_{in} = \frac{2\pi(17000)}{60}$$
$$\omega_{in} = 1780.24\ rad/s$$

Thus, by using equation (4.9(4.9),

$$\omega_{out} = 1780.24/191.93$$
$$\omega_{out} = 9.275\ rad/s$$

The theoretical vehicle speed,

$$v_{max} = r_{wheel}\omega_{out} \tag{4.10}$$

$$v_{max} = 0.1143(9.275)$$

$$v_{max} = 1.060\ m/s$$

$$v_{max} = 1.060\frac{m}{s} \times \frac{3600s}{1h} \times \frac{1km}{1000m}$$

$$v_{max} = 3.816\ km/h$$

Figure 4.14: RS380 motor specification (“3V, 6V, 12V”, n.d.).

On the other hand, the new setup for RS895 motor swap has used different gear ratio than the stock setup. The pinion gear of the motor was using 14T hardened steel gear with module, M1 to match the middle gear. Figure 4.15 depicts the internal geartrain of the modified motor gearbox.

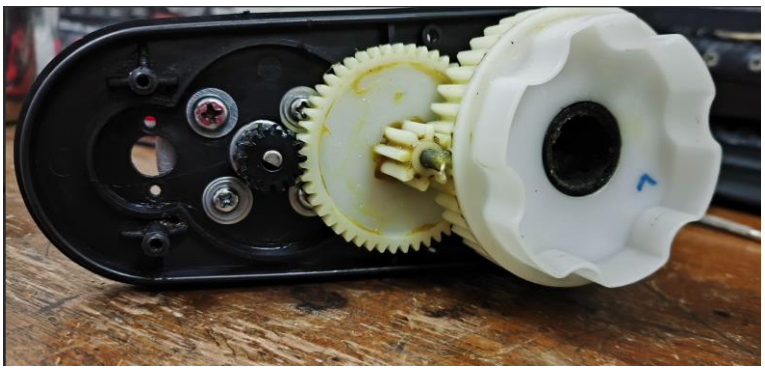

Figure 4.15: First gear deletes RS895 motor gearbox.

When the first gear has been removed, the new train value becomes,

$$TV = \frac{50 \times 44}{14 \times 8}$$
$$TV = 19.64$$

By using the datasheet of the RS895 motor, the rated maximum speed was 6000 rpm at 24V. Hence, the wheel speed could be calculated as shown below,

$$TV = \omega_{in}/\omega_{out}$$
$$\omega_{in} = \frac{2\pi(6000)}{60}$$
$$\omega_{in} = 628.32\, rad/s$$

Thus,

$$\omega_{out} = 628.32/19.64$$
$$\omega_{out} = 31.99\, rad/s$$

The theoretical vehicle speed,

$$v_{max} = r_{wheel}\omega_{out}$$
$$v_{max} = 0.1143(31.99)$$
$$v_{max} = 3.657\, m/s$$

$$v_{max} = 3.657 \frac{m}{s} \times \frac{3600s}{1h} \times \frac{1km}{1000m}$$

$$v_{max} = 13.16\ km/h$$

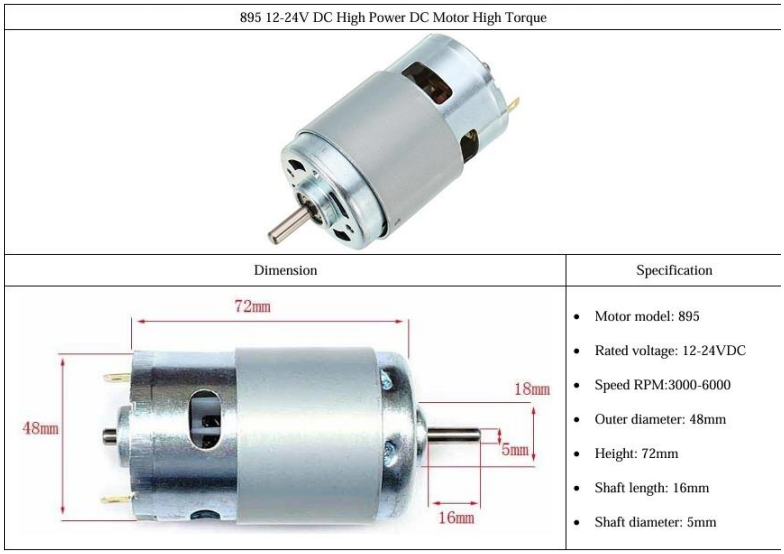

Figure 4.16: RS895 motor datasheet (“3V, 6V, 12V”, n.d.).

4.5 First testing result (stock powertrain)

By referring to Figure 4.17, the acceleration test of the stock ride-on-car was done by repeating 3 times in a 13-meter-long route at the subbasement parking.

Figure 4.17: Acceleration test for 0-13 meters.

In the acceleration testing, the result was captured by using phone's stopwatch and phone's GPS apps shown in Figure 4.18 and the result was recorded as shown in the Table 4.5.

Table 4.5: Acceleration test result.

Test (0-13 m)	Time (s)
1	21.45
2	20.16
3	21.32
Average time	20.98
Top speed (km/h) from GPS	3

Figure 4.18: Maximum speed of the car from GPS speedometer apps.

The next result measured was the total power draw (peak value) based on the power consumption meter reading. When the car was stationary, the total power draw was equal to 1.19 W at 12.5 V of battery voltage. However, the voltage drops to 11.9 V with the peak power of 67.4 W when the car has launched for 3 to 4 seconds. This was also equal to 33.7 W power input per motor approximately. Finally, the power input to the dual RS380 motor was fluctuating about 40 to 46 W when the ride on car reached constant speed.

Figure 4.19: Power reading when the car starts to move for 3 to 4 second.

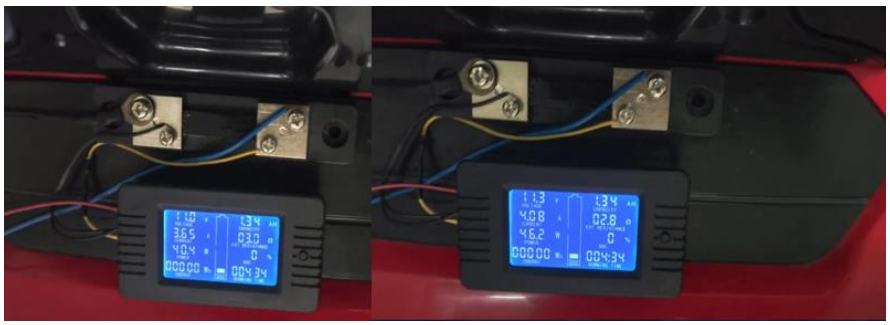

Figure 4.20: Power reading when the car reached constant speed.

Furthermore, the result for g-force values were recorded by using another GPS application during 3 acceleration tests shown in

Table 4.6. The results demonstrated the relationship between the car's g-force over a time interval. The GPS application measured the resultant g-force, which included components in the X, Y and Z directions. This was also indicating that the acceleration of the car due to gravity was also incorporated into the resultant g-force. The value obtained was the experimental results and it represented time required by the car to achieve maximum of torque during the acceleration from standstill condition. The graph further indicated that the ride-on-car that equipped with a 12 V dual RS380 motor setup was capable of generating a maximum g-force in the range of 0.05 g to 0.13 g during 3 to 5 seconds. It was also predicted that the peak torque did not occur immediately after the motor on/off switch was triggered as the motor controller itself contained the soft start features initially.

Table 4.6: G-force measurement from 0-25 seconds.

	Resultant G-force (g)			
Time, t (s)	1	2	3	Average
0	0	0	0	0.00
1	0.01	0.01	0.02	0.01
2	0.01	0.01	0.02	0.01
3	0.08	0.04	0.03	0.05
4	0.12	0.11	0.15	0.13
5	0.1	0.14	0.14	0.13
6	0.05	0.07	0.08	0.07
7	0.06	0.08	0.07	0.07
8	0.09	0.06	0.07	0.07
9	0.07	0.07	0.08	0.07
10	0.08	0.05	0.05	0.06
11	0.08	0.08	0.05	0.07
12	0.08	0.05	0.05	0.06
13	0.07	0.08	0.06	0.07
14	0.03	0.03	0.06	0.04
15	0.02	0.06	0.06	0.05
16	0.01	0.04	0.04	0.03
17	0.04	0.02	0.02	0.03
18	0.01	0.03	0.05	0.03
19	0.02	0.03	0.03	0.03
20	0.02	0.03	0.03	0.03
21	0.02	0.03	0.02	0.02
22	0.01	0.01	0.01	0.01
23	0.01	0.01	0.01	0.01
24	0.01	0.01	0.01	0.01
25	0.01	0.01	0.01	0.01

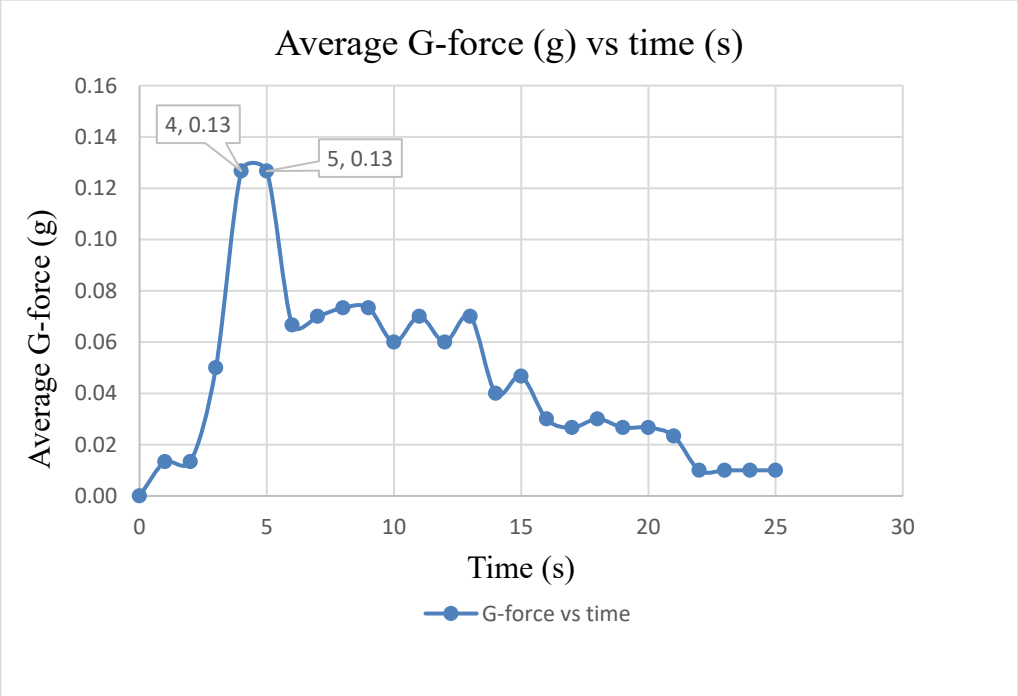

Figure 4.21: Graph of average g-force versus time in stock condition.

Assume that the maximum speed (v_{max}= 3 km/h) of the ride-on-car occur at t= 5 second when the peak g-force has occurred. The acceleration of the car in 1 dimension, a_x can be calculated as,

$$maximum\ speed, v_{max} = 5\ km/h$$

$$v_{max} = \frac{3km}{1\ h} \times \frac{1000\ m}{1\ km} \times \frac{1\ h}{3600\ s}$$

$$v_{max} = 0.83\ m/s$$

Acceleration in x-direction is given by,

$$a_x = \frac{\Delta v}{t} \tag{4.11}$$

$$a_x = \frac{0.83 - 0}{5}$$

$$a_x = 0.167\ m/s^2$$

Figure 4.22 illustrated the combined version of kinematic and free body diagram of the ride-on-car. Since the car was dual rear wheel drive motor, the traction force would be provided at the rear of the car, which was equal to $2F_{RT}$. The car was tested inside the parking basement which the floor was made from concrete instead of tarmac. Hence, the traction force could be calculated as shown in the step below.

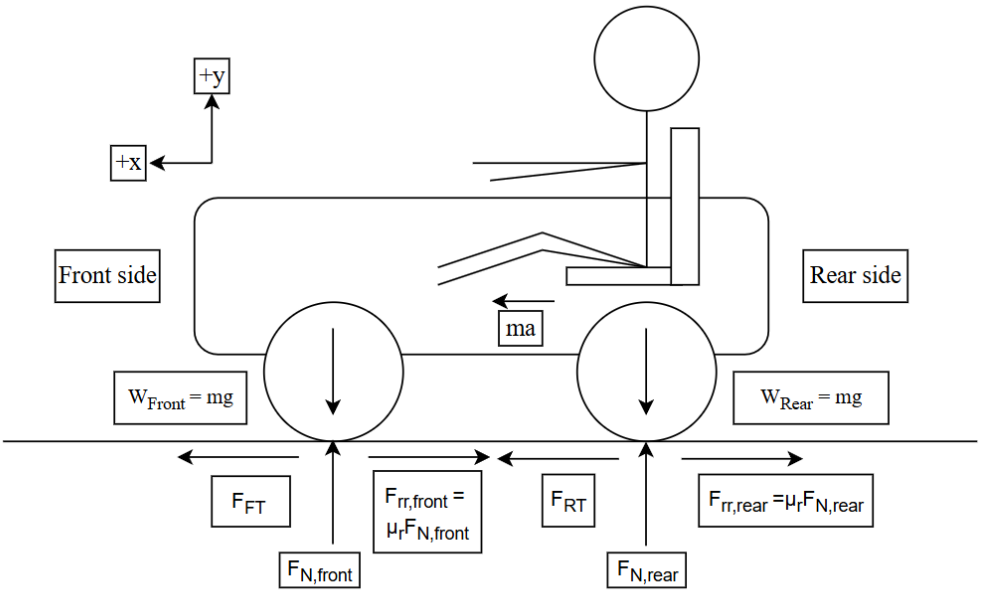

Figure 4.22: Kinematic and free body diagram of ride-on-car.

The rear tractive force, F_{RT} provided by dual RS380 motor was calculated based on equation (4.12),

$$\sum F_x = ma \tag{4.12}$$

$$2F_{RT} - 4F_{rolling\ resistance} = ma_x$$

$$F_{rolling\ resistance} = \mu_r F_N$$

Where F_N was the normal force that located at the front wheel and rear wheel. The additional mass, m_1 would be the mass from dual RS380 motor-gearboxes and a 12 V battery located at the rear.

$$Additional\ mass, m_1 = 2.35\ kg$$

$$Total\ mass, m = 119.45 + 2.35 = 121.8\ kg$$

Rolling resistance, μ_r when the was moving with certain speed could be obtained by following relationship,

$$\mu_r = \mu_0 + \mu_1 v_x^2\ (Jazar, 2008, pp\ 119, eqn\ 3.76) \tag{4.13}$$

Assume that the $\mu_0 = 0.02$ for concrete road in poor condition based on Figure 4.23 and constant value $\mu_1 = 7 \times 10^{-6} s^2/m^2$ (Jazar, 2008, pp 119, eqn 3.78). When, the car was moving in top speed which was 5 km/h or 1.39 m/s. By using equation (4.13), the rolling resistance, μ_r is given by,

$$\mu_r = (0.02) + (7 \times 10^{-6})(1.39)^2 = 0.02$$

Since the car's weight distribution ratio was 39:61 which was 39% of total weight and 61% of the total weight at the rear. The rolling resistance (rr) could be divided into front and rear part which were $F_{rr,front}$ and $F_{rr,rear}$ shown in equation (4.14) and (4.15).

$$F_{rr,front} = \mu_r F_{N,front} \tag{4.14}$$

$$F_{rr,front} = (0.02)(0.39 \times 121.8)(9.81) = 9.32\ N$$

For the rear rolling resistance,

$$F_{rr,rear} = \mu_r F_{N,rear} \tag{4.15}$$

$$F_{rr,rear} = (0.02)(0.61 \times 121.8)(9.81) = 14.58\ N$$

Rewrite the newton equation,

$$2F_{RT} - 2F_{rr,front} - 2F_{rr,rear} = ma_x \tag{4.16}$$

$$2F_{RT} = ma_x + 2F_{rr,front} + 2F_{rr,rear}$$

Then, the total rear traction force becomes,

$$2F_{RT} = (121.8)(0.167) + 2(9.32) + 2(14.58)$$
$$2F_{RT} = 68.14\ N$$

Table 3.1 - The value of μ_0 on different pavements.

Road and pavement condition	μ_0
Very good concrete	0.008 – 0.1
Very good tarmac	0.01 – 0.0125
Average concrete	0.01 – 0.015
Very good pavement	0.015
Very good macadam	0.013 – 0.016
Average tarmac	0.018
Concrete in poor condition	0.02
Good block paving	0.02
Average macadam	0.018 – 0.023
Tarmac in poor condition	0.23
Dusty macadam	0.023 – 0.028
Good stone paving	0.033 – 0.055
Good natural paving	0.045
Stone pavement in poor condition	0.085
Snow shallow (5 cm)	0.025
Snow thick (10 cm)	0.037
Unmaintained natural road	0.08 – 0.16
Sand	0.15 – 0.3

Figure 4.23: Initial rolling resistance coefficient value, μ0 (Jazar, 2008, pp 121, table 3.1).

The wheel torque could be obtained as shown below based on equation (4.17),

$$T_w = 2F_{RT} r_{wheel} \quad (4.17)$$
$$r_{wheel} = 0.1143\ m$$
$$T_w = 68.14(0.1143)$$
$$T_w = 7.788\ Nm$$

For the on-wheel power can be calculated by using equation (4.18),

$$P_w = T_w \omega \quad (4.18)$$

By converting wheel speed into angular speed,

$$v = r\omega$$

$$\omega = \frac{0.83}{0.1143} = 7.26\ rad/s$$

$$P_w = T_w\omega = 7.788 \times 7.26$$

$$P_w = 56.54\ W$$

Thus, efficiency, η of the whole powertrain was,

$$\eta = \frac{P_w}{P_{in}} \times 100\% \tag{4.19}$$

$$\eta = \frac{56.54}{67.40} \times 100\%$$

$$\eta = 83.89\ \%$$

Figure 4.24 below showed the second top speed test to ensure the data accuracy in the same parking basement. However, the GPS app was showing the top speed of the 12 V setup ride-on-car was able to reach 5 km/h which was slightly higher than the result shown in Figure 4.18 and theoretical top speed calculated in equation (4.10). If using the data measured on the second top speed measurement and repeated the calculation steps above, the efficiency of the whole powertrain would be higher than 100 % which was not possible as maximum efficiency could only cap at 100 %. Consequently, the GPS top speed measurement was low in accuracy at the parking basement and 3 km/h was selected as it more near to the theoretical top speed.

Figure 4.24: Second top speed test for checking the data accuracy.

Based on the result obtained, the spec of the 12V stock ride-on-car could be summarised as shown in Table 4.7,

Table 4.7: Summary of the powertrain performance at stock condition.

	Result
Top speed (km/h)	3
0-3 km/h	5 seconds
Total wheel torque (Nm)	7.788 Nm
Total wheel power (W)	56.54 W
Wheel horsepower (whp)	0.076 hp
Efficiency	83.89 %

Furthermore, the power consumption test has also been conducted after the acceleration test as shown in Figure 4.25. Table 4.8 below represented the results of power consumption test for a total of 27 m/lap track for 5 laps. The recorded results showed that the total power consumed after running for 5 laps was equal to 2 Wh based on the power consumption meter reading as shown in Figure 4.26. The average lap time recorded was 39.91 seconds.

Figure 4.25: Power consumption test for 5 laps.

Table 4.8: Lap time in power consumption test.

Lap	Time (s)	Power consumption per lap (Wh/lap)	Cumulative Power consumption (Wh)
1	40.53	0.41	0.41
2	39.70	0.40	0.81
3	39.18	0.39	1.20
4	39.68	0.40	1.60
5	40.44	0.41	2.00
Total time (s)	199.53	-	
Average time (s)	39.91	-	
Total track length (m)	27.00		
Power consumption (Wh)	2.00		
Average power per length (Wh/m)	0.01481		
Average power per second (Wh/s)	0.01002		

Figure 4.26: Power consumption of the ride-on-car after 5 laps.

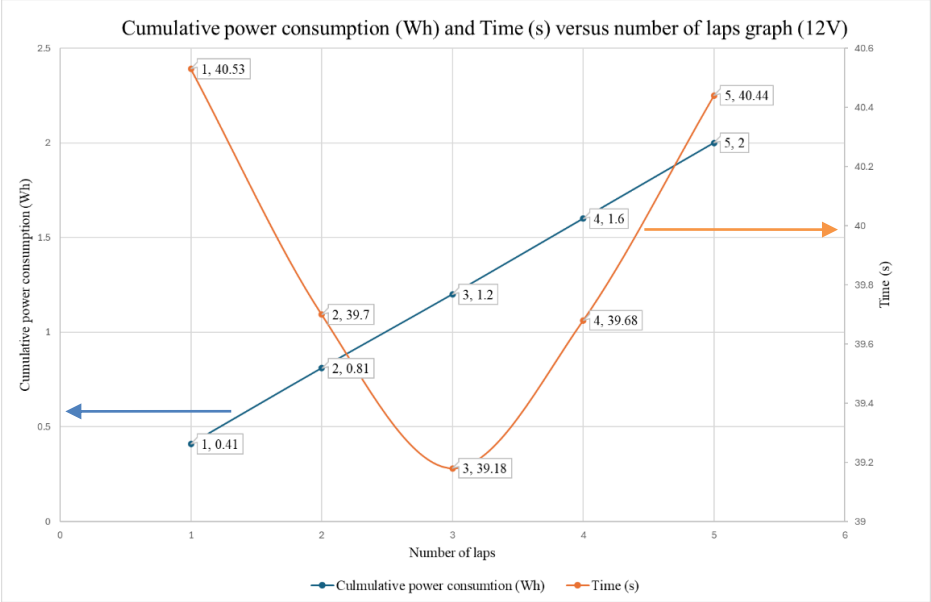

Figure 4.27: Cumulative power consumption (Wh) and time (s) versus number of laps graphs (12V).

Based on the battery specifications which was 12 V with 7 Ah. Thus, the theoretical battery watt hour could be obtained as shown in below,

$$Watt\ hour = Amp\ hour \times Voltage$$

$$Watt\ hour = 84\ Wh$$

The theoretical ride-on-car maximum distance could travel was,

$$Maximum\ distance, d_{max} = 84\ Wh \times \frac{1m}{0.01481\ Wh}$$

$$d_{max} = 5670\ m$$

Next, after the test has been completed, the motor temperature that has been measured which was equal to 44℃ as shown in Figure 4.28.

Figure 4.28: Motor temperature measurement after the first test.

4.6 Second testing result (modified powertrain)

After the ride-on-car has been modified with 24 V system, the acceleration test has been carried out in parking basement also as shown in Figure 4.29.

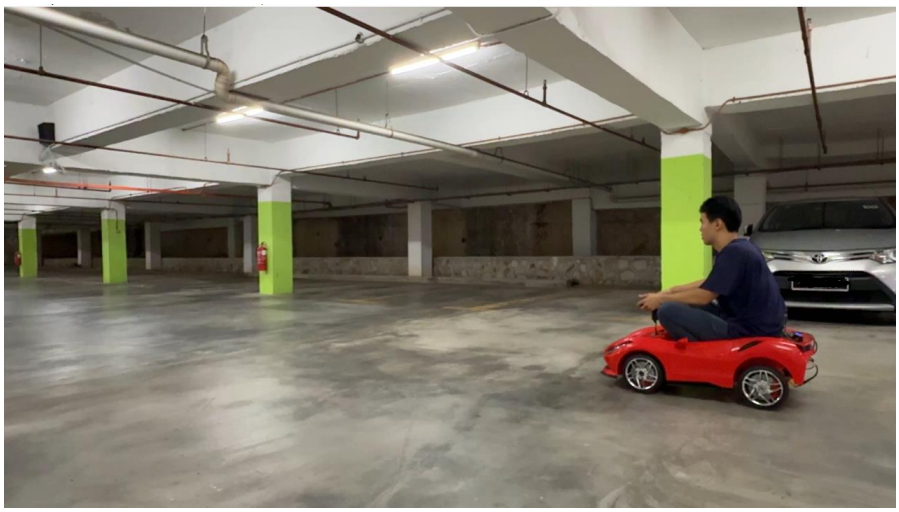

Figure 4.29: Acceleration test for the modified ride-on-car.

In the acceleration test, the top speed of the modified ride-on-car was equal to 11 km/h as shown in Figure 4.30 below by using the GPS application. In this testing, the 13 m long straight road was used and the time required for the ride-on-car start from 0 to 13 m was recorded in Table 4.9.

Table 4.9: Acceleration test result.

Test (0-13 m)	Time (s)
1	5.57
2	5.72
3	6.43
Average time	5.91
Top speed (km/h) from GPS	11

Figure 4.30: Top speed measurement result from GPS app.

On the other hand, the subsequent results obtained were the peak power reading from the power consumption meter. According to Figure 4.31, the peak power recorded was 761 W for 1 to 2 seconds after starting from stationary The initial voltage recorded by the meter was 25 V, which dropped to 22 V when the peak power was reached. This indicated that the peak power per motor was approximately 380.5 W. When the car has reach constant speed, the power drawn by the dual RS895 motors fluctuated between 400 to 500 W.

Figure 4.31: Peak power reading from stationary condition.

Figure 4.32: Power reading when the car run in constant speed.

In addition, g-force logging data were recorded to estimate the time at which the peak power occurred under heavy load conditions. Based on the Table 4.10, the average peak G-force was equal to 0.22 g when the car starts to move from the starting line when time, t equal 2 seconds. The record value also shown that the G-force value was vary from 0.09 to 0.33 g from 7 seconds onward until 9 second in test 1. This was due to the vibration in the car persisted even after the throttle padel has been released.

Table 4.10: G-force measurement from 0-11 seconds.

	Resultant G-force (g)			
Time (s)	1	2	3	Average
0	0	0	0	0.00
1	0.05	0.03	0.03	0.04
2	0.27	0.19	0.21	0.22
3	0.25	0.27	0.14	0.22
4	0.25	0.22	0.16	0.21
5	0.19	0.17	0.01	0.12
6	0.10	0.15	0.01	0.09
7	0.33	0	0.07	0.13
8	0.11	0.04	0.06	0.07
9	0.09	0.04	0.07	0.07
10	0.03	0.12	0.05	0.07
11	0	0.04	0.02	0.02

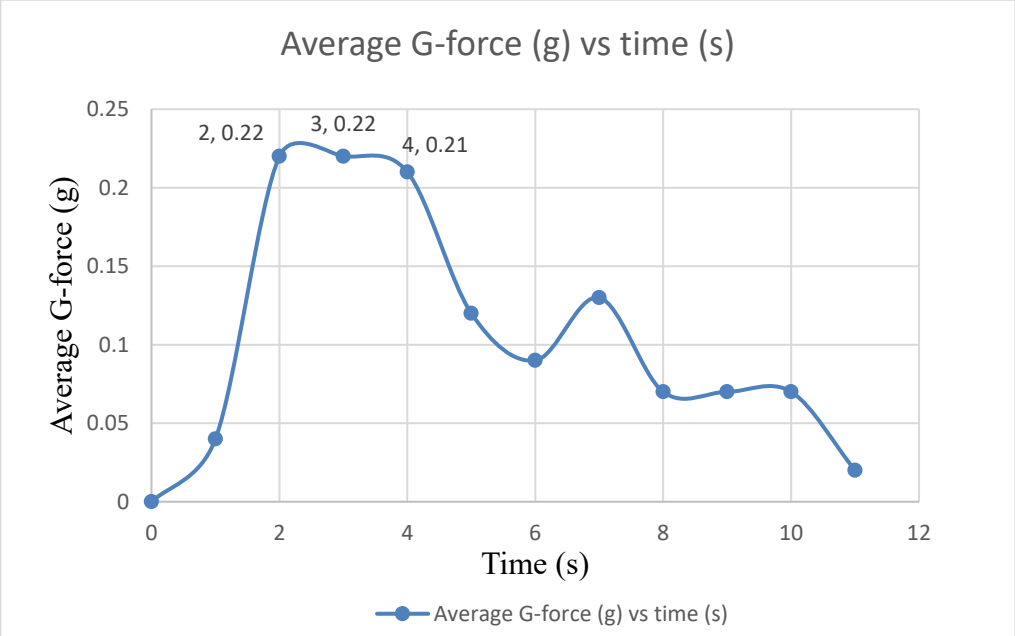

Figure 4.33: Average G-force vs time graph for modified ride-on-car.

Assume the top speed of the ride-on-car (v_{max}= 11 km/h) occur when the time, t = 3 s, the acceleration of the car in x-direction could be obtained as shown below,

$$v_{max} = \frac{11km}{1h} \times \frac{1000m}{1km} \times \frac{1h}{3600s}$$

$$v_{max} = 3.06\ m/s$$

$$a_x = \frac{3.06 - 0}{3}$$

$$a_x = 1.02\ m/s^2$$

The tractive force provided by dual RS895 motor could be obtained by following equation same as equation (4.12),

$$\sum F_x = ma$$

The additional mass, m_1 would be the mass from dual RS895 motor-gearboxes and two 12 V battery. One of the batteries was put at the front of the car and the rest still maintain at the rear side.

$$Additional\ mass, m_1 = 5.05\ kg$$
$$total\ mass, m = 119.45 + 5.05 = 124.50\ kg$$

After adding one 12 V battery at the front of the car, the new weight distribution ratio would become, 38:62. By using the same rolling resistance, μ_r formula in equation (4.13),

$$\mu_r = \mu_0 + \mu_1 v_x^2$$
$$\mu_r = (0.02) + (7 \times 10^{-6})(3.06)^2 = 0.02$$

By using the front rolling resistance formula shown in equation (4.14),

$$F_{rr,front} = (0.02)(0.38 \times 124.50)(9.81) = 9.282\ N$$

For the rear rolling resistance which mentioned in equation (4.15),

$$F_{rr,rear} = \mu_r F_{N,rear}$$
$$F_{rr,rear} = (0.02)(0.62 \times 124.50)(9.81) = 15.14N$$

Rewrite the newton equation,

$$2F_{RT} - 2F_{rr,front} - 2F_{rr,rear} = ma_x$$
$$2F_{RT} = ma_x + 2F_{rr,front} + 2F_{rr,rear}$$

Then, by using equation above the total rear traction force becomes,

$$2F_{RT} = (124.50)(1.02) + 2(9.282\ ) + 2(15.14)$$
$$2F_{RT} = 175.83\ N$$

The wheel torque could be obtained as shown below by using equation (4.17),

$$T_w = 2F_{RT} r_{wheel}$$
$$r_{wheel} = 0.1143\ m$$

$$T_w = 175.83(0.1143)$$
$$T_w = 20.10\ Nm$$

For the on-wheel power from equation (4.18),

$$v = r\omega$$
$$\omega = \frac{3.06}{0.1143} = 26.77\ rad/s$$
$$P_w = T_w\omega = 20.10 \times 26.77$$
$$P_w = 538.00\ W$$

By using efficiency, η equation (4.19), the powertrain efficiency was,

$$\eta = \frac{P_w}{P_{in}} \times 100\%$$
$$\eta = \frac{538}{761} \times 100\%$$
$$\eta = 70.70\ \%$$

Based on the result obtained, the spec of the 24V mod ride-on-car could be summarised as shown in Table 4.11,

Table 4.11: Summary of the powertrain performance at modified condition.

	Result
Top speed (km/h)	11
0-11 km/h	3 seconds
Total wheel torque (Nm)	20.10
Total wheel power (W)	538.00
Wheel horsepower (whp)	0.7212
Efficiency (%)	70.70

Moreover, the following testing would be the power consumption test with the modified ride-on-car after the acceleration test as shown in Figure 4.34.

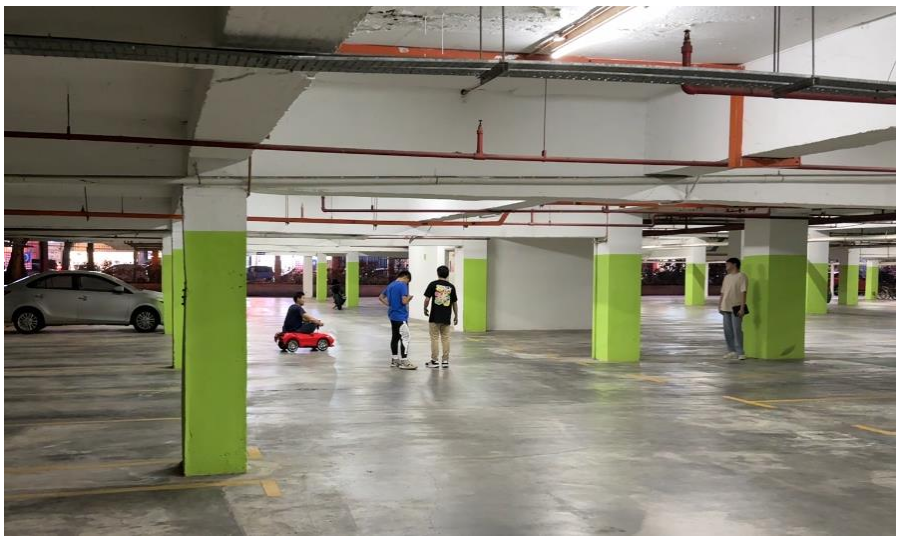

Figure 4.34: Power consumption test for the mod ride-on-car.

Table 4.12 shows the results of power consumption test for a total of 27 m long of track per lap for 5 laps. It was recorded that the total power consumed after running for 5 laps was equal to 19 Wh based on the power consumption meter reading shown in Figure 4.35. The average time per lap was equal to 17.36 seconds.

Table 4.12: Lap time in power consumption test.

Lap	Time (s)	Power consumption per lap (Wh/lap)	Cumulative power consumption (Wh)
1	19.62	4.30	4.3
2	17.51	3.83	8.13
3	16.21	3.55	11.68
4	17.54	3.84	15.52
5	15.90	3.48	19
Total time (s)	86.78	-	
Average time (s)	17.36	-	
Total track length (m)	27.00		
Power consumption (Wh)	19.00		
Average power per length (Wh/m)	0.1407		
Average power per second (Wh/s)	0.2189		

Figure 4.35: Power consumption of the modified ride-on-car after driving for 5 laps.

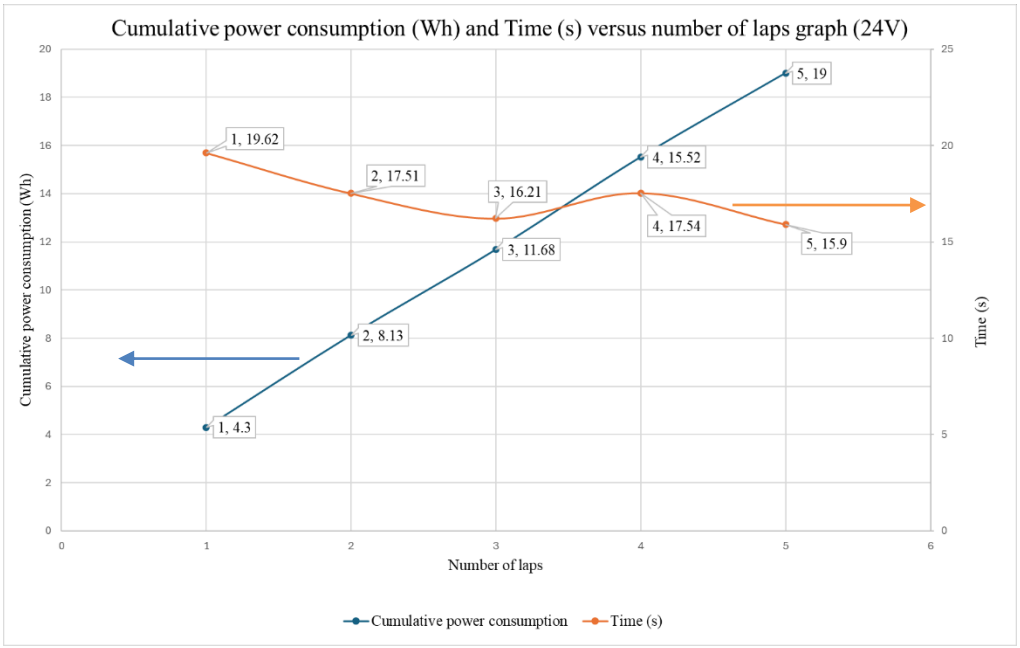

Figure 4.36: Cumulative power consumption (Wh) and time (s) versus number of laps graphs (24V).

Based on the battery specifications which was 12 V with 7 Ah and total of 2 batteries being used in series. Thus, the theoretical battery watt hour could be obtained as shown in below,

$$Watt\ hour = Amp\ hour \times Voltage$$

$$Watt\ hour = 7 \times 24$$

$$Watt\ hour = 168\ Wh$$

The theoretical ride-on-car maximum distance could travel was,

$$Maximum\ distance, d_{max} = 168\ Wh\ \times \frac{1m}{0.1407\ Wh}$$

$$d_{max} = 1193.68\ m$$

Next, after the test has been completed, the motor temperature that has been measured which was equal to 57℃ as shown in Figure 4.37.

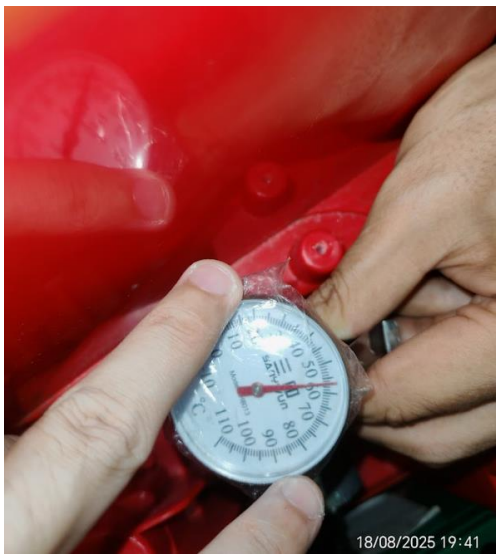

Figure 4.37: Motor temperature measurement after the second test.

4.7 Comparison of the stock and modified ride-on-car specifications

After all the necessary values were recorded in test 1 and test 2. A summary of improvements and changes has occurred on the modified ride-on-car was represented in Table 4.13. According to average time recorded for 0-13 m in acceleration test, the time has been shortened greatly from 20.98 seconds to 5.91 seconds. By combining the graph shown in Figure 4.21 and Figure 4.33, Figure 4.38 was obtained as shown in below. The graph showing that the 24V setup has the greater peak resultant G-force (peak torque) of 0.22 g than 12V setup which was 0.13 g. This value depicts the 24 V setup's peak torque occur around 2 to 3 seconds and the peak torque for 12 V setup occur slightly slower

which was 4 to 5 seconds. Figure 4.40. This was the expected result as the rated motor power output was higher than the stock motor.

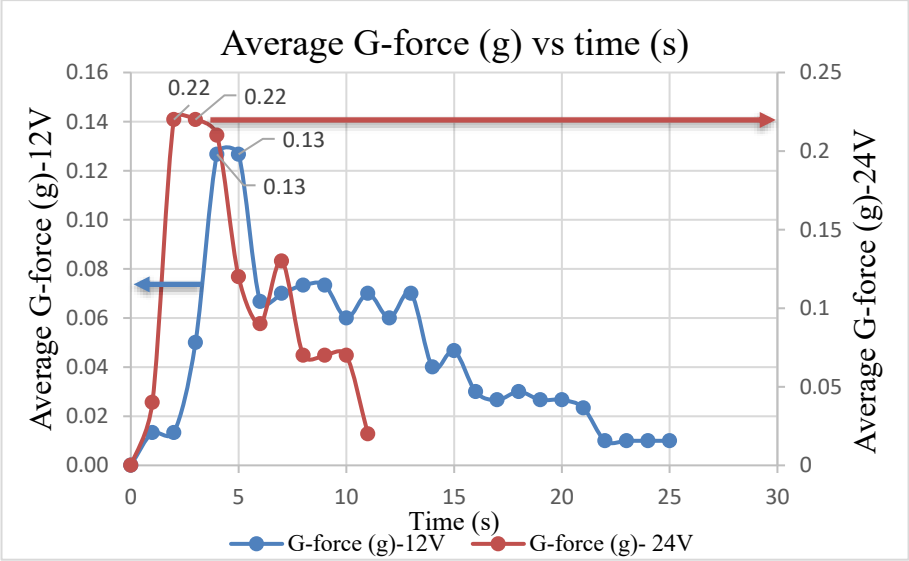

Figure 4.38: Combined graph for acceleration test for 12V and 24V setup.

Similarly, the average lap time was also reduced sharply from 39.91 seconds to 17.36 seconds as shown in Table 4.13. These results could also be further illustrated based on the graph shown Figure 4.39. The lap time during this test was fluctuating between 39.18 to 40.53 seconds and 15.90 to 19.62 seconds for 12 V and 24 V setup respectively. However, the total power consumption of 24 V (19 Wh) was higher than 12 V setup (2 Wh). These improvements were consistent with the motor specifications provided by the manufacturer where a single RS380 motor was capable of producing a peak power of 40 W and the RS895 motor produced a peak power of 360 W. Consequently, the power consumption result and acceleration test result proof that the ride-on-car improved significantly in terms of performance.

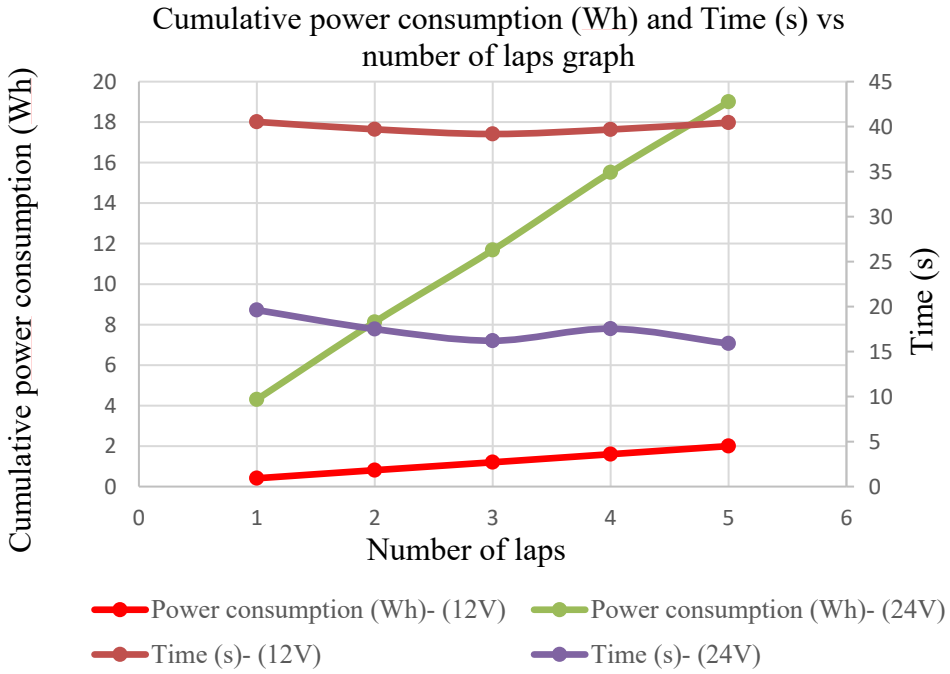

Figure 4.39: Combined graph for power consumption test for 12V and 24V setup.

In contrast, the power efficiency chart shown in Figure 4.40 illustrated that the 24 V setup was 13.19 % less efficient than the 12 V stock setup which was a negative impact for this modification plan. Not only this, but the consequence of using bigger motor was the temperature of the motor itself become higher which increased from 44 °C to 57 °C based on Table 4.13. This showed that the 24 V setup was generating more heat than stock 12 V configuration setup and the power consumption per meter of the ride-on-car increased from 0.0148 Wh/m to 0.1407 Wh/m. This was showing that the effect of using bigger motor was the power consumption would be increased significantly. The increase in motor temperature also indicated that more heat was generated due to the decrease in powertrain efficiency from 83.89 % to 70.70 % and the motor was running slightly out of its efficiency range. However, this could also be due to measuring equipment error as elaborated in the following paragraph.

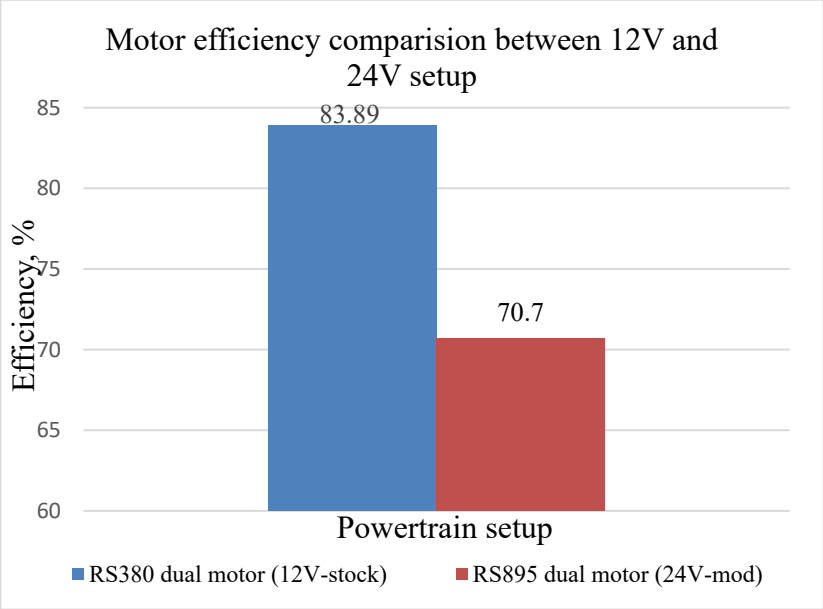

Figure 4.40: Comparison of motor power efficiency between 12 V and 24 V powertrain setup.

GPS calculates speed by measuring how the ride-on-car position changes over time using satellite signals. In ideal conditions, such as under open sky, well-designed GPS receivers are accurate to about 3 m or 95 % of accuracy (5 % GPS error), while smartphones are typically accurate within 4.9 m on a horizontal road. Factors such as the number and distribution of satellites, signal reflections from buildings or trees and atmospheric disturbances can all reduce accuracy. As long as the GPS signal was stable, the speed accuracy would be within about 0.2 km/h ("Why GPS, OBD", n.d.). Moreover, the conducted acceleration test in parking basement with top speed measurement was utilising the GPS application which could lead to positional error which could translate to speed inaccuracies. The data concluded such as wheel power and efficiency for the ride-on-car in Table 4.13 was calculated based on vehicle dynamic equation by using the top speed measured which were 3 km/h and 11 km/h. As illustrated based on Figure 4.24, a slight change of top speed could result in tremendous changes of efficiency which was higher than 100 % efficiency. Due to the accuracy of the GPS reading and this could explain the reason of the efficiency was decreasing for 24 V setup testing in another parking basement. Supposing, the efficiency should be higher than 70.70 % as all the powertrain setup was the same except swapping

to RS895 motor and first gear delete gearbox. Decreasing in number of gears in the gearbox with higher motor torque should improve the gearbox efficiency with higher top speed than 11 km/h and hence the overall powertrain efficiency should be higher.

Table 4.13: Comparison of performance for stock and modified ride-on-car.

Parameter	Stock (12 V- dual RS380 motor)	Mod (24 V- dual RS895 motor)
Average time (s) for 0-13 m	20.98	5.91
Top speed (km/h)	3	11
Theoretical top speed (km/h)	3.816	13.16
Acceleration time (s)	5	3
Average lap time (s) for 27 m	39.91	17.36
Gear ratio	191.93:1	19.64:1
Total wheel torque (Nm)	7.788	20.10
Total wheel power (W)	56.54	538.00
Wheel horsepower (whp)	0.0758	0.7212
Power consumption per meter (Wh/m)	0.0148	0.1407
Power consumption (Wh)	2	19
Efficiency (%)	83.89	70.70
Temperature (°C)	44	57

In addition, by using the ±5 % error of the smartphone GPS speed reading, the improvement range of the could be obtained based on step below. The top speed measured for the 12 V setup is 3 km/h and the highest and lowest possible speed is given by,

$$Highest\ possible\ speed, v_{max,12V} = 3 + (3 \times 5\%) = 3.15\ km/h$$

$$Lowest\ possible\ speed, v_{min,12V} = 3 - (3 \times 5\%) = 2.85 km/h$$

For the 24 V, the recorded top speed was 11 km/h,

$$Highest\ possible\ speed, v_{max,24V} = 11 + (11 \times 5\%) = 11.55\ km/h$$
$$Lowest\ possible\ speed, v_{min,24V} = 11 - (11 \times 5\%) = 10.45\ km/h$$

Thus, the improvement of the speed can be further divided into 2 categories which included highest speed gain and lowest speed gain. For the first scenario, highest speed gain was comparing the relative change of highest possible speed for 24 V and lowest possible speed 12 V,

$$Relative\ change\ of\ highest\ speed\ gain, \frac{v_{max,24V} - v_{min,12V}}{v_{min,12V}}$$
$$= \frac{11.55 - 2.85}{2.85} = 3.05$$

For the comparison of lowest possible speed for 24 V and highest possible speed for 12 V, the relative change is given by,

$$Relative\ change\ of\ lowest\ speed\ gain, \frac{v_{min,24V} - v_{max,12V}}{v_{max,12V}}$$
$$= \frac{10.45 - 3.15}{3.15} = 2.32$$

Based on the GPS measurement and calculation above with an assumed ±5% error margin, the ride-on-car's top speed improvement can be further expressed as a range rather than a single fixed value. At the lower bound, when the modified car's speed was underestimated and the stock car's speed was overestimated, the performance gain was approximately 2.32 times. At the upper bound, when the modified car's speed was overestimated and the stock car's speed was underestimated, the gain increases to about 3.05 times. This indicated that, even when accounting for potential GPS inaccuracies, the modification consistently demonstrated a significant improvement in speed performance, confirming the effectiveness of the design changes.

By using the 4 possible speed, the efficiency of the car could be obtained by using the identical steps in section 4.5 and section 4.6 by using vehicle dynamic equation and the comparison of the speed gain and relative change and powertrain efficiency was recorded as shown in Table 4.14.

Table 4.14: Relative change of speed gain and efficiency comparison between 2 powertrain setup.

Speed gain	Powertrain setup	Top speed (km/h) with ±5% error margin	Relative change	Efficiency (%)
Highest speed gain	Stock-12 V	2.85	3.05	78.80
	Mod- 24 V	11.55		76.73
Lowest speed gain	Stock-12 V	3.15	2.32	89.73
	Mod- 24 V	10.45		64.58

Figure 4.41 below illustrated the discrepancy of efficiency for stock and mod ride-on-car in 2 categories which were highest speed gain and lowest speed gain. At the highest speed gain, both configurations demonstrated relatively similar efficiency, with values of 78.8% for the 12V system and 76.73% for the 24V system. This indicates that under higher load transmission, the efficiency loss between the two systems was minimal. In contrast, at the lowest speed gain, a significant gap was observed. The 12V configuration achieved an efficiency of 89.73% but the efficiency dropped to 64.58% when using 24V setup. Thus, this result demonstrated that the apparent efficiency of the powertrain was greatly influenced by the stability of the GPS signal used for speed measurement. This also indicated that the current GPS readings shown in Table 4.13 for the ride-on-car were more strongly affected under the low speed gain category, as the limited accuracy of GPS at lower top speed introduced greater measurement uncertainty.

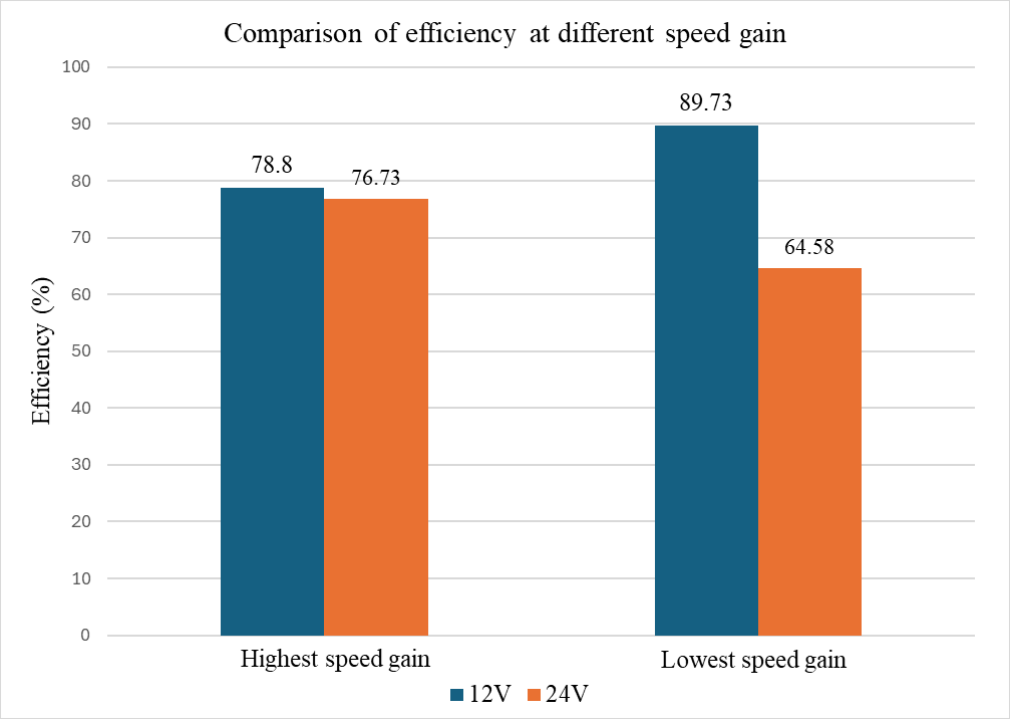

Figure 4.41: Speed gain versus efficiency for 12V and 24V setup.

CHAPTER 5

CONCLUSIONS AND RECOMMENDATIONS

5.1 Conclusions

As a conclusion, the electric ride-on-car that initially manufactured for the kids to play has been successfully reinforced it to enable the adult or young people to drive. By using the fundamental engineering knowledge and skills, both the structure and component of the car were reinforced to withstand higher load while maintaining the required functionality. For example, the issue of excessive camber gain and deflection at the front and rear assemblies was mitigated by installing aluminium strut bars (camber change reduced about 79.07% and 75% for left and right wheels respectively) and enlarging the rear shaft diameter (deflection reduced from 19.75 mm to 8 mm). To achieve higher top speed of the ride-on-car, the motor was swapped with larger size motor with a compatible gear pitch and gear ratio for the modified motor–gearbox assembly. From electrical perspective, the battery voltage was increased from 12 V to 24 V to provide sufficient power to propel the load.

Furthermore, every modification in this project was guided by the important considerations such as safety, cost, simplicity, weight, efficiency, and performance in order to be replicated by the children and high school students. For instance, the steering linkage was reinforced with two aluminium strut bars was due to the cost-effectiveness, strength and lightweight. This was because the aluminium strut bar could be easily fabricated with normal hand tools and minimizing the tool wear despite it was less durable than steel. Nylon wheels bushing were selected was due to the constraint of selecting suitable bearing to fit the 16 mm rear shaft and original plastic wheel housing. Special size bearing was still available in the market, however the price of this type of bearing was expensive than standard size bearing. Alternatively, custom made nylon bush method was chosen due to the cheaper price while offering excellent mechanical material properties.

Last but not least, the weight of the car was increased from 16.90 kg to 23.80 kg due to the reinforcement done on the car. Despite this increased,

significant performance improvements were achieved like the top speed rose from 3 km/h to 11 km/h which were measured by GPS application and the calculated wheel horsepower increased from 0.0758 whp to 0.7212 whp. This result proven that the goal to enhance the performance of the ride-on-car has been achieved based on the data recorded in Table 4.13. However, this result in higher power consumption than 12 V setup, which increased from 0.0148 Wh/m to 0.1407 Wh/m. Due to the instability of GPS signal, the powertrain efficiency was reduced from 83.89% (12 V) to 70.70% (24 V) based on the calculated results. The significance efficiency gap between 12 V and 24 V setup was also attributed from the low speed gain category which obtained from the general percentage error of the phone GPS signal.

Most importantly, the car was able to complete all testing without components failure, demonstrating that the modifications successfully balanced enhanced performance with structural integrity.

5.2 Recommendations for future work

Despite the modified ride-on-car which was originally designed for children has successfully completed the planned tests. However, there were few potential issues could be happening and to be improved in the future. Firstly, the wheels that made from plastic could cause the vibration issue and decrease the drivetrain efficiency for the car. Although the rear wheels were using the custom-made nylon bush and functions as wheel bearing but the wheels could not rotate with full concentricity due to fabrication limitations. As stated in section 3.2.1.2 fabrication process, the nylon bushing was fabricated using lathe machine with relatively low accuracy. During test 2, the steering was observed to be slightly difficult to control when the on/off switch was triggered while cornering. This was mainly due to the insufficient traction of the front tires, which caused understeer when the motor was engaged during cornering. In order to solve these problems, replacing the plastic wheels with rubber wheels equipped with pneumatic tubes and bearing was recommended.

Since the modified gearbox that originally designed for the RS380 motor was using nylon gears, these gears were transmitting higher torque (1 Nm) and power from the RS895 motor (380 W of input power) in the race.

Over time, the nylon gears were likely to wear out rapidly under such conditions. A suitable improvement would be to replace the nylon gears with metal gears that consist of ball bearing and lubricated with high-temperature grease to withstand the increased mechanical stresses. Due to the soft start feature from the motor controller, the motor could only be either turning on or off, the time during cornering has been wasted as the speed of motor could not be controlled. Therefore, a variable speed controller is recommended in the future to control the speed of the motor.

Finally, the current battery setup was using 2 sets of 12 V lead acid battery. Based on prior modifications observed in similar power-wheel applications, lithium-ion battery was selected due to their higher discharge rate, reduced weight and compact size. This eventually can enhance the efficiency of the electric system of the ride-on-car. Therefore, the lighter and smaller size battery with high voltage rating can be done be done in the future work with better motor controller.

CHAPTER 6

REFERENCES

Aarniovuori, L., Cao, W.P., Shah Bukhari, A.A. (2018) 'Review of Electrical Motor Drives for Electric Vehicle Applications'. *Mehran University Research Journal of Engineering & Technology*, vol. 38(3), pp: 526-530. Available at: https://search.informit.org/doi/epdf/10.3316/informit.502648737477789 (Accessed date: 5 March 2025).

Badal. J. (2019) 'Analysis of different powertrain configurations for a formula style electric race car'. *LUND University*, pp. 11-39. Available at: https://upcommons.upc.edu/bitstream/handle/2117/171833/master-thesis.pdf?sequence=1&isAllowed=y (Accessed date: 4 March 2025).

Bellwood. O. (2024). *The Dads Are Taking Their Modded Power Wheels Drag Racing*. Jalopnik. Available at: https://www.jalopnik.com/dad-modifies-power-wheels-to-hit-30-miles-per-hour-and-1851676039/ (Accessed: 2 July 2025).

BENTLEY JE1008-CEN APOCADAY Kids Electric Ride On Car, n.d. Manuals plus. [Online]. Available at: https://manuals.plus/bentley/je1008-cen-apocaday-kids-electric-ride-on-car-manual#assembly_tools_required_not_included (Accessed: 18 September 2025).

"Central Ohio Power Wheels Drag Racing Keeps Growing" (2022). Drag Champion. Available at: https://dragchamp.com/2022/bracket-racing/central-ohio-power-wheels-drag-racing-keeps-growing/ (Accessed: 2 July 2025).

DeLuca, C. (2020) 'DC Dynamic Braking'. *PDHonline Course E246 (4 PDH)*, pp: 1-3. Available at: https://pdhonline.com/courses/e246/e246content.pdf (Accessed date: 24 March 2025).

Electrathon, n.d. Electrathon of Florida. [Online]. Available at: https://electrathonofflorida.org/index.php/about-us/?utm_source (Accessed: 5 September 2025).

EViE – Electric Vehicles in Education, n.d. BUFORI EViE. Available at: https://bufori.com/evie/#:~:text=In%202022%2C%20Bufori%20received%20a,realm%20of%20the%20EViE%20project (Accessed: 18 September 2025).

Hideaki, S., Hiroki, M., Kenichi, H., Mamoru, T., Masahiro, Y., Michiru, H., Norikazu, S., Takaaki, O., Takuya, T., Yasuhiro, O. (2024) 'Visualization of oil-lubrication ball bearings at high rotational speeds'. *Frontiers in Mechanical Engineering*, 10, pp.7-8. Doi: 10.3389/fmech.2024.1416656. (Accessed date: 6 March 2025).

Hindle, C., n.d. Polypropylene (PP). British Plastic Federation. [Online]. Available at: https://www.bpf.co.uk/plastipedia/polymers/PP.aspx (Accessed: 18 September 2025).

"How to Start Modifying Power Wheels and Ride-On Toys" (n.d.). MLToys. Available at: https://www.mltoys.com/pages/how-to-start-modifying-power-wheels-and-ride-on-toys (Accessed: 12 May 2025).

Jazar, R.N. (2008) 'Vehicle Dynamics: Theory and Application*'. Springer*, vol.45(11), pp:38-52. Available at: https://ftp.idu.ac.id/wp-content/uploads/ebook/tdg/TERRAMECHANICS%20AND%20MOBILITY/epdf.pub_vehicle-dynamics-theory-and-application.pdf (Accessed date: 25 March 2025).

Kanzaki, S., Moritomi, S., Watanabe, S., 2010. Polypropylene Compounds for Automotive Applications. Sumitomo Chemical Co., Ltd. Petrochemicals Research Laboratory. [Online]. Available at: https://www.sumitomo-chem.co.jp/english/rd/report/files/docs/01_2010-1e.pdf (Accessed: 18 September 2025).

Kinnaird, C., 2024. Bulk Capacitor Sizing for DC Motor Drive Applications. Texas Instruments. Available at: https://www.ti.com/lit/an/slvaft0/slvaft0.pdf?ts=1759987900598&ref_url=https%253A%252F%252Fwww.google.com%252F#:~:text=Experienced%20engineers%20often%20use%20general,each%20Watt%20of%20motor%20power. (Accessed: 9 October 2025).

Maker Faire Milwaukee (2025). *Power Racing Series Archives*. Available at: https://milwaukee.makerfaire.com/category/power-racing-series/ (Accessed: 12 May 2025).

Melanson, D., 2020. Public-private Partnership to Provide STEM Education Through Electric Vehicles. UKNOW. [Online]. Available at: https://uknow.uky.edu/research/public-private-partnership-provide-stem-education-through-electric-vehicles (Accessed: 18 September 2025).

Mohammed Salah, S. Z. (2009) 'Parameters Identification of a Permanent Magnet Dc Motor'. *The Islamic University of Gaza Deanery of Graduate Studies Faculty of Engineering Electrical Engineering Department*, pp. 11-17. Available at: https://scispace.com/pdf/parameters-identification-of-a-permanent-magnet-dc-motor-2jm6mkxyq3.pdf (Accessed date: 5 March 2025).

Mohd. Ali, S., Mohd. Gausa, P., Mohd. Kaif, S., Zeeshan, S. (2022) 'Determination of Mechanical Properties of ABS Plastic Material used in Automobile Bumper'. *International Journal of Research Publication and Reviews*, 3(5), pp: 3430-3434. Available at: https://ijrpr.com/uploads/V3ISSUE5/IJRPR4395.pdf (Accessed date: 4 March 2025).

Moore, E.L.T., 2024. Max energy: East Central students hone STEM skills as they build electric race cars. San Antonio Express News. [Online]. Available

at: https://www.expressnews.com/news/article/east-central-electric-cars-competition-19946812.php?utm_source (Accessed: 5 September 2025).

Power Racing Series (2025). *Power Racing Series – Growing up is overrated*. Available at: https://powerracingseries.org/ (Accessed: 12 May 2025).

"Power Wheels Racing: The Next Big Thing?" (2019). Drag Champion. Available at: https://dragchamp.com/2019/bracket-racing/power-wheels-racing-the-next-big-thing/ (Accessed: 2 July 2025).

Redaktionsteam, 2025. Capacitor Motor Calculation: This is how you dimension the right capacitor. ATEK. Available at: https://www.atek.de/en/capacitor-motor-calculation-this-is-how-you-dimension-the-right-capacitor/ (Accessed: 9 October 2025).

Sharma, M., 2025. Types of Car Chassis: What They Are & Why They Matter. Spinny Post. Available at: https://www.spinny.com/blog/types-of-car-chassis/#:~:text=Tubular%20chassis%2C%20or%20space%20chassis,realise%20high%20agility%20and%20speed (Accessed: 18 September 2025).

Serteller, N.F., Ustundag, D. (2017) 'Analysis of Dynamic Behavior of Direct Current Motor with Electrical Braking Techniques'. *Marmara University*, pp: 1-7. Available at: https://www.researchgate.net/publication/321319736_Analysis_of_Dynamic_Behavior_of_Direct_Current_Motor_with_Electrical_Braking_Techniques (Accessed date: 24 March 2025).

SLS, 2020. How Ball Bearings Reduce Friction? SLS Bearing. Available at: https://blog.slsbearings.com/how-ball-bearings-reduce-friction (Accessed: 18 September 2025).

"Staged Motor - Gearboxes Explained" (n.d.). MLToys. Available at: https://www.mltoys.com/pages/staged-motor-gearboxes-explained (Accessed: 12 May 2025).

"Understanding EV Technology: Current Trends and Future Prospects" (2024) *Pulse Energy* [online] Available at: https://pulseenergy.io/blog/ev-technology (Accessed: 14 March 2025).

Why GPS, OBD scanner and speedometer show different speed, n.d. HUDWAY. Available at: https://hudway.co/blog/difference-in-gps-obd-and-speedometer-speed-readings (Accessed: 29 September 2025).

Wu, S. (2016a). *Lamborghini Aventador Teardown*. Fictiv. Available at: https://www.fictiv.com/teardowns/lamborghini-aventador-teardown (Accessed: 12 May 2025).

Wu, S. (2016b). *Power Racing Series Build Part 1*. Fictiv. Available at: https://www.fictiv.com/articles/power-racing-series-build-part-1 (Accessed: 12 May 2025).

Wu, S. (2016c). *Power Racing Series Build Part 2*. Fictiv. Available at: https://www.fictiv.com/articles/power-racing-series-build-part-2 (Accessed: 12 May 2025).

Wu, S. (2016d). *Power Racing Series Car Build Part 3: The Bananaghini on the Track*. Fictiv. Available at: https://www.fictiv.com/articles/power-racing-series-car-build-part-3-the-bananaghini-on-the-track (Accessed: 12 May 2025).

Yokota, K. (2020). 'Technological Trends and Outlook of Automotive Bearing'. *JTEKT ENGINEERING JOURNAL English Edition No. 1017E (2020)*, pp. 25-34. Available at: https://www.jtekt.co.jp/e/engineering-journal/assets/1017/1017e_05.pdf (Accessed date: 6 March 2025).

Yu, H.L. (2017). 'Optimal Powertrain Design and Control of an Electric Race Car'. *Politecnico di Milan*, pp. 1-5. Available at: https://www.politesi.polimi.it/handle/10589/134573 (Accessed: 14 March 2025).

12V Kids Electric Ride on Cars Toys Vehicles for Toddlers 1-3 with Remote Control, Licensed Bentley Car for Kids, Power Wheels for Boys Girls to Drive w/Bluetooth/MP3/Light/3 Speeds (Green), n.d. Amazon. Available at: https://www.amazon.com/APOCADAY-Electric-Licensed-Toddlers-Bluetooth/dp/B0CKBPYBRX?th=1 (Accessed: 18 September 2025).

3V, 6V, 12V, 24V, High Speed DC Small Motor RS 130, 140, 180, 260, 280, 300, 310, 365, 380, 385, 390, 395, 500, 545, 550, 555, 775, 795, 895, Basic Info, n.d. SYNACORP Technologies Sdn Bhd. Available at: https://synacorp.my/v3/en/index.php?controller=attachment&id_attachment=691 (Accessed: 23 August 2025).

"7R First Gear Delete & Dual 775 Motor Mounting Plates" (n.d). MLToys. Available at: https://www.mltoys.com/products/7r-first-gear-delete-dual-775-motor-mounting-plates (Accessed: 12 May 2025).

APPENDICES

Appendix A: Detail review diagram for methodology

On the rear side, the two wheels were inserted into the same shaft using a clip mechanism. The bottom casing at the rear served as the support for both the rear shaft and the dual spring system of the ride-on-car as shown in Figure A.1. Each spring had its own base casing and blind hole to allow compression and extension. Indirectly, the spring's base casing exerted pressure on the rear shaft when it was installed at the back of the car as illustrated in Figure A.2.

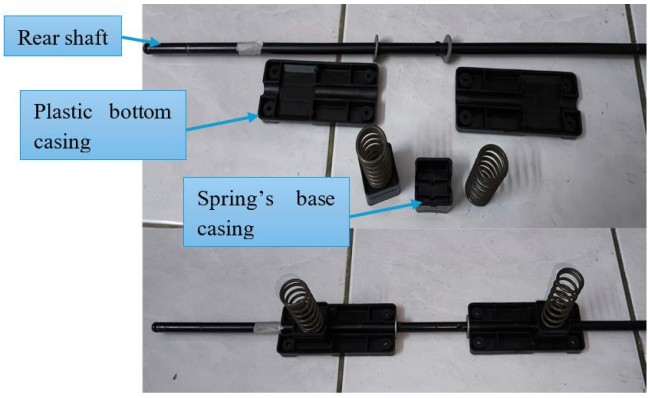

Figure A.1: Suspension part and assembly of rear axle suspension system

Figure A.2: Side view of assembled rear powertrain

The shaft was mounted on the rear section of the car and was produced from mild steel with two axle grooves near each end of shaft which was designed to be inserted clips as shown in Figure A.3. This allowed the shaft to be inserted directly into the wheel using clips alone, without the need of fastener locking mechanisms. Near the center of the shaft, two additional welds were used to secure it to the bottom chassis of the car. A clip holder,

placed on the outside of each wheel, was responsible for retaining the axle grooves in place. Another side of the shaft holder was used to insert and release the rear shaft by pressing and holding the release button as shown in Figure A.4.

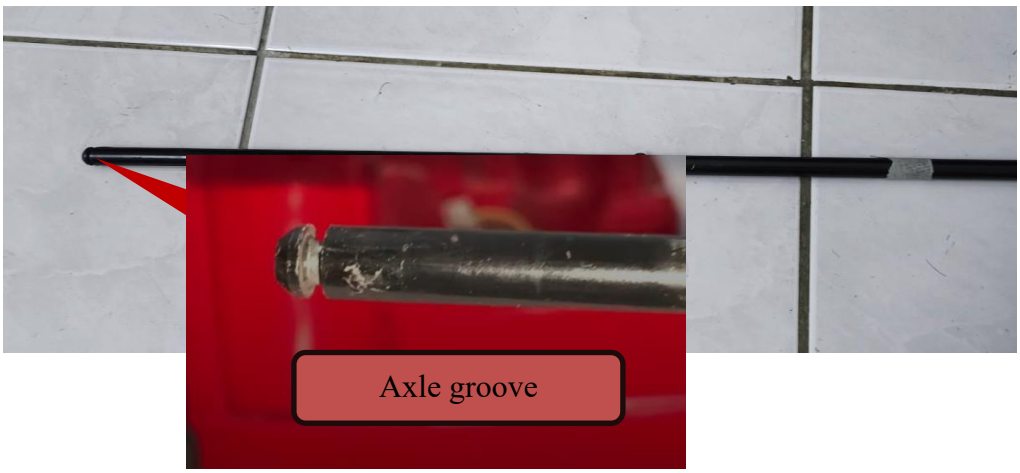

Figure A.3: Rear axle shaft (length: 550mm and diameter: 9.5mm)

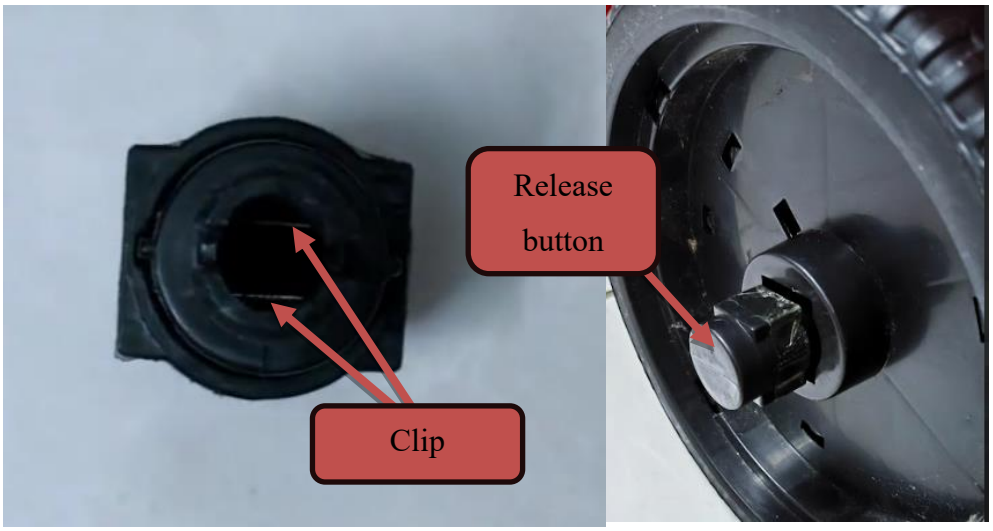

Figure A.4: Axle clip holder

Each wheel has a slot that was designed to attach to the output gear of the gearbox as shown in Figure A.5. The slot on the wheel was intentionally designed with a slightly larger diameter, allowing the wheel to lock securely onto the gearbox gear. At the center of the gearbox casing, a 10 mm diameter through-hole was designed for the shaft to pass through and slide into the wheel where it was secured by the clip holder via the axle groove.

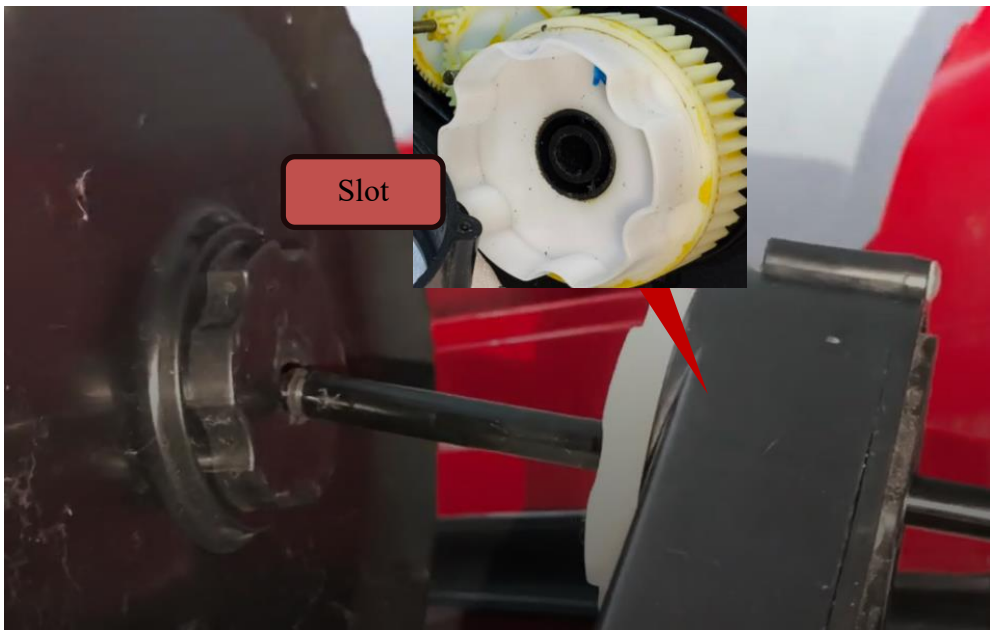

Figure A.5: Illustration of wheel-gearbox attach method

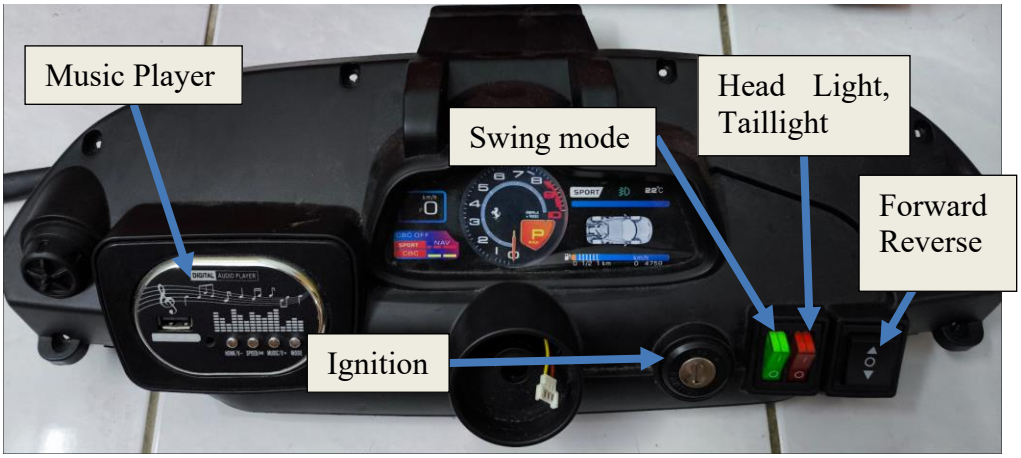

Figure A.6: Detail view of dashboard panel

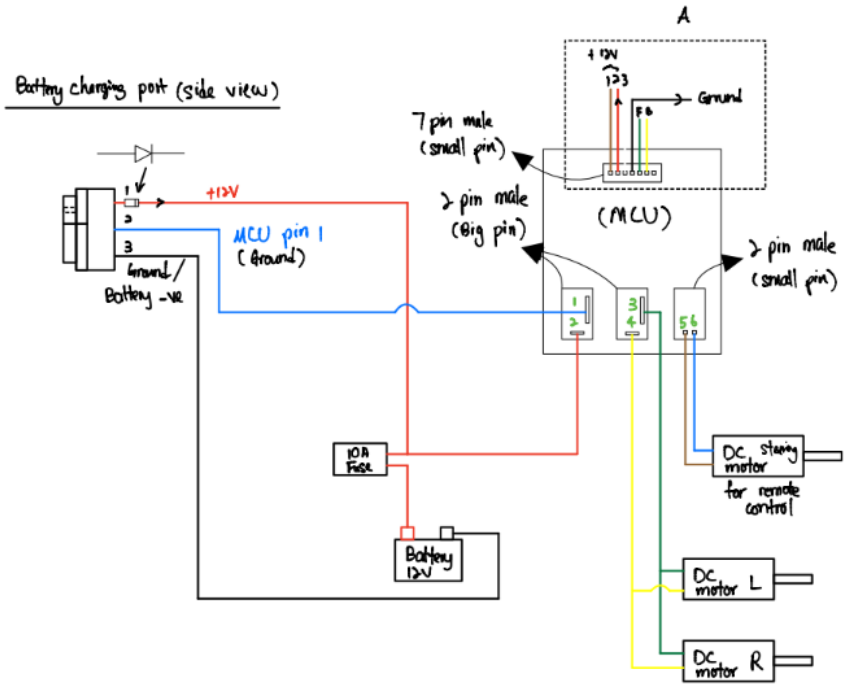

Figure A.7: Original wiring diagram for the car

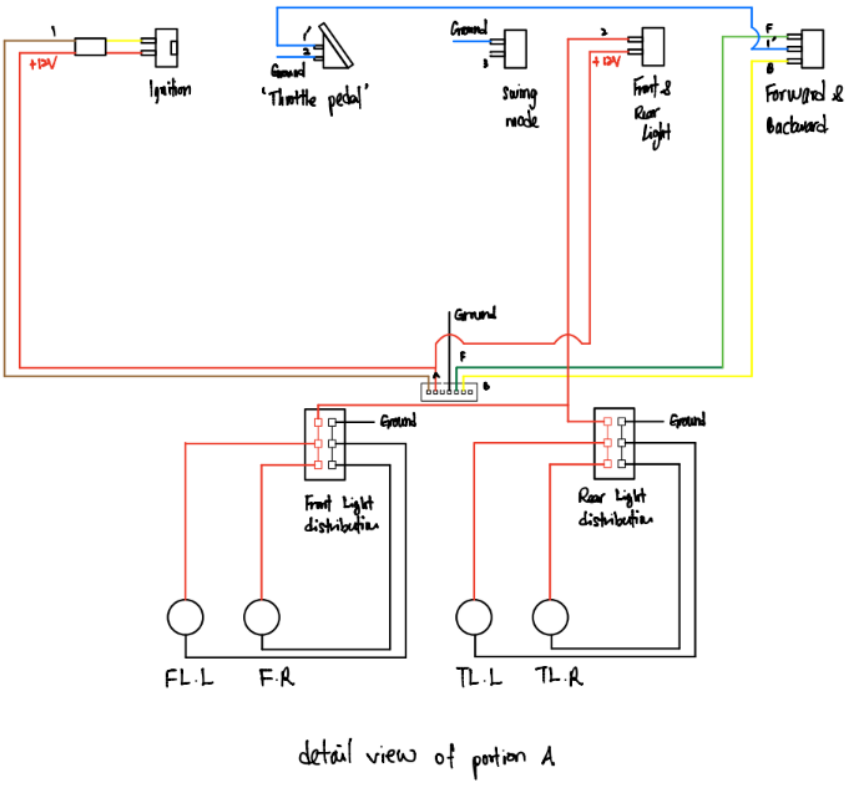

Figure A.8: Detail of wiring diagram for portion A

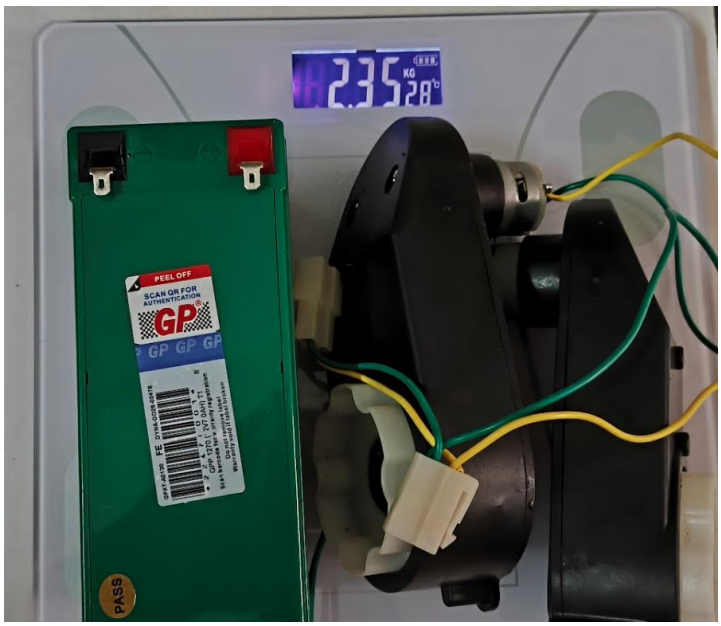

Figure A.9: Stock 12 V motor gearbox weight

Figure A.10: Upgraded 24 V motor gearbox weight

Appendix B: Gantt Chart

Project title: DEVELOPMENT OF AN SMALL ELECTRIC RACE CAR (FYP1)						Feb 2025 Trimester												
No.	Project Activities	Start	End	Duration	Predecessor	W1	W2	W3	W4	W5	W6	W7	W8	W9	W10	W11	W12	W13	W14
1.0	**Problem Formulation & Project Planning**	10/2/2025	28/2/2025	3 week															
1.1	Attend project briefing in Teams.	10/2/2025	14/2/2025	1 week	-														
1.2	Contact the project supervisor for arranging the first meeting about the project.	17/2/2025	21/2/2025	1 week	1.1														
1.3	Research about purchasing the small EV with planned budget	17/2/2025	21/2/2025	1 week	1.1														
1.4	Negotiate about the product's price and identifing small electric car's specification	24/2/2025	28/2/2025	1 week	1.2, 1.3														
1.5	Purchased small electric car	24/2/2025	28/2/2025	1 week	1.2, 1.4														
2.0	**Literature review**	3/3/2025	21/3/2025	3 week															
2.1	Research about the journal to be written in the literature review	3/3/2025	7/3/2025	1 week	1.5														
2.2	Powertrain layout and electric motor review for EV	10/3/2025	14/3/2025	1 week	2.1														
2.3	Research of ABS Material used for electric toys car	10/3/2025	14/3/2025	1 week	2.1														
2.4	Study for the car traction calculation E-book	17/3/2025	21/3/2025	1 week	2.2, 2.3														
2.5	Evaluation of the information that had been reviewed	17/3/2025	21/3/2025	1 week	2.2, 2.3														
3.0	**Identifing the methodology and work plan**	3/3/2025	2/5/2025	9 week															
3.1	Disemble the car for condition investigation	3/3/2025	28/3/2025	3 week	1.5														
3.2	Determine the part of the vehicle that need to be modified first	3/3/2025	7/3/2025	1 week	3.1														
3.3	Preparing several feasible design concept by hand sketching	17/3/2025	21/3/2025	1 week	2.2, 2.3														
3.4	Testing the DC motor speed without load and inverstigate battery condition	31/3/2025	4/4/2025	1 week	3.3														
3.5	Modification plan of DC motor	31/3/2025	4/4/2025	1 week	3.3														
3.6	Designed reinforce bar	7/4/2025	18/4/2025	2 week	3.4, 3.5														
3.7	Material and shape selection for the reinforce bar.	7/4/2025	18/4/2025	2 week	3.4, 3.5														
3.8	Front and rear suspension delete plan	21/4/2025	2/5/2025	2 week	3.6, 3.7														
3.9	Powertrain modification plan	21/4/2025	2/5/2025	2 week	3.6, 3.7														
4.0	**Simulation of design plan**	7/4/2025	2/5/2025	4 week															
4.1	Reinforce bar simulation	7/4/2025	25/4/2025	3 week	3.4, 3.5,3.6,3.7														
4.2	Rear fixed axle suspension simulation	28/4/2025	2/5/2025	1 week	3.9														
5.0	**Report Writing & Presentation**	3/3/2025	9/5/2025	10 week															
5.1	Preparation of Report	3/3/2025	9/5/2025	9 week	1.2														
5.2	Preparation of Presentation	28/4/2025	9/5/2025	2 week	5.1														

Figure B.1: Gantt Chart for FYP 1 February Trimester 2025

Project title: DEVELOPMENT OF AN SMALL ELECTRIC RACE CAR (FYP2)						June 2025 Trimester												
No.	Project Activities	Start	End	Duration	Predecesor	W1	W2	W3	W4	W5	W6	W7	W8	W9	W10	W11	W12	W13	W14
1.0	**Frabrication process for drivetrain**	23/6/2025	18/7/2025	4 weeks															
1.1	Preparing 16 mm rear shaft with require length and thread	23/6/2025	27/6/2025	1 week	-														
1.2	Cutting shaft cover from sheet metal and drilling holes to mount on the car body	23/6/2025	27/6/2025	1 week	-														
1.3	Rebuidling the gearbox with bigger motor	30/6/2025	4/7/2025	1 week	-														
1.4	Welding 16 mm rear shaft on the mild steel shaft cover	30/6/2025	4/7/2025	1 week	1.1,1.2														
1.5	Farbication of wheel bushing and its housing	7/7/2025	18/7/2025	2 weeks	1.4														
2.0	**Installation of drivetrain and electronic parts**	14/7/2025	18/7/2025	1 week															
2.1	Installing the 16 mm rear shaft assembly and wheel bushing assembly	14/7/2025	18/7/2025	1 week	1.4,1.5														
2.2	Assembly of original electronic component and test drive the car	14/7/2025	18/7/2025	1 week	-														
3.0	**Reinforcement of steering linkage assembly**	21/7/2025	1/8/2025	2 weeks															
3.1	Fabrication on upper and lower strut bar by using aluminium hollow square bar	21/7/2025	25/7/2025	1 week	2.2														
3.2	Reinforce the steering turning rod	21/7/2025	25/7/2025	1 week	2.2														
3.3	Reposition of steering coloumn and steering wheel	28/7/2025	1/8/2025	1 week	3.1,3.2														
3.4	Test drive the car to ensure the reinforcement was done correctly	28/7/2025	1/8/2025	1 week	3.1,3.2,3.3														
4.0	**First testing on the stock ride on car**	4/8/2025	15/8/2025	2 weeks															
4.1	Acceleration test and power consumption test	4/8/2025	8/8/2025	1 week	3.4														
4.2	Fabrication of 24V system wiring hardness with proper wiring route	11/8/2025	15/8/2025	1 week	4.1														
4.3	Remove the stock motor and swap with bigger motor with first gear delete	11/8/2025	15/8/2025	1 week	4.1,4.2														
5.0	**Second testing on the modified car**	18/8/2025	22/8/2025	1 week															
5.1	Acceleration test and power consumption test for modride on car	18/8/2025	22/8/2025	1 week	4.2,4.3														
6.0	**Completion of Project**	23/6/2025	26/9/2025	14 weeks															
6.1	Report Writing	23/6/2025	29/8/2025	10 weeks	-														
6.2	Preparation of Poster	25/8/2025	29/8/2025	2 weeks	1.0,2.0,3.0,4.0,5.0														
6.3	Preparation of Presentation	8/9/2025	26/9/2025	3 weeks	6.1,6.2														

Figure B.2: Gantt Chart for FYP 2 June Trimester 2025

Appendix C: Engineering drawing for fabrication part

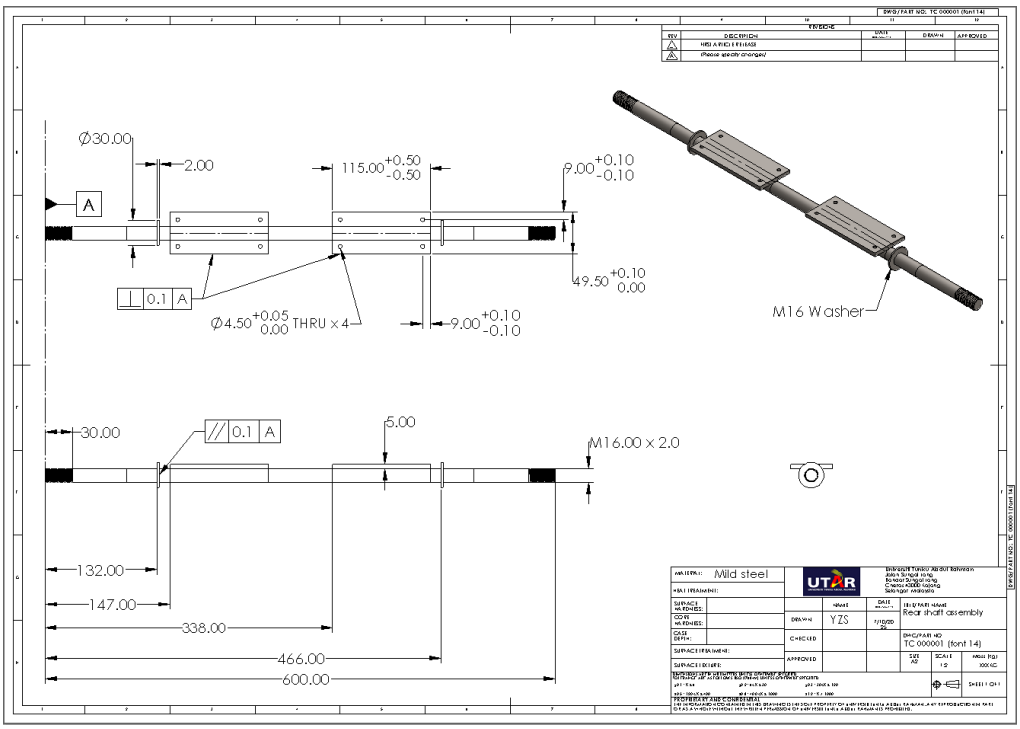

Figure C.1: 16 mm rear shaft assembly

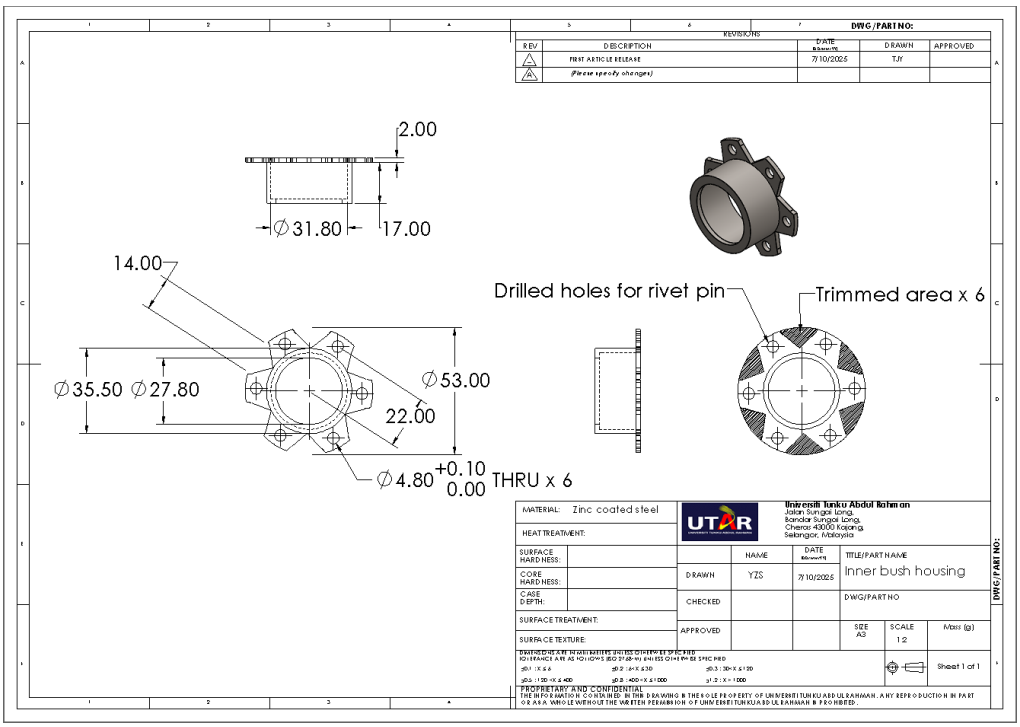

Figure C.2: Wheel bush housing (inner wheels)

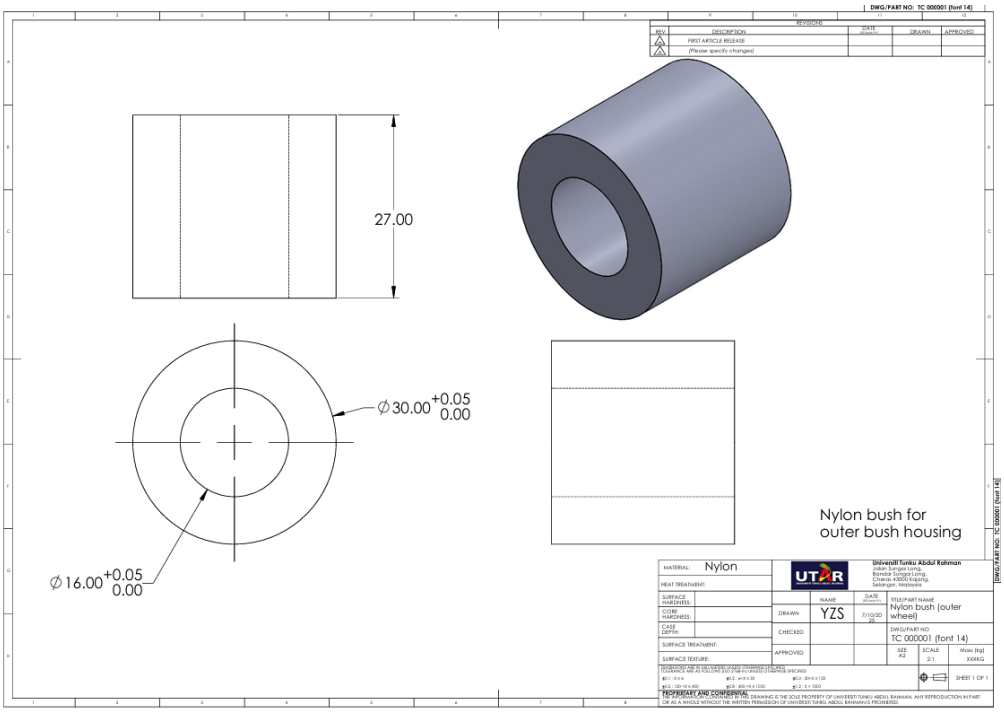

Figure C.3: Nylon bushing (Outer wheels)

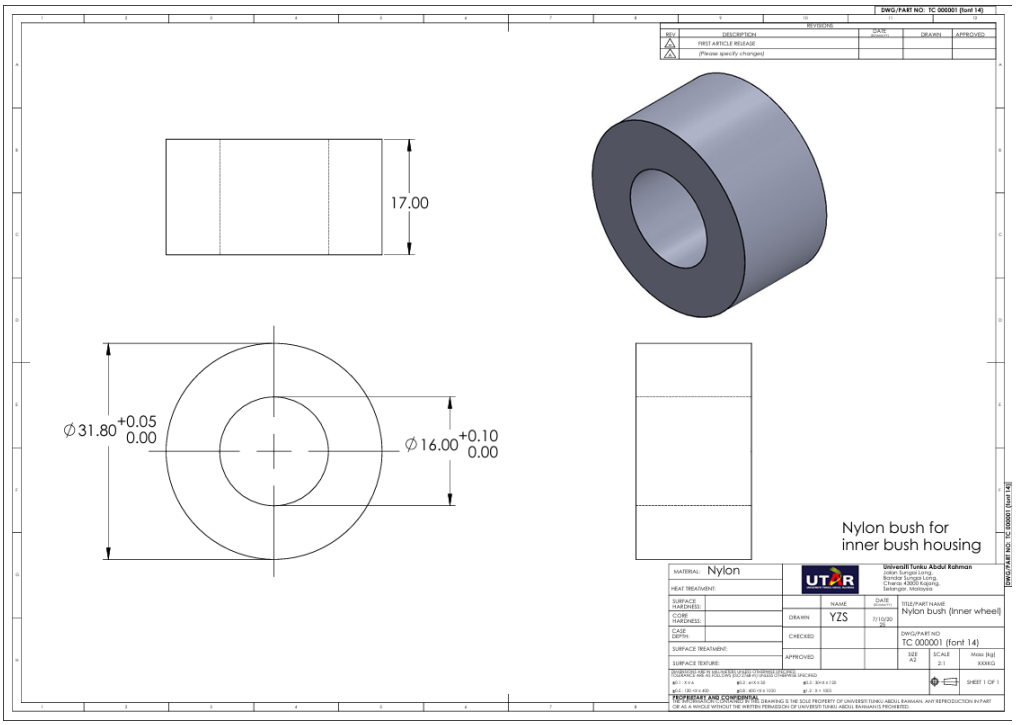

Figure C.4: Nylon bushing (inner wheels)

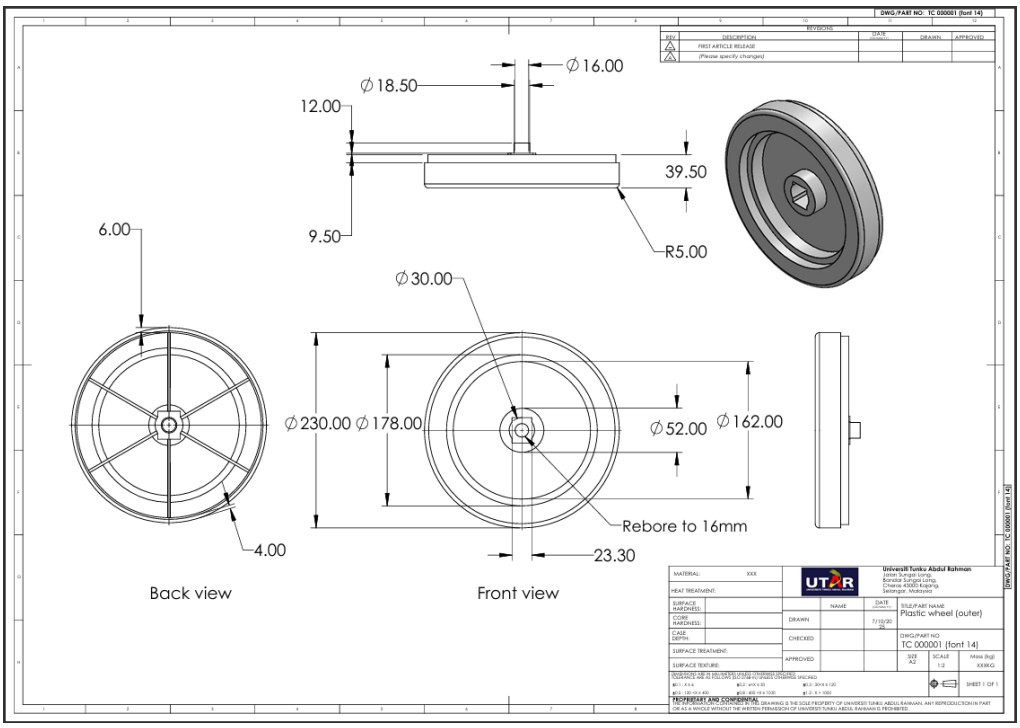

Figure C.5: Plastic wheels (outside)

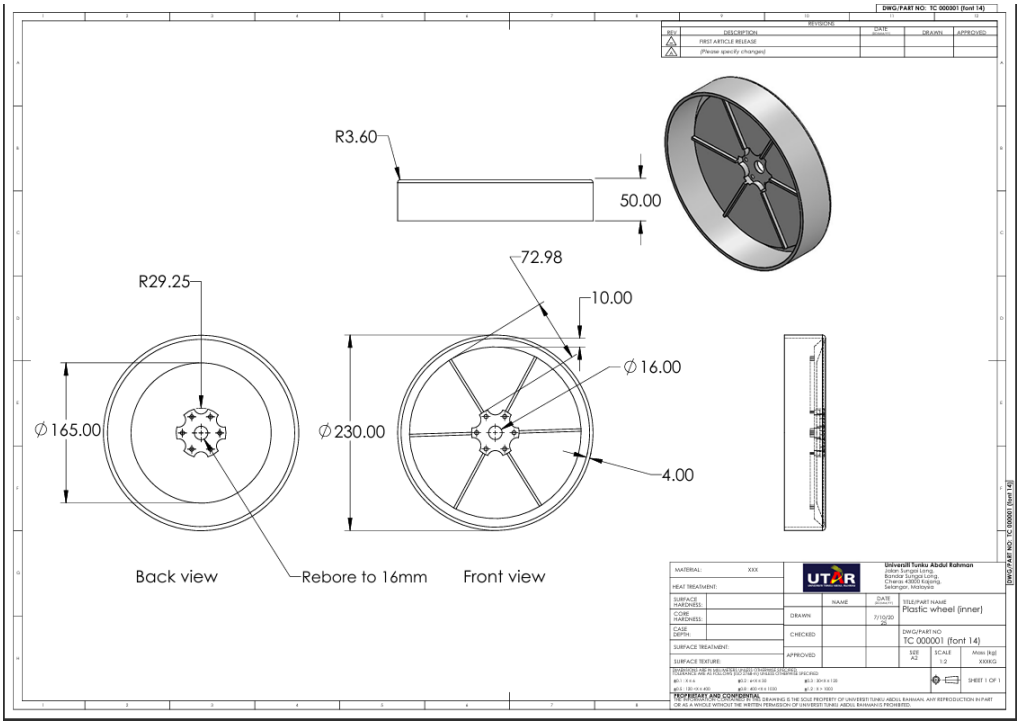

Figure C.6: Plastic wheels (inside)

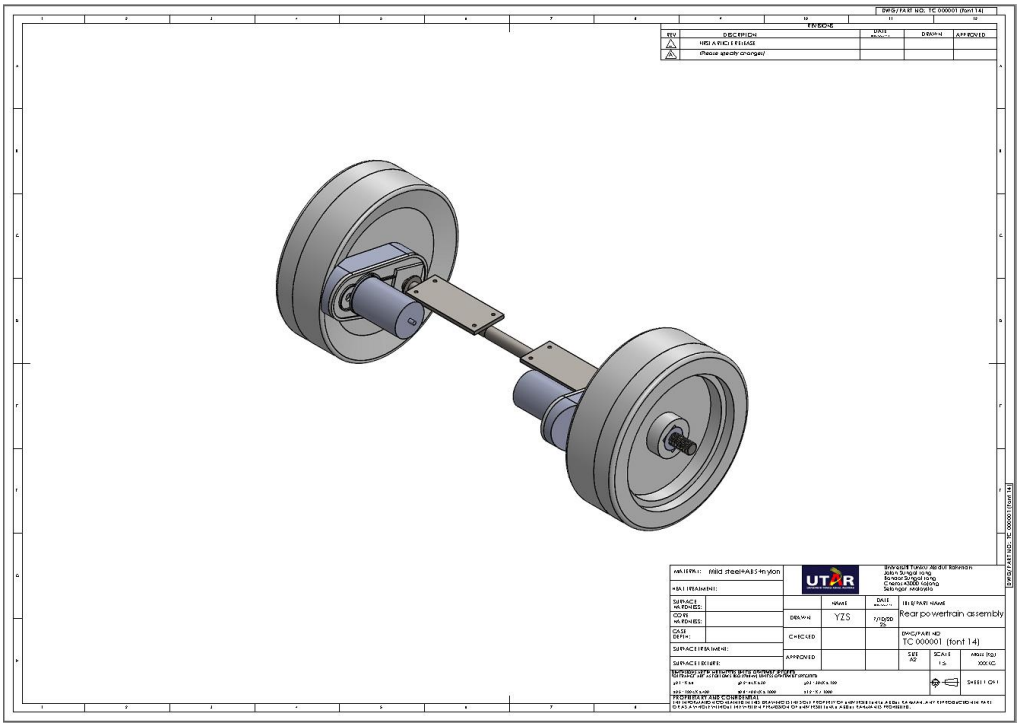

Figure C.7: Rear powertrain assembly

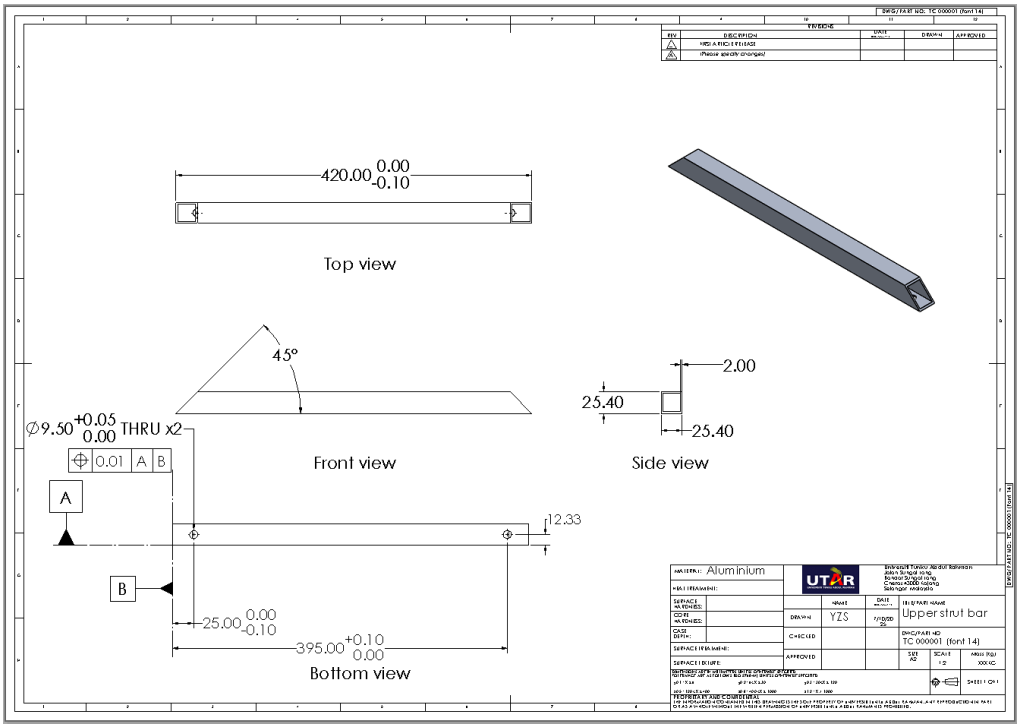

Figure C.8: Upper strut bar

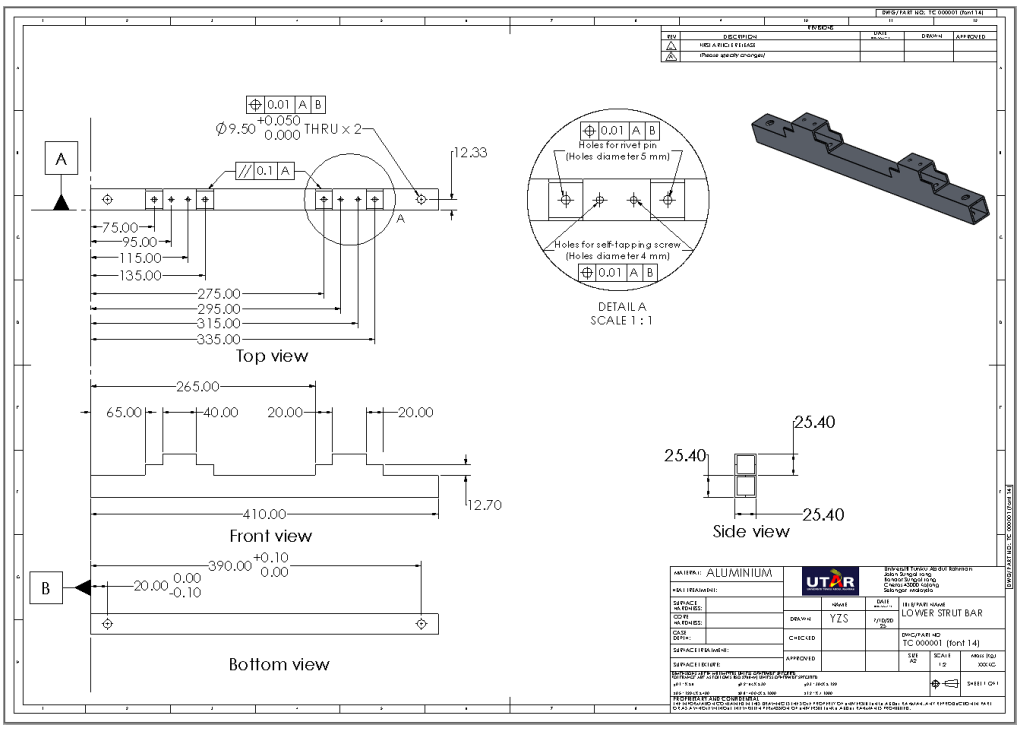

Figure C.9: Lower strut bar

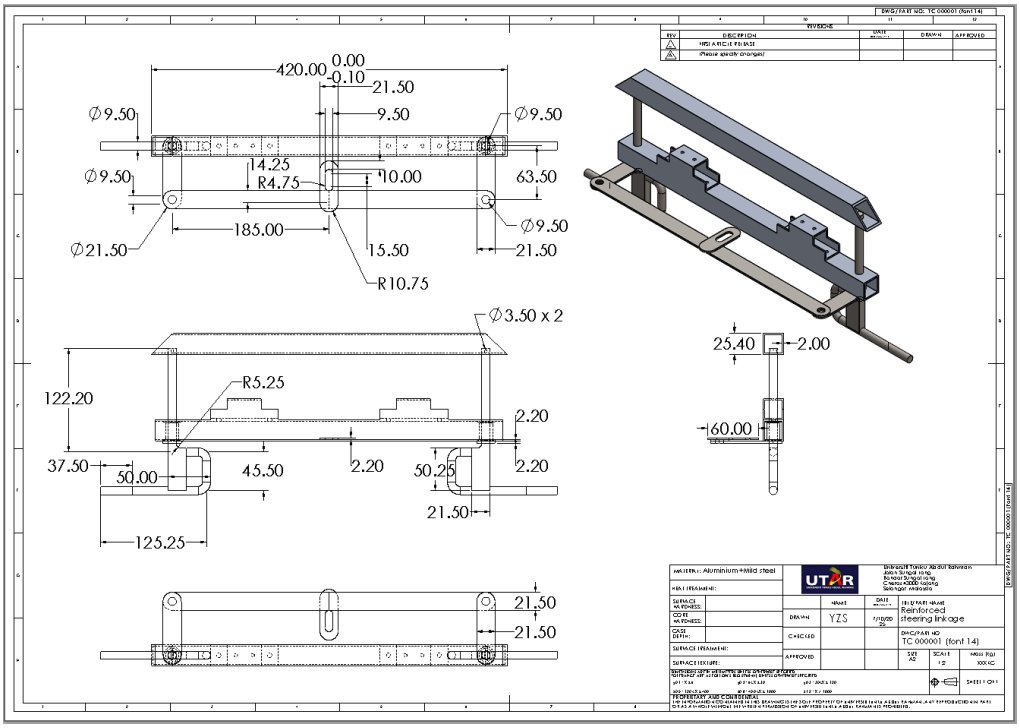

Figure C.10: Reinforced steering linkage

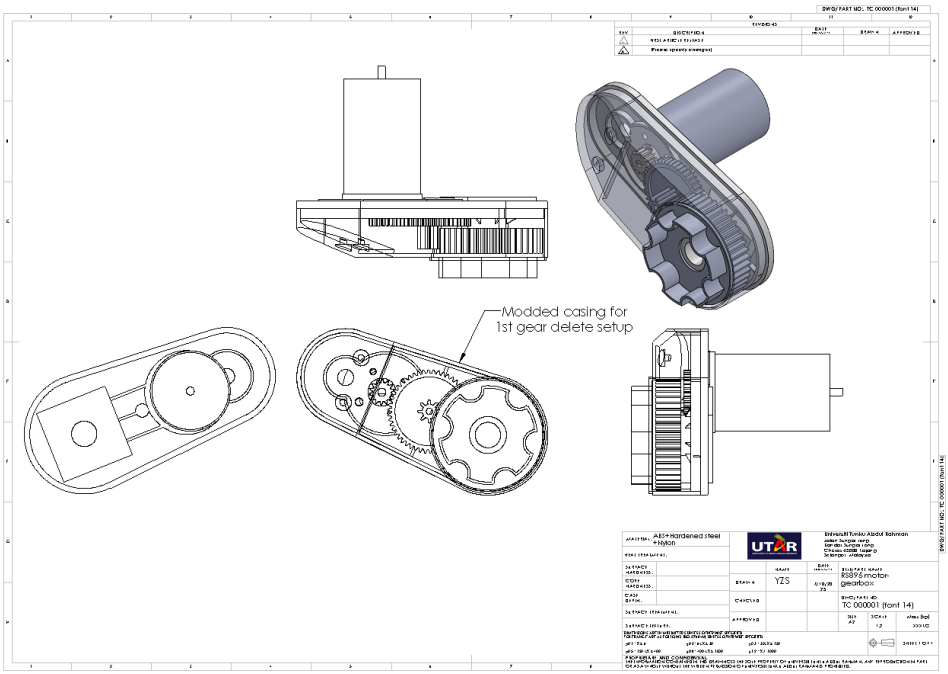

Figure C.11: RS895 motor gearbox assembly (with first gear delete)

Appendix D: Simulation results

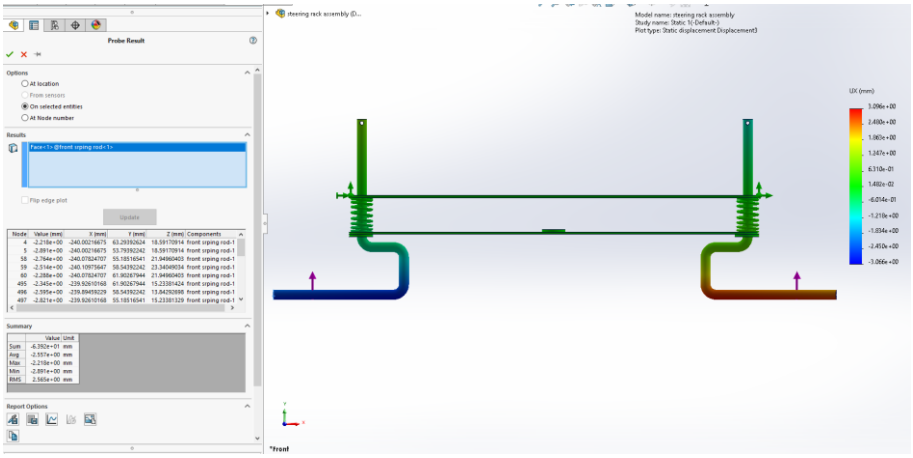

Figure D.1: Average X-displacement (2.557 mm) of stock steering linkage (400 N each side)

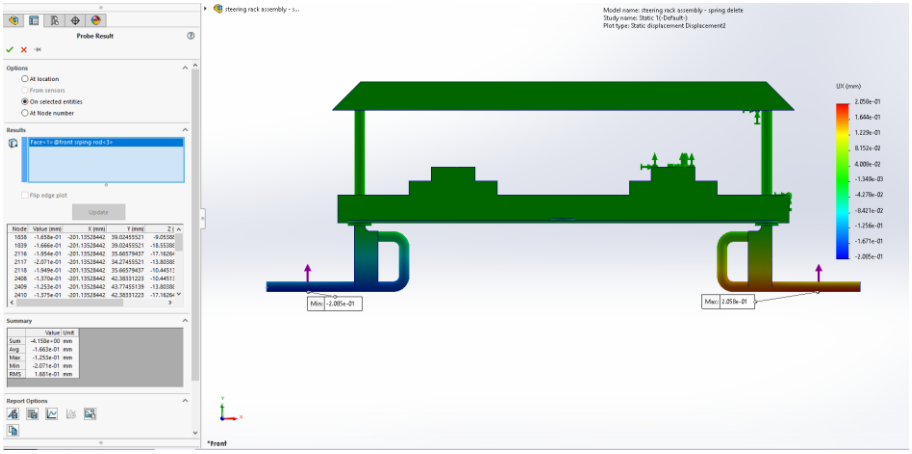

Figure D.2: Average X-displacement (-0.1663 mm) of reinforced steering linkage (400 N each side)

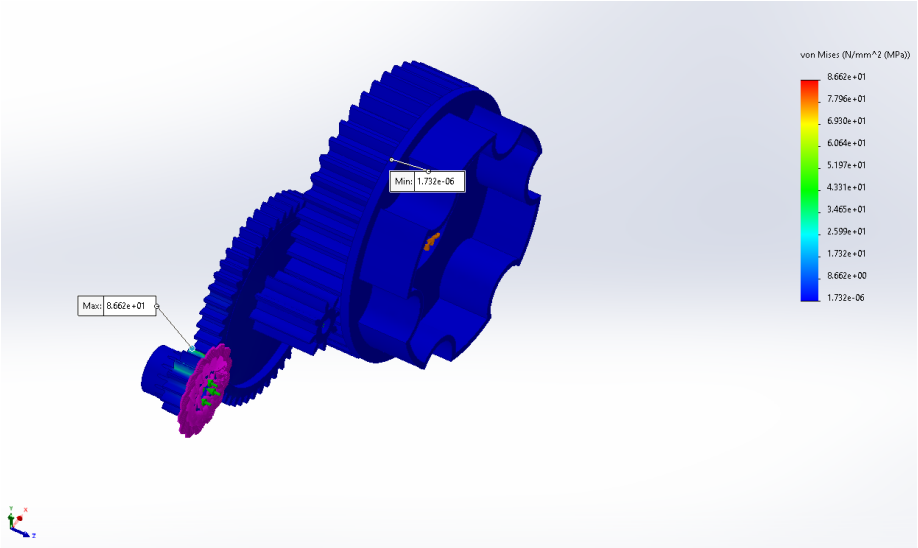

Figure D.3: Motor swapped geartrain simulation (τ_{in}: 1 Nm)

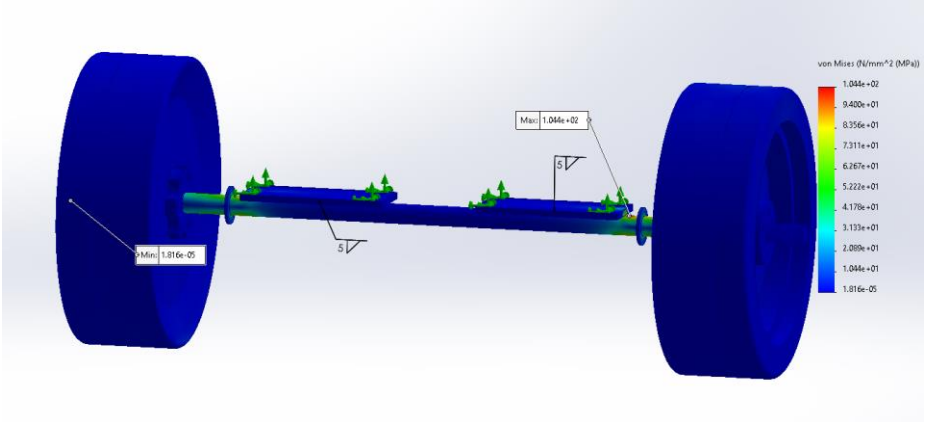

Figure D.4: Maximum stress (104.4 MPa) of reinforced rear shaft assembly under 400N point load on each wheel.

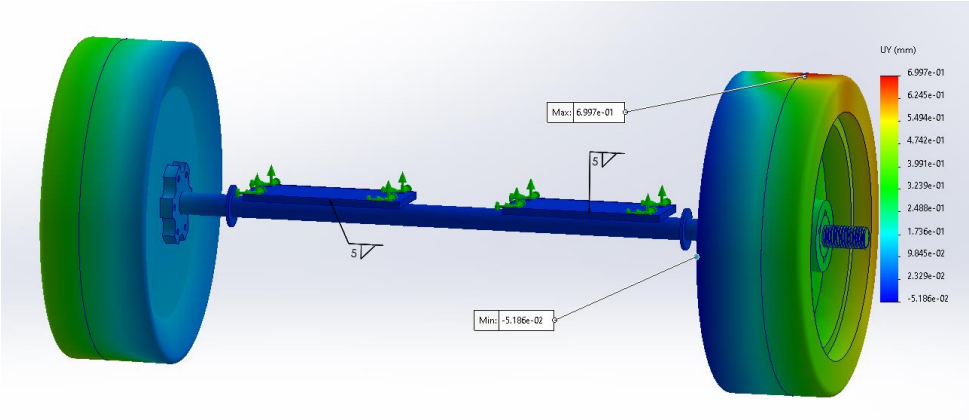

Figure D.5: Maximum Y-displacement (0.6997 mm) for reinforced rear shaft assembly under 400 N of point load on each wheel.

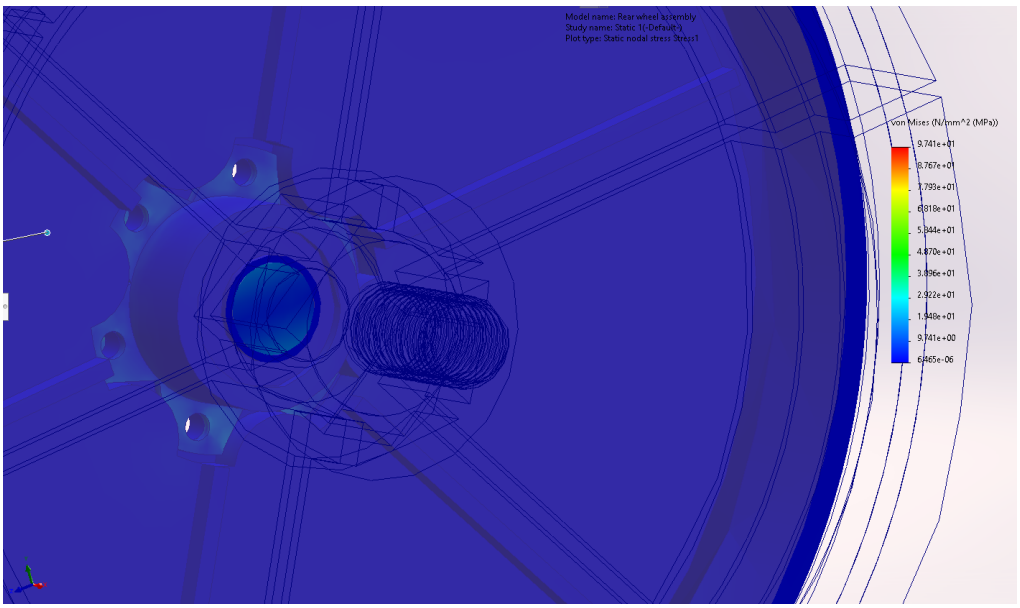

Figure D.6: Stress distribution of inner wheel bush housing

Appendix E: Ride-on-car model in SolidWorks

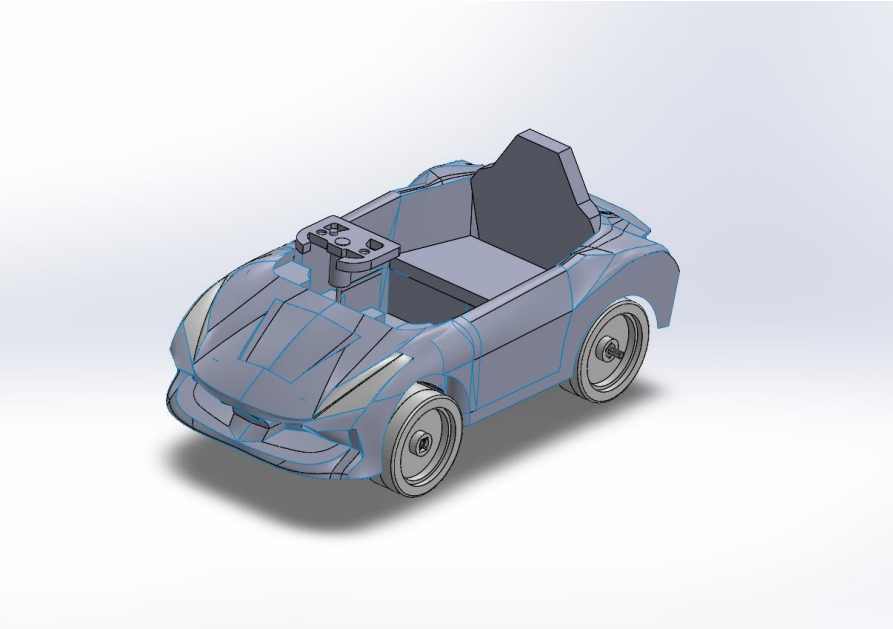

Figure E.1: Ride-on-car assembly model